RHIC Multi-Year Beam Use Request For Runs 10 and 11

The STAR Collaboration

May 27, 2009

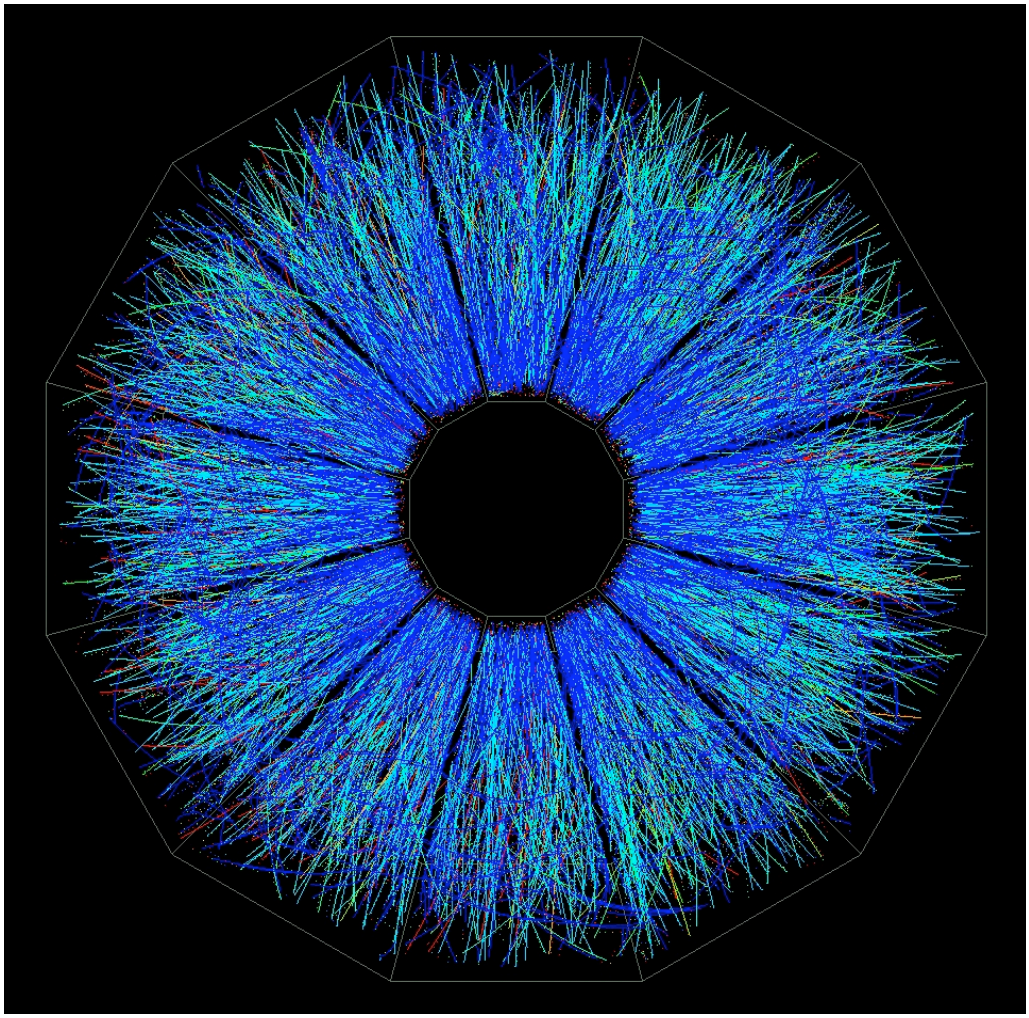

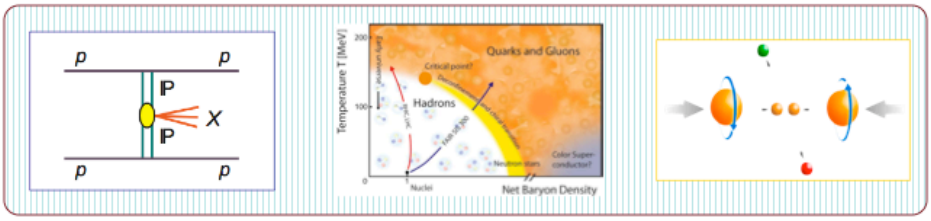

Table of Contents

1. Executive summary 4

2. Report on data taking in Run 9 7
2.1. Run 9 enhancements in STAR detector performance 7
2.2. 500 GeV Run Performance and Goals 9
2.3. Run 2009 Goals for 200 GeV pp 12

3. Experimental Study of the QCD Phase Diagram and Search for the Critical Point: Selected Arguments for the Run-10 Beam Energy Scan at RHIC 14
3.1. Introduction & Summary 14
3.2. The QCD Phase Diagram 16
3.3. A: Search for Phase Transition and a Critical Point 18
3.4. B: Turn-off of QGP Signatures and Other New Phenomena 25
3.5. Flexibility of STAR and Readiness for Unanticipated Observations 30
3.6. STAR Run Plan for First Energy Scan 31

4. Returning to Au+Au at 200 GeV in Run 10 37
4.1. Introduction and rationale 37
4.2. Triggered Datasets and Heavy Flavor 37
4.2.1. Run 10 in the longer-term context of luminosity improvements 47
4.3. Untriggered Datasets in Au+Au at 200 GeV 47
4.3.1. High-p_T kaon measurements as Probe of Nuclear matter with jet conversion 47
4.3.2. Full Jet Reconstruction 51
4.3.3. Future EM probes in STAR 53
4.3.4. Hypernuclei and anti-hypernuclei 54
4.3.5. Ultra-Peripheral Collisions 58
4.4. Au+Au Beam Use Request at 200 GeV for Run 10 59

5. Run 11: U+U Collisions at 200 GeV 61
5.1. Physics of U+U collisions at RHIC Top Energy 61
5.2. U+U Beam Use Request for Run 11 65

6. Run 11: Return to p+p Collisions 67
6.1. Recent spin physics results 67
6.1.1. STAR transverse spin program 67
6.1.2. STAR longitudinal spin program 69
6.2. Run 11 spin physics request 72
6.3. Transverse spin program at 200 and 500 GeV 73
6.4. Longitudinal spin program at 500 GeV 78
6.5. Longitudinal spin program at 200 GeV 81

7. Physics with Tagged Forward Protons: Run 11 and Beyond 87
7.1. Introduction 87
7.2. Beam Use Request for Run 11 87
7.3. Request beyond Run 11, Phase II 89

RHIC Multi-Year Beam Use Request
For Runs 10 and 11

The STAR Collaboration

May 24, 2009

1. Executive summary

The STAR Collaboration makes the following two-year beam-use proposal, in order to achieve its spin and relativistic heavy ion physics goals on a timescale consistent with intense international interest and competition in these areas, as well as to utilize RHIC beams effectively, taking full advantage of planned improvements in machine and detector capability as a function of time:

Table I: Beam Use Request for Runs 10 and 11

Run	Energy	System	Time	Goal
10[(1)]	$\sqrt{s_{NN}}$ =7.7-39 GeV	Au + Au	16 weeks	Critical Point search
	$\sqrt{s_{NN}}$ = 5 GeV	Au + Au	1 week[(a)]	Commissioning and first look at data
	$\sqrt{s_{NN}}$ = 200 GeV	Au + Au	8 weeks	250M central 300M minbias 2 nb^{-1} sampled
11[(2)]	$\sqrt{s}$ = 200 GeV[(b)]	$p_{\rightarrow}$ $p_{\rightarrow}$ $p_{\uparrow}$ $p_{\uparrow}$	13 weeks	~30 pb^{-1} long.[(d)] 15 pb^{-1} transverse
	$\sqrt{s}$ = 500 GeV[(c)]	$p_{\rightarrow}$ $p_{\rightarrow}$ $p_{\uparrow}$ $p_{\uparrow}$		15 pb^{-1} longitudinal 6.5 pb^{-1} transverse
	$\sqrt{s}$ = 200 GeV	$p_{\rightarrow}$ $p_{\rightarrow}$	5 days	pp2pp at high β*
	$\sqrt{s_{NN}}$ =200 GeV	U + U	4 weeks[(e)]	400M events

(1) 30 cryo weeks, 25 weeks production with one species
(2) 25 cryo weeks, 18 weeks production with two species.
(a) C-AD test for higher luminosity at the lower energy
(b) 60% or higher polarization in both yellow and blue rings is needed.
(c) 50% or higher polarization in both yellow and blue ring is needed.
(d) Request is to finish the minimum 50 pb^{-1} goal and make progress towards the portion of the long-term goal of 80 pb^{-1} at 60% polarization remaining after Run 9 is completed
(e) Contingent on EBIS operation at moderate rates (5-10 kHz)

Table II: Detailed breakdown of Critical Point search and Beam Energy Scan

Beam Energy	Event Rate	8-hr Days/ 1M Events	Events proposed	8-hr days proposed
5	0.8	45	100 k	5
7.7	3	11	5 M	56
11.5	10	3.7	5M	19
17.3	33	1.1	15M	16
27	92	0.4	33M	12
39	190	0.2	24M	5

In this proposed physics-driven plan, the STAR Collaboration intends to make the most efficient use of RHIC beam time and upgrades in order to make timely progress in determining the properties of the new state of matter produced at RHIC, to map the x dependence of the gluon polarization in the proton, $\Delta g(x)$, and to perform a definitive search for the phase boundary and the existence and location, if it exists, of the QCD critical point.

The primary goals of the proposed program are:

Run 10: 30 cryo-weeks, 25 weeks for physics production with a single species

a) Search for the existence and location of the QCD Critical point. First energy scan from $\sqrt{s_{NN}}$ = 7.7 to 39 GeV Au+Au collisions, combined with C-AD test to increase luminosity for $\sqrt{s_{NN}}$ = 5 GeV Au+Au collisions

b) 200 GeV Au+Au low material run with full Time-of-Flight and DAQ1000, in order to study in more detail the properties of matter produced at top RHIC energy

Run 11: 25 cryo-weeks, 18 weeks for physics production with two species

a) Return to $\sqrt{s}$ = 200 GeV to make progress towards the long term goal of 80 pb^{-1} sampled at 60% polarization, necessary to map the x dependence of gluon polarization in the proton, $\Delta g(x)$

b) First statistically significant measurement of the large parity violating single spin asymmetry, A_L, in W production at mid-rapidity.

c) Make progress towards the transverse spin milestone to search for evidence of repulsive color-charge interactions in the Sivers effect in correlations between forward photons and mid-rapidity jets

d) First run with U+U collisions to study hydrodynamic behavior of matter at energy densities up to 50% higher than that achievable with Au+Au collisions at 200 GeV

e) Continue the pp2pp program begun in Run 9, with longitudinally polarized beams, for studies of diffractive physics and search for glueballs at central rapidity

Comment on possible extension of Run 10

Run 10 presents a unique configuration of the machine and the detectors for the Critical Point Search. Additionally, there are uncertainties in the performance of the machine in this first wide-ranging exploration of the QCD phase diagram. Should the run be extended to 30 weeks, our top priority is to use the additional beam time to complete the program outlined in Table II.

We argue that the most important energy region for the physics of the BES program is the lower end of the proposed energy span, and therefore we propose to start the energy scan at 7.7 GeV. After about two weeks of data taking, we will be able to test and refine the accuracy of the estimates provided in Tables 3-1 and 3-2 of this document, and adjust the allocation of time, if needed.

2. Report on data taking in Run 9

2.1. Run 9 enhancements in STAR detector performance

A number of upgrades were added to STAR before the beginning of Run 9 to increase the data rates. The largest impact comes from the TPX or DAQ1000 upgrade to the TPC readout. This provides near dead-timeless readout of the STAR TPC up to rates approaching 1 kHz. This has been very successful and Fig. 2-1 shows a DAQ rate of 450 Hz (a) with a dead time of only a few percent (b). The barrel shower maximum detector (BSMD) is essential for electron and gamma physics. Its readout was also reworked this past year. By restricting its readout only to those triggers for which the detector is important, low dead times (15% in typical runs as shown in the figure) for rates over 200 Hz of such triggers are possible.

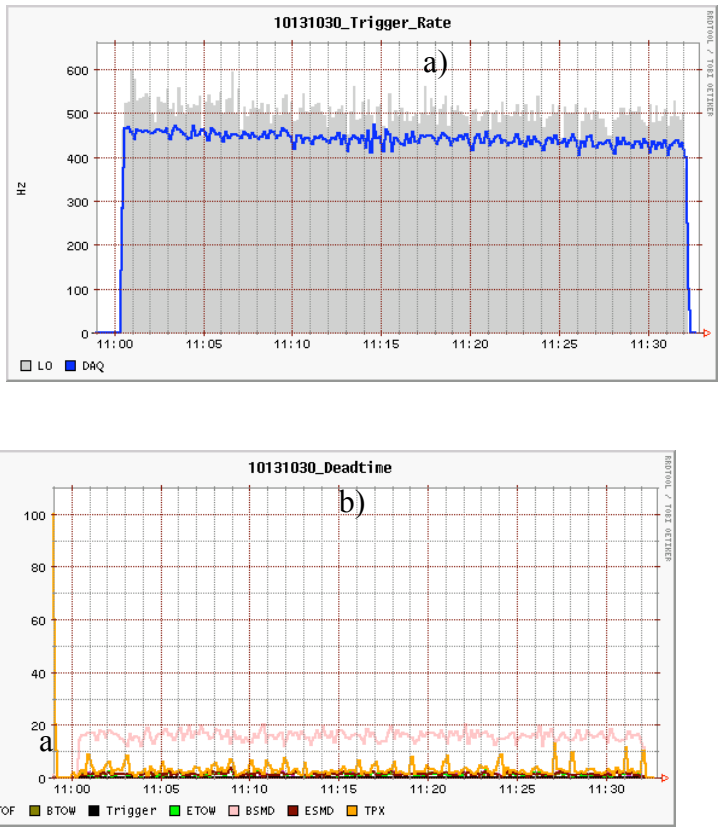

Figure 2-1: Typical trigger rates (a) and dead times (b) during run 9.

Another important modification was made to the hardware trigger logic. In previous runs the east barrel of the electromagnet calorimeters, the west barrel and the endcap triggers were essentially independent for jets, not allowing jets spanning two of these detectors to fire efficiently. Not only did this reduce overall acceptance, these overlap regions are correlated with certain kinematic regions in the gluon distribution $\Delta g(x)$ we wish to

measure. By rewiring the level 0 trigger electronics it was possible to create overlap patches that allow much more efficient triggering in the overlap regions as shown in Fig. 2-2. The pseudorapidity dependence from offline reconstructed jet distributions for run 6 is compared to that of run 9 in Fig. 2-3, showing the increased acceptance in the overlap region.

Through all these enhancements to our sub-systems we have greatly increased the yield of data we can record from a given amount of delivered luminosity, and are taking full advantage of this in run 9 for the polarized pp program.

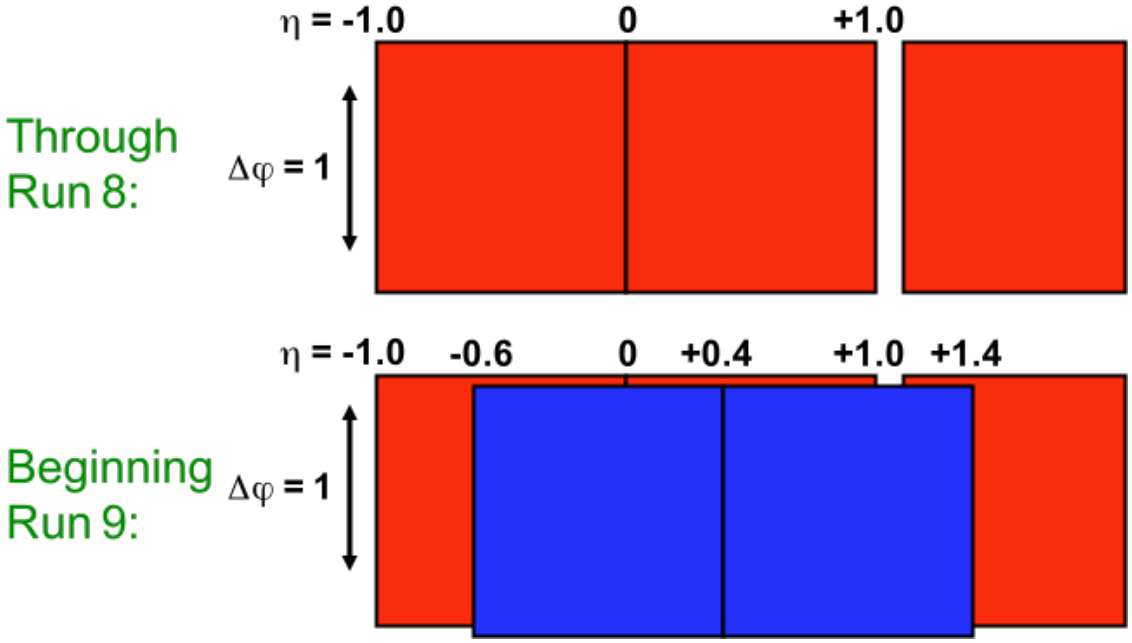

Figure 2-2. Through run 8 each unit of eta triggered on jets independently as indicated by the top figure. For the present run adjacent jet patches were defined that spanned the boundaries as shown in the lower figure.

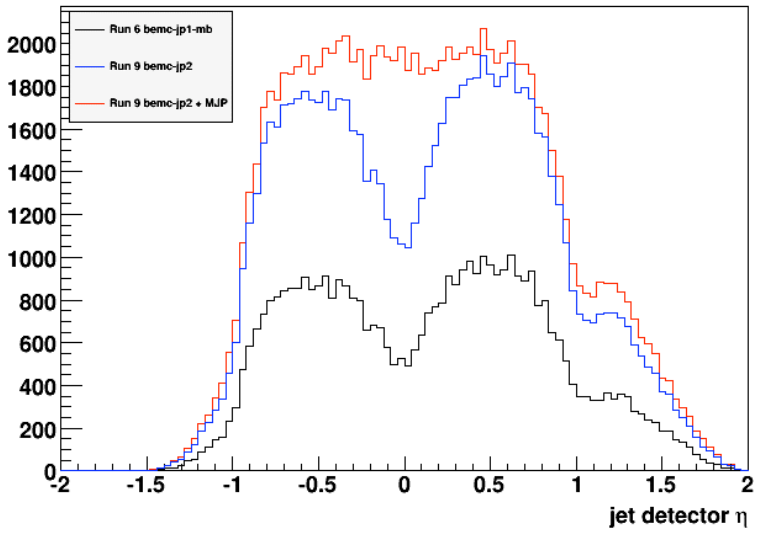

Figure 2-3: η distribution of offline reconstructed jets from 2006 data (black), with run 9 triggers (blue) and with adjacent jet patches spanning η=0 (red).

2.2. 500 GeV Run Performance and Goals

Run 9 began with 10 weeks of RHIC operations devoted to developing polarized proton collisions at 500 GeV center-of-mass energy. About 5 weeks were available for physics running. Our goals included the commissioning and operation of STAR in the 500 GeV environment, including, in particular, the development of local polarimetry at this new energy as well as initial physics goals of measuring the W production cross section in the leptonic decay channel and a first longitudinal spin asymmetry A_L provided that sufficient luminosity and polarization could be achieved.

Local polarimetry is essential at the experiments to verify that the transverse components of the beam polarization are minimized during longitudinal running through appropriate feedback on tuning of the spin rotators. Previous experience had indicated that the asymmetries in the beam-beam counters might be even smaller than they are at 200 GeV and thus difficult to use for this purpose at the higher energy. We had previously added crossed scintillator strip detectors between the forward and middle modules of the zero degree hadronic calorimeters allowing us to discern small angle scattering to the left, right, up and down of particles with respect to the beam. It was found that triggers that required significant energy deposit in the front and back portion of the ZDC resulted in usefully large analyzing powers for polarimetry as shown in Fig. 2-4. Here we plot the spin dependent asymmetry from flipping spin from nominally up to down vs. the azimuthal angle of the scattering plane. The magnitude of the sinusoidal oscillation is proportional to the beam polarization times analyzing power. This is a success and was used throughout the 500 GeV period for feedback on the direction of the beam polarization.

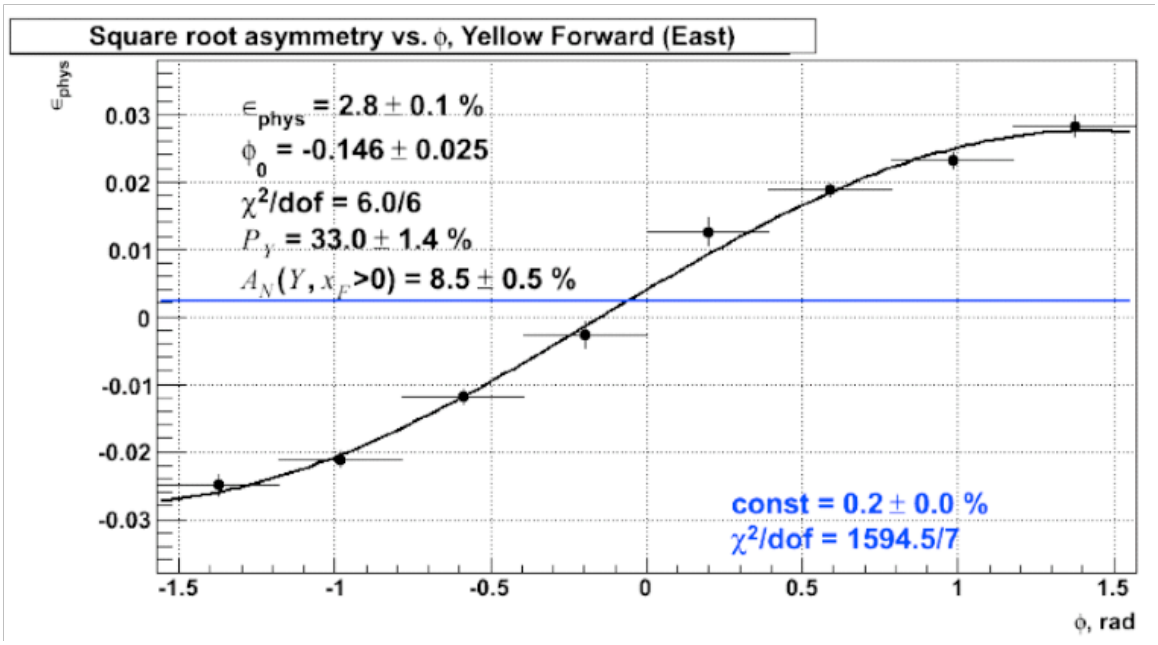

Fig. 2-4. The spin dependent asymmetry in a zero degree calorimeter with phi of the scattering determined by crossed scintillator strips inserted between the front and middle modules of the calorimeter. The magnitude of the sinusoid is proportional to the beam polarization

With the guidance provided on possible integrated luminosity provided by CAD we developed a physics program based on 10 pb^{-1} and 50% beam polarization. We have recently completed full detailed simulations comparing signal to backgrounds in the W production program. A strategy for cuts based on shower shapes analysis in the EM calorimeters and vetoing on away-side energy are indicating sufficient background suppression to get good signal to background ratios as shown in Fig. 2-5. At mid-rapidity we benefit from the fact that there is a peak in the W spectrum due to the Jacobian of the 2-body kinematics despite the fact that the neutrino is not detected. Our primary goal was to detect this peak if sufficient luminosity could be integrated.

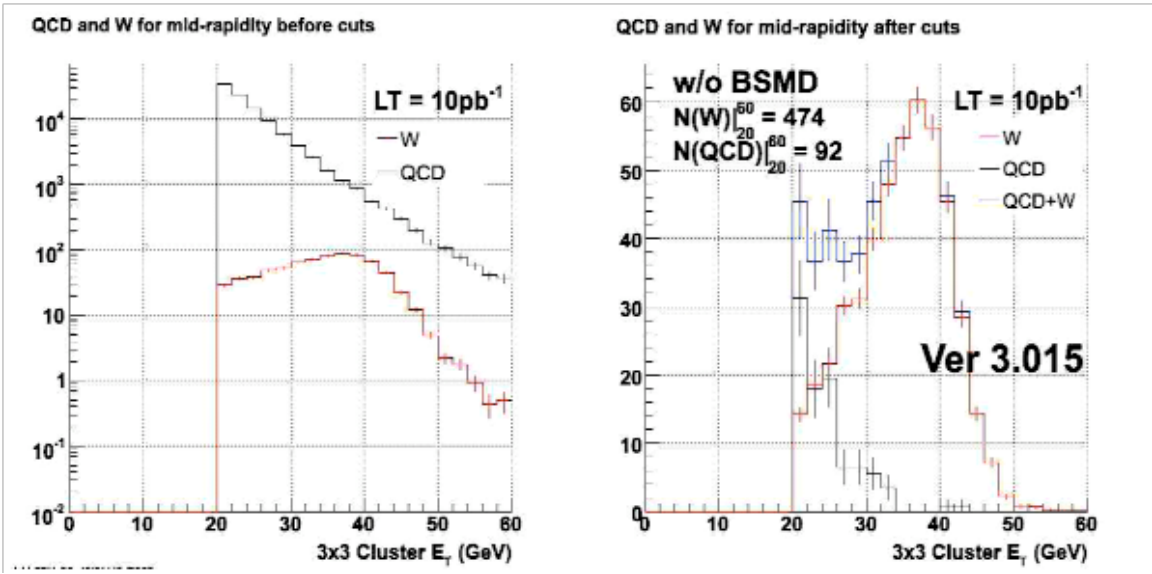

Figure 2-5. Simulations of background reduction in W production.

If in addition there would be 50 % beam polarizations we expected that we would be able to measure a statistically non-zero parity violating longitudinal single spin asymmetry as shown in Fig. 2-6. Note that this is more challenging not only because of the required 50% beam polarization but also because the charge sign separation must be fully developed at mid-rapidity using only the TPC and a beamline constraint.

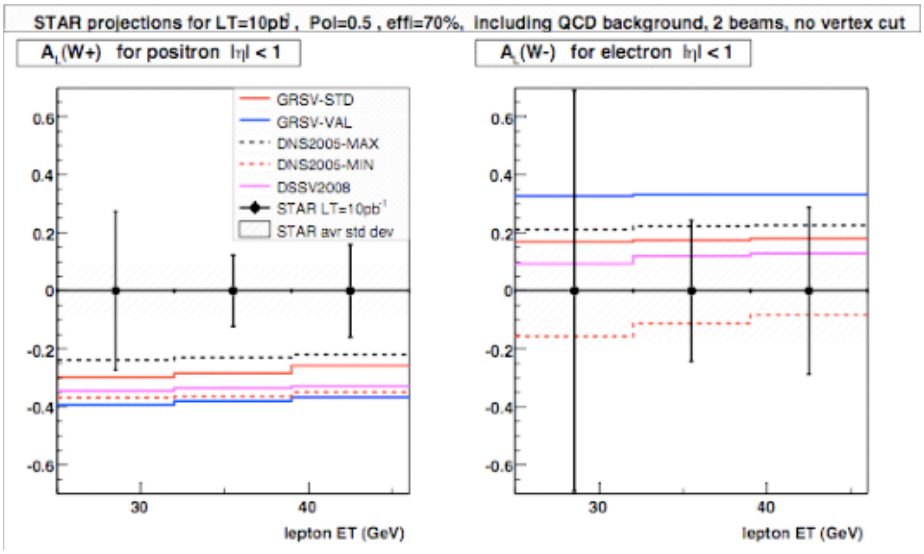

Fig. 2-6 Expected longitudinal single spin asymmetry, A_L, assuming 10 pb^{-1} and 50% beam polarization.

As shown in Fig. 2-7 we were successful in recording our integrated luminosity goal in the 500 GeV portion of run 9 and the analysis of events triggered for the W program, including tracking with the TPC, is underway. However the polarization of the beams delivered was well below the 50% assumed in our goals. Since the figure of merit involves the square of the polarization for single spin asymmetries the achieved FOM reached only about half our goal.

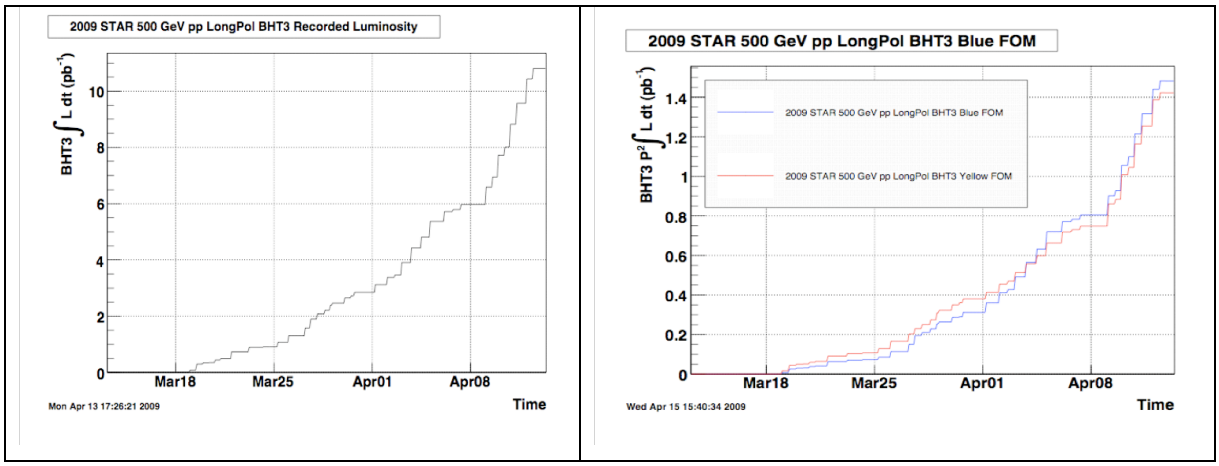

Fig. 2-7: STAR recorded integrated luminosity (left) and figure of merit, P^2L, (right).

2.3. Run 2009 Goals for 200 GeV pp

The physics goal for the ongoing 200 GeV p+p running in 2009 is to advance our understanding of the gluon polarization based on measurements of inclusive jets and other probes to high p_T and on measurements of di-jet and photon-jet correlations to map the kinematic dependence, $\Delta g(x)$. The figure of merit goal for this run was originally set based on a 12 week run commencing after startup was complete. Picking a mid-point between the RHIC projected max. and min. delivered luminosity and factoring in our improved DAQ capabilities we estimated we could record 50 pb^{-1}. With a polarization of 60% this leads to a goal FOM (P^4L) of 6.5 pb^{-1}. Subsequent projections based on a changeover from the 500 GeV run indicated that we could hold these projections for a 10 week run as shown in Fig. 2-8. Extrapolation of beam performance at the time of writing indicates that a substantial portion of this FOM will need to be acquired in a future run. Thus the detailed description of the physics goals appears below in the proposed physics section.

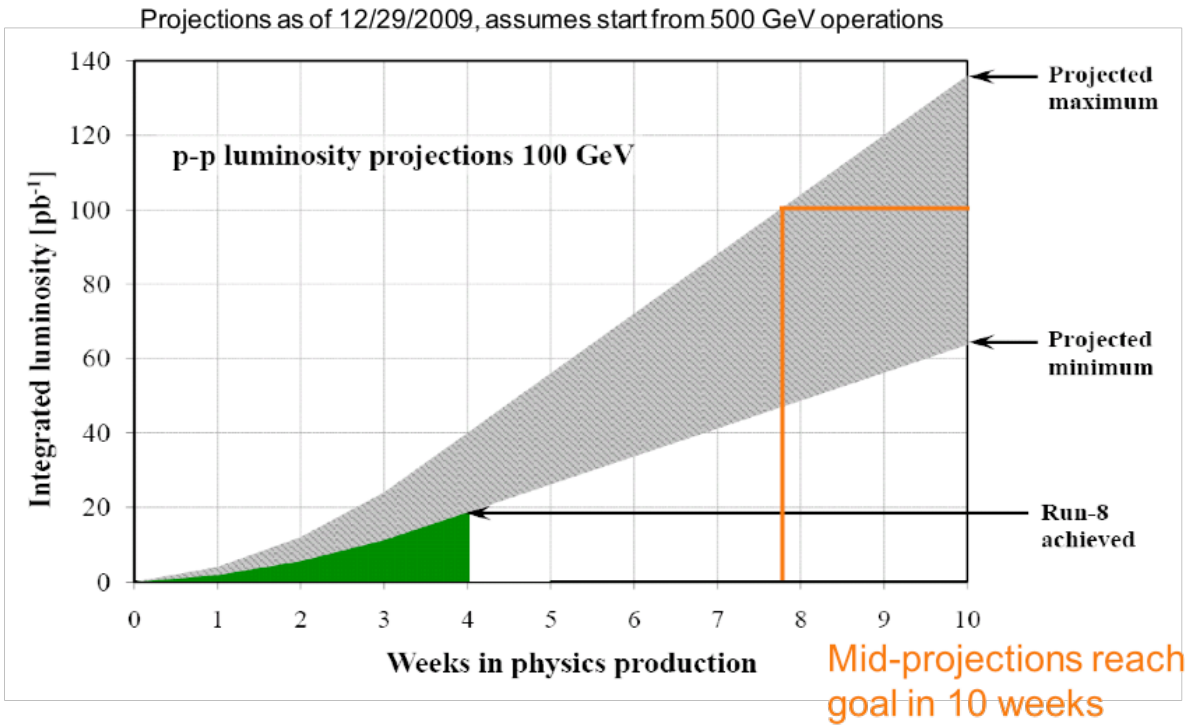

Fig. 2-8. Projected delivered integrated luminosity at 200 GeV assuming a warm start from the 500 GeV run.

3. Experimental Study of the QCD Phase Diagram and Search for the Critical Point: Selected Arguments for the Run-10 Beam Energy Scan at RHIC

3.1. Introduction & Summary

We present an overview of the main ideas that have emerged from discussions within STAR for the Beam Energy Scan (BES). The formulation of these arguments has been facilitated by the preparation of a much longer and more comprehensive companion document entitled *Experimental Exploration of the QCD Phase Diagram: Search for the Critical Point* [1]. The compelling arguments and motivations for the physics of our proposed Beam Energy Scan program, which have a particular role in guiding the run plan as set out in our discussion of Tables 3-1 and 3-2, are:

A: Search for signatures of a phase transition and a critical point.
The particular observables that we have identified as the essential drivers of our run plan are:

(A-1) Elliptic & directed flow for charged particles and for identified protons and pions, which have been identified by many theorists as highly promising indicators of a "softest point" in the nuclear equation of state;

(A-2) Azimuthally-sensitive femtoscopy, which adds to the standard HBT observables by allowing the tilt angle of the ellipsoid-like particle source in coordinate space to be measured; these measurements hold promise for identifying a softest point, and complements the momentum-space information revealed by flow measurements, and

(A-3) Fluctuation measures, indicated by large jumps in the baryon, charge and strangeness susceptibilities, as a function of system temperature – the most obvious expected manifestation of critical phenomena.

B: Search for turn-off of new phenomena already established at higher RHIC energies
QGP signatures are the most obvious example, but we define this category more broadly. If our current understanding of RHIC physics and these signatures is correct, a turn-off must be observed in several signatures, and such corroboration is an essential part of the "unfinished business" of QGP discovery [2]. The particular observables that STAR has identified as the essential drivers of our run plan are:

(B-1) Constituent-quark-number scaling of v_2, indicating partonic degrees of freedom;

(B-2) Hadron suppression in central collisions as characterized by the ratio R_{CP};

(B-3) Untriggered pair correlations in the space of pair separation in azimuth and pseudorapidity, which elucidate the ridge phenomenon;

(B-4) Local parity violation in strong interactions, an emerging and important RHIC discovery in its own right, is generally believed to require deconfinement, and thus also is expected to turn-off at lower energies.

Approaching the proposed BES program with the realization that a lesson from the past history of relativistic heavy-ion physics is to expect surprises, we offer a physics vision that is presented in Table 3-2, in which we emphasize the highly diverse analysis options made possible by the large acceptance and general-purpose capabilities of the STAR detector, especially with the enhanced particle ID capabilities added by the full Time-of-Flight barrel coming online in Run 10. Table 3-2 is a concise illustration that STAR is highly adaptable and flexible, and we are ready to find and characterize the almost-inevitable surprises that will be in store as we explore the new frontier of the BES.

Recent analyses of a few thousand Au + Au events at $\sqrt{s_{NN}}$ = 9.2 GeV, recorded during a short beam development test in spring 2008, provide ample evidence that the STAR detector is fully ready and capable of successful operation at sub-injection energies.

Many factors constrain our planning for BES running at STAR. These include the upcoming Heavy Flavor Tracker and Forward GEM Tracker subsystems, which will impact the future availability of one or both Forward Time Projection Chambers (FTPC) – proven existing subsystems that provide information about the reaction plane needed for measuring the v_1 component of flow and considerably extend pseudorapidity coverage. New 4-cm-diameter beam pipes are also coming to both PHENIX and STAR in Run-11. The implication for BES of these new pipes is still under study, but there is a danger of very serious degradation of RHIC performance at low beam energies. Therefore, we view Run-10 as a unique opportunity for an exploratory Energy Scan.

3.2. The QCD Phase Diagram

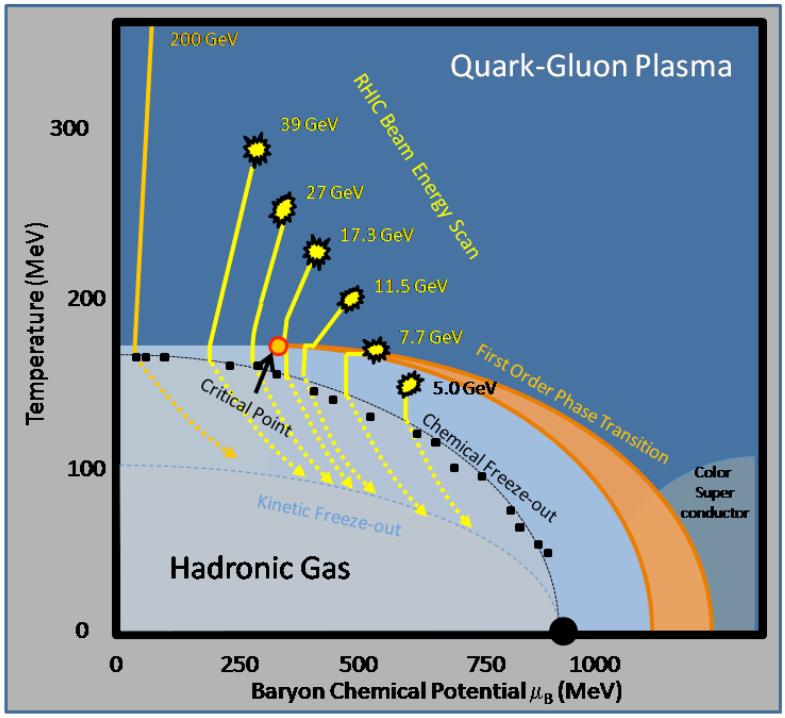

Fig. 3-1: A schematic representation of the QCD Phase Diagram. The location of the critical point, the separation between the 1st-order transition and chemical freeze-out, and the focusing of the event trajectories towards the critical point, are not based on specific quantitative predictions, but are all chosen to illustrate plausible possibilities.

The QCD phase diagram, schematically sketched in Fig. 3-1, lies at the heart of what the RHIC Physics Program is all about. It contains information about the location of phase boundaries (the phase transition is indicated by the orange band) and the physics of the phases, hadronic gas (HG, light blue) and quark-gluon plasma (QGP, navy), that are separated by this boundary.

So far, our understanding of this diagram is limited to the "edges"[3]: Lattice QCD calculations at vanishing chemical potential μ_B indicate a rapid, but smooth cross-over transition at a large temperature T [4], while various models representing matter at vanishing T predict a strong first-order phase transition at a large μ_B [5]. If both classes of models are correct, then a critical point (marked by the red circle in Fig. 3-1) must be located where the transition changes from a smooth cross-over to first-order [6]. Exploring the rest of the QCD phase diagram ($T \neq 0$ and $\mu_B \neq 0$) presents a formidable challenge. Several methods have been applied to lattice QCD to overcome existing numerical problems at non-vanishing μ_B, but there is no agreement in the predictions of the location, or even the existence, of the critical point so far. An additional complication comes from

the fact that the systematic errors of lattice calculations are neither understood nor constrained.

Given the very significant theoretical difficulties, it falls to the experiments to resolve the questions. The BES experimental program at RHIC with heavy ion collisions at energies in the range $\sqrt{s_{NN}}$ = 5 to 39 GeV is designed to provide observational evidence for the existence of the critical point and to explore the unknown "territories" of the QCD phase diagram. Heavy ion collisions provide a unique experimental opportunity for such exploration; by varying the center-of-mass energy of the colliding nuclei, one can access different values of μ_B (collisions with higher energies probe lower μ_B values). The yellow lines in Fig. 3-1 represent possible reaction trajectories at energies proposed for the first run of the BES program (from right to left: $\sqrt{s_{NN}}$ = 5, 7.7, 11.5, 17.3, 27 and 39 GeV).

While stepping in μ_B, one needs to pay close attention to many observables, in particular the signatures predicted for phase transition and the critical point. A non-monotonic dependence of variables on $\sqrt{s_{NN}}$ and an increase of long-wavelength fluctuations should become apparent only near the critical point. The rise and then fall of this signal as μ_B increases should allow us to ascertain the (T, μ_B) coordinates of the critical point. The onset of the non-equilibrium "lumpy" final state is expected after cooling through a first-order phase transition. Those fluctuations will have non-Gaussian character.

Note that the magnitude of these non-monotonic excursions, as well as the probability that they will survive the final state interactions, is difficult to predict. Fortunately for the experiments, there may not be a need for a trajectory to "pass" precisely through the critical point in the (T, μ_B) plane to see the signatures, as some hydrodynamic calculations show that the critical point "attracts" trajectories [7]. In such a case, if the trajectory misses the critical point by a few tens of MeV along the μ_B axis, the signature will be just as strong as if it were to pass directly through it. Note, however, that this "attraction" is not generic, and relies on specific features of the EOS near the critical point [7]. The exact position of the critical point in Fig. 3-1, as well as the associated attraction of trajectories, was chosen for illustration purposes only [7]. Although subsequent running can use smaller steps in μ_B to verify and trace the possible effect of focusing and to pin down the critical point, the first exploration of unknown territories of (T, μ_B) space will be done with a few steps in $\sqrt{s_{NN}}$ to narrow down an area of interest for further study (see Table 3-1).

Establishing the existence of the critical point, or the existence of both a cross-over and a first/second order transition, would surely place RHIC results into textbooks around the world.

3.3. A: Search for Phase Transition and a Critical Point

(A-1) Elliptic and Directed Flow

The search for a critical point can follow two parallel strategies: the first is to find direct evidence of the divergence of fluctuations expected at the critical point, while the second is to bracket the location of the critical point by finding evidence for a first order phase transition at lower μ_b. For collision energies that result in trajectories that cross the 1st-order phase transition region, there is expected to be a significant softening of the equation of state. Thus signatures of the 1st-order phase transition will be found in the hydrodynamic evolution of the phase-space distribution.

Elliptic flow (v_2) has been studied at RHIC, SPS, AGS, and lower energies. The most extensive energy systematic is p_T integrated for unidentified particles, as shown in Fig. 3-2. At energies below $\sqrt{s_{NN}}$ = 3.8 GeV, the elliptic flow is negative (out-of-plane). This is interpreted as a squeeze-out due to the interaction between the spectators and the participant zone [8]. Ideal hydrodynamics had predicted a non-monotonic dependence of v_2 with collision energy due to the softening near T_c [9], however, this has not been seen in this general study; above 3.8 GeV, the elliptic flow becomes positive and increases with collision energy. In order to remove the effects of the initial conditions, v_2/ε (where ε is the initial state eccentricity) has been studied as a function of centrality for RHIC energies and compared to hydrodynamic predictions [10]. It is only at the highest particle densities that the systems seem to approach the ideal hydro limits [11].

Measuring v_2 with a selection on transverse momentum is important for at least two reasons. First, comparison with any model should only be done within the range of validity of that model. Hydrodynamics is typically assumed to be valid below 1.5 GeV/c [9], and the shape of the p_T-dependence of v_2 is a good indication of when viscous effects dominate. Secondly, it has recently been stressed [12] that focus on some specific range in p_T can generate apparently exciting but actually-trivial artifacts in the excitation function of v_2. In addition to p_T selection, it is crucial to have good particle identification, for two important reasons. Firstly, several authors [13,14] have pointed out the much stronger sensitivity on the EOS for particles much heavier than the pions, which dominate inclusive charged particle measurements. For example, a potential signature of the phase transition is the collapse of the proton elliptic flow [15]. NA49 had made an initial report of an observation of this effect in $\sqrt{s_{NN}}$ = 8.77 GeV data [16]; however, more precise results and more detailed comparisons to the theoretical models are needed in order to draw firm conclusions. Secondly, the defining characteristic of collectivity in hydrodynamical scenarios is the interplay of the velocity field with thermal motion; this gives rise to an unavoidable and characteristic mass scaling of spectra and v_2. The observation of this scaling signals that hydro concepts may be applied, whereas its breakdown suggests strong viscous corrections, or particle-dependent mechanisms such as quark coalescence or particles escaping early from the collision (e.g. phi meson).

The directed flow (v_1) is generated during the nuclear passage time, T_{pass}, and therefore it can probe the onset of the bulk collective dynamics as long as this passage time is greater than the time required to achieve thermalization, τ_0. The nuclear passage time can be estimated as $T_{pass}=2R/\gamma$, which varies from ~ 5.6 fm/c for $\sqrt{s_{NN}}$ = 5 GeV to ~ 0.35 fm/c for

$\sqrt{s_{NN}}$ = 39 GeV; the timescale for thermalization is expected to be proportional to $(dN/dy)^{-1/2}$ and varies from ~ 1.2 fm/c for $\sqrt{s_{NN}}$ = 5 GeV to ~ 0.7 fm/c for $\sqrt{s_{NN}}$ = 39 GeV ($T_{pass} > \tau_0$ for all collision energies proposed in Table 3-1 except 39 GeV). The shape of v_1 vs. rapidity is of special interest because it has been identified as a key phase transition signature [17]. At low energies, the v_1 is almost directly proportional to the rapidity. In the energy range proposed in Table 3-1, the directed flow is predicted to be near zero and to even exhibit a characteristic "*wiggle*". In Fig. 3-3, we show suggestive preliminary results of a v_1 analysis of 9.2 GeV test run data.

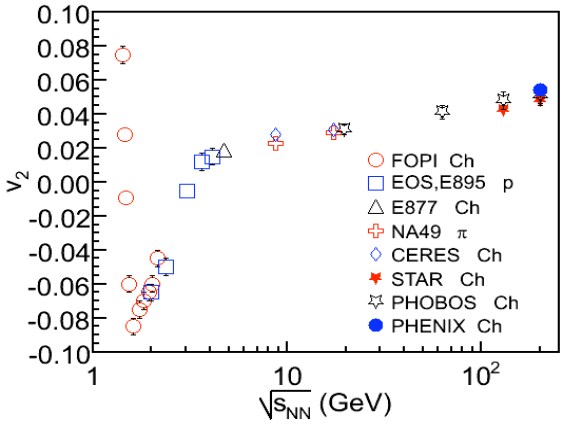

Fig. 3-2: The charged particle v_2 collision energy excitation function shows a change from out-of-plane to in-plane.

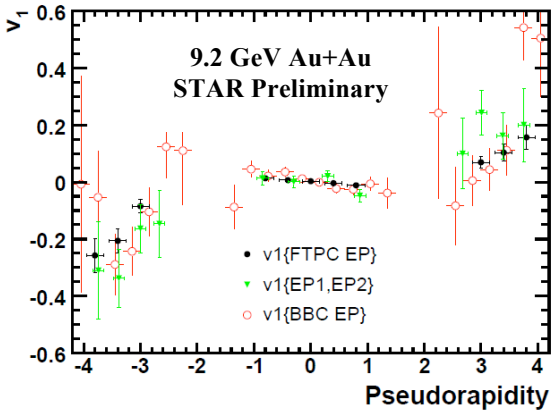

Fig. 3-3: A "*wiggle*" in v_1 near $y = 0$ is a promising phase transition signature; however it is important to distinguish pion from proton v_1, which the full ToF will allow.

(A-2) Azimuthally Sensitive HBT

Momentum-space correlations tell only half of the story of the hydrodynamic evolution. HBT radii measured relative to the event plane are the coordinate-space analogs of directed and elliptic flow [18, 19], and are expected to be sensitive to a softening in the EOS related to a 1st-order phase transition [20].

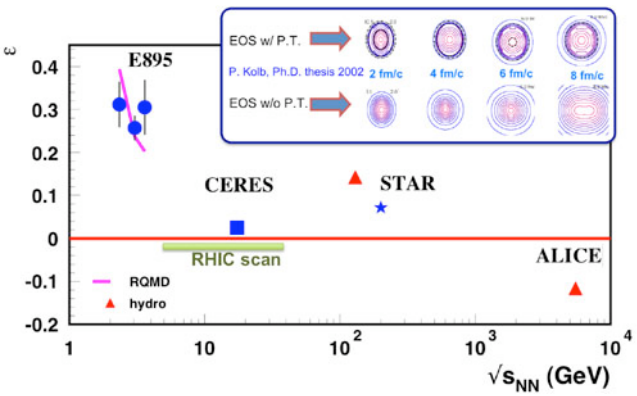

Fig. 3-4: Freeze-out anisotropy from 2nd -order oscillations of HBT radii. All measurements are subject to ~30% systematic uncertainty. Inset shows hydro evolution of source shape for an equation of state with (upper) and without (lower) softening due to finite latent heat. [23]

STAR has measured the azimuthal dependence of the π HBT radii with respect to the reaction plane [21]. In addition to the overall size of the source, this analysis reveals the transverse *shape* (described by the eccentricity, $\varepsilon = (\sigma_y^2 - \sigma_x^2)/(\sigma_y^2 + \sigma_x^2)$, where σ_x^2 is the in-plane axis, and σ_y^2 is the out-of-plane axis). The shape is found to be extended out-of-plane at freeze-out. Quantitatively, however, it has a lower eccentricity than the initial system, reflecting the dynamic evolution of the system.

The eccentricity has been measured at a few lower energies, as well. Since the

lifetime of the system and the elliptic flow increase with collision energy, one naively expects that the freeze-out shape becomes less out-of-plane extended, and may even become in-plane extended (as predicted [20] for example at the LHC). However, Fig. 3-4 shows instead an intriguing non-monotonic behavior. A possible explanation may be that at low energies the stiff EOS of a hadronic system generates a large pressure, pushing the system towards a round shape ($\varepsilon = 0$). At some energy, a threshold required to generate a phase transition is crossed. This generates a "soft point" in the EOS, and the push towards a round state is reduced. At still higher energies, the stiff EOS of the QGP phase leads again to a decreasing eccentricity with increasing $\sqrt{s_{NN}}$.

This would be the direct analog of the non-monotonic excitation function of v_2 originally predicted by ideal hydro models with a softening due to a phase transition [9, 22]. The signal in v_2 has not been observed. However, the spatial anisotropy probed by HBT is weighted in the time evolution differently, so may retain sensitivity to the softest point. In any event, Fig. 3-4 represents one of the very rare bulk-sector probes with an unexplained non-monotonic excitation function, demanding further exploration.

The 3-dimensional shape of the spatial configuration approximates a tri-axial ellipsoid. One can extract the angle between its major axis and the beam direction. This "*tilt angle*" [19] is the spatial analog of the "*flow angle*" [23] formerly used to characterize directed flow. Simultaneous measurement of both the tilt angle and v_1 provides unique insight into the nature and physics of directed flow at lower energies. As discussed above, crossing a threshold to a phase transition will generate a "wiggle" in the directed flow at midrapidity. This same physical scenario is predicted to generate a non-trivial fingerprint [24] of the coordinate-space configuration. The geometry will probe the physics *behind* the "third component" of flow generating the v_1 wiggle.

(A-3) Fluctuations

It is important to understand the characteristics of the fluctuations and correlations expected in case the system passes through the region near the critical point, or in case it passes through a first order phase transition. Those correlations and fluctuations must be disentangled from backgrounds such as resonance decays, jet fragmentation, elliptic flow, and other sources of correlations not related to the critical point or to clumping due to spinodal phase separation at the hadronization phase boundary [25].

Understanding the origin of the already observed non-statistical correlations and fluctuations [26] requires highly differential information at a variety of centralities. Of particular experimental interest are the longitudinal and azimuthal width of any anomalous correlations and the system size dependence of the associated fluctuations. With particle identification and a large uniform acceptance in $\Delta\eta$ and $\Delta\varphi$, STAR provides unprecedented capabilities for these studies. This will allow STAR to disentangle the various sources of correlations and identify those related to a first order phase transition or a critical point. Since they are formed later in the system's evolution, these correlations should be narrow in longitudinal extent, while the azimuthal width will depend on the strength of the radial flow and the temperature of the system. Once backgrounds have been accounted for, the centrality dependence of the correlations can reveal information about the order of the phase transition [27]. In particular, a first order phase transition will lead to a centrality dependence, whereas a smooth cross-over will not [28]. Performing these differential

correlations and fluctuations analyses at a variety of centralities will require approximately 5 million events per energy.

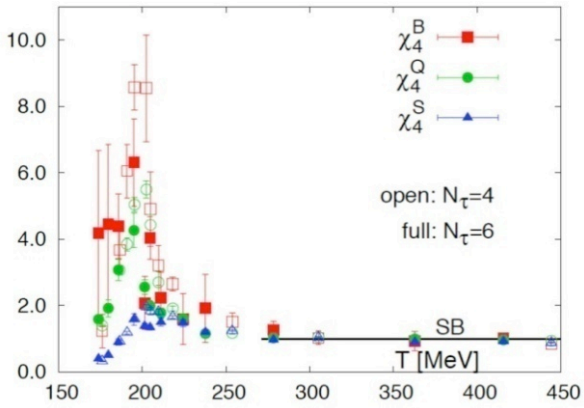

Fig. 3-5: Quadratic fluctuations of baryon number, electric charge and strangeness. All quantities have been normalized to the corresponding free quark gas values [29].

The characteristic signature of the existence of a critical point is an increase, and divergence, of fluctuations [29]. Lattice QCD calculations [30] indicate large jumps in the baryon, charge, and strangeness susceptibilities as a function of the temperature of the system; see Fig. 3-5. These susceptibilities can be related to event-by-event moments of various observables in heavy-ion collisions, in particular to fluctuations of conserved quantities (net charge, net baryon and net strangeness). Theoretical calculations show that the net proton fluctuations, which are experimentally accessible, are a good substitute for net baryon fluctuations [31]. Particle ratios, e.g. K/π and p/π, probe medium dynamics at chemical freeze-out. They are also convenient to study because volume effects are canceled.

The fluctuations of momentum of the charged pions are expected to be sensitive to critical fluctuations [32], because pions couple strongly to the fluctuations of the sigma field (the magnitude of the chiral condensate), which is the order parameter of the phase transition. Since the condensate magnitude is predicted to show increased fluctuations in the vicinity of a critical point, these signatures should be imprinted on the pion [32].

Preliminary studies show [33] that they are all within the reach and capabilities of the STAR detector.

K/π fluctuations: The changes in susceptibilities as a function of the temperature illustrated in Fig. 3-5 might be observable as deviations of fluctuations from a monotonic dependence on incident energy in central collisions. However, changes in the underlying physics can also induce changes in the fluctuations as a function of incident energy. To gain insights into what might be expected from K/π fluctuations as a function of beam energy, the experimental results were compared to predictions from the UrQMD [34] and the HSD [35] models, as illustrated in Fig. 3-6. The UrQMD and HSD models reproduce results at RHIC energies, however at lower energies, UrQMD under-predicts the fluctuations, while HSD reproduces the lowest and the highest energies, but over-predicts in the range $\sqrt{s_{NN}}$ = 8-20 GeV. Detailed discussion and comparisons with the AMPT model [36] will be found in Ref. [1]. The fact that all presently-available models have a serious problem with reproducing observed data, combined with the lack of experimental data in the range of $\sqrt{s_{NN}}$ = 20 - 60 GeV, means that the question of non-monotonic behavior of K/π fluctuations must be answered with additional measurements. Of particular interest is the magnitude of K/π fluctuations at the lower end of the proposed energy scan range, as this may shed light on the monotonic vs. non-monotonic behavior of the NA49 "horn". With the proposed run

scenario, the fluctuations at 7.7 GeV will be analyzed with adequate statistics, while the proposed number of events for 5 GeV K/π fluctuation analysis may only indicate the trend.

STAR is perfectly suited to perform these measurements. Fig. 3-7 shows the estimated statistical error for STAR's σ_{dyn} for the charge-integrated K/π ratio. The measurements were assumed to be based on only 100k central events. Also shown, for comparison, are the current NA49 and STAR measured data points. With the ToF, STAR's relative error is ~ 5%. To make these measurements, one needs to attempt to measure all the kaons and pions. The K reconstruction efficiency at low p_T is rather low, mainly due to kaon decays. STAR's ToF will extend the clean PID range to higher p_T and thus gain essential coverage. As already mentioned, not only coverage, but clean PID is needed. The ToF plays an essential role in eliminating electron contamination at low p_T.

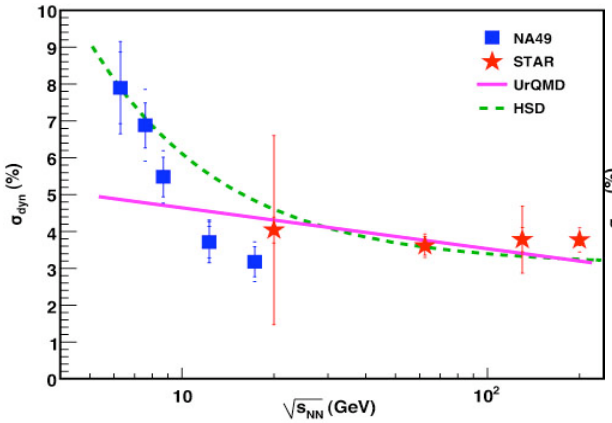

Fig. 3-6: Comparison of the predictions of the HSD and UrQMD models to the experimental data for σ_{dyn} for K/π.

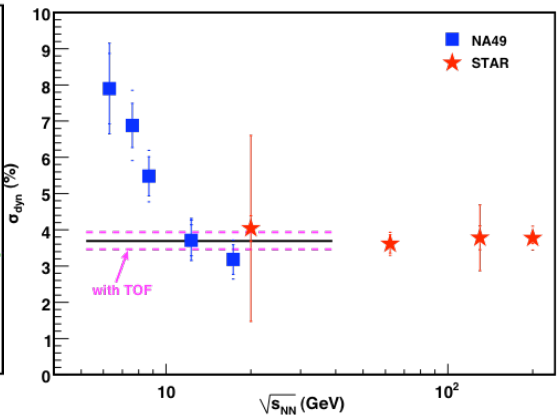

Fig. 3-7: Estimate of the error in σ_{dyn} for charge-integrated K/π fluctuations, based on 100K central events analyzed in the STAR detector (with the newly completed ToF). Shown for comparison are the current measurements from NA49 and STAR.

p/π fluctuations: The study of p/π fluctuations may provide information about baryon fluctuations. The quadratic baryon susceptibilities show a marked peak at temperatures near the critical temperature (see Fig. 3-5). p/π fluctuations have been studied as a function of $\sqrt{s_{NN}}$ by NA49 [37] and by STAR at the same energies as used to study K/π fluctuations. Results were compared to UrQMD and AMPT models. Both models are reasonably close to the experimental data. And again, as in the case of K/π, there is a gap in experimental information at lower energies, which needs to be remedied with new data.

$\langle p_T \rangle$ fluctuations: Average transverse momentum fluctuations are discussed in the literature in the context of a search for the QCD critical point [32], [38]. It is expected that close to the critical point, long-range correlations are very strong, resulting in enhanced momentum fluctuations, especially for small momenta (small p_T values are important because correlation length r diverges at the Critical Point and $\Delta r\, \Delta p < h/2\pi$). The signature in this case would be a maximum in the excitation function of $\langle p_T \rangle$-fluctuations at the energy corresponding to the location of the critical point. In addition to the transverse momentum fluctuations for all charged particles, one can investigate p_T fluctuations of the negative and positive charges independently, as well as the cross-correlations between them [39].

Measurements of $\langle p_T \rangle$ fluctuations are extremely challenging if the experiment does not have 2π acceptance, because there are a number of effects that can compromise the strength of the signal and are not fully correctable without 2π coverage (for instance elliptic flow can cause a non-statistical fluctuation of the $\langle p_T \rangle$ if the experiment does not have 2π acceptance). This is not a concern for the STAR detector, which has full azimuthal symmetry. STAR analyzed successfully those fluctuations in Au+Au collisions at energies from 20 to 200 GeV. The $\langle p_T \rangle$ was measured for all events and also estimated for mixed events. The results were compared, and a difference between the data and mixed events was interpreted as an indication of non-statistical fluctuations; see an example in Fig. 3-8. Current results show significant non-statistical fluctuations at all energies measured by STAR [40]. $\langle p_T \rangle$ fluctuations have been also investigated at the CERN SPS (CERES [41] and NA49 [42] experiments). Together these measurements cover a wide range of beam energies. The compilation of all $\langle p_T \rangle$-fluctuation measurements is shown in Fig. 3-9 (the variable Σp_T represents the dynamical contribution to event-by-event $\langle p_T \rangle$ fluctuations in units of the overall average $\langle p_T \rangle$ [43,44]). The fluctuations are of the order of 1% of $\langle p_T \rangle$ in all cases, and show virtually no beam-energy dependence.

Currently there are no measurements with full azimuthal coverage in collider geometry below $\sqrt{s_{NN}}$ = 20 GeV where, most probably, the CP is located. This fact, together with a relatively large gap in the measurements between 20 and 60 GeV, does not yet allow us to draw conclusions regarding non-statistical fluctuations, their magnitude and nature, and possible relation to the critical point. The BES program, particularly the part of the scan below injection energy, will allow us to clarify the situation. It is important to stress that all measurements will be done with the same apparatus, and therefore, with the same systematics.

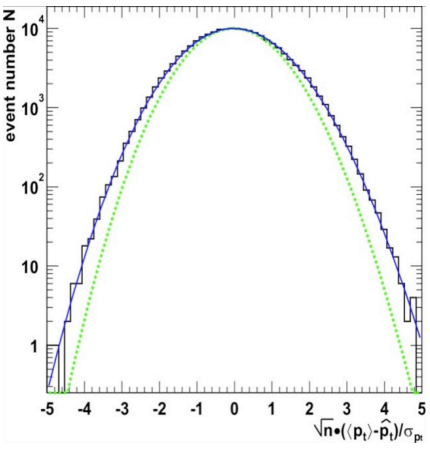

Fig. 3-8: The measured $\langle p_T \rangle$ in Au+Au collisions at 200 GeV (solid histogram), and from event mixing (green curve). The fit to the data is shown as the blue curve.

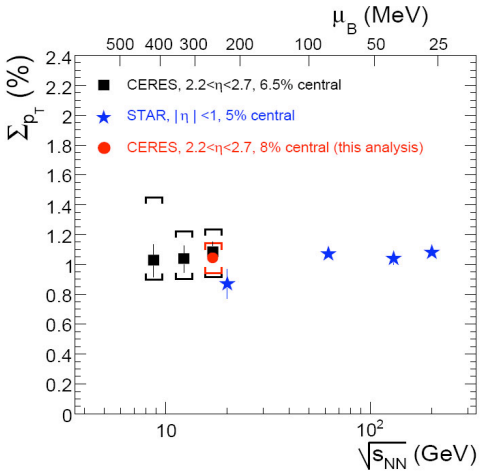

Fig. 3-9: Normalized dynamical fluctuation observable Σp_T in central Pb+Au and Au+Au collisions for different center of mass energies. The figure is from Ref. [41].

Higher Moments, Kurtosis: To date, most experimental fluctuation measures have concentrated on the second moments (proportional to the square of the correlation length). However, estimates of the magnitude of correlation length in heavy-ion collisions indicate it could be small around the critical point (of the order of 2-3 fm) [44], making it challenging to be detected in experiments. It has been proposed that higher moments of event-by-event pion and proton multiplicities are significantly more sensitive to the existence of the critical point compared to measures based on second moments. The fourth moment, the kurtosis, of these multiplicity distributions is expected to be proportional to the seventh power of the correlation length [45]. In addition, it is expected that the evolution of fluctuations from the critical point to the freeze-out point may lead to a non-Gaussian shape in the event-by-event multiplicity distributions. Due to the above reasons, the kurtosis of multiplicity distributions would then provide a more sensitive observable for the search of the QCD critical point. Further in lattice calculations, which assume the system to be in thermal equilibrium, the kurtosis of event-by-event net-baryon number, net-charge and net-strangeness are related to the respective susceptibilities. These susceptibilities show large values or diverge at the critical temperature in presence of a QCD critical point [29, 30, 45, 46]. The measurement of higher moments of event-by-event identified particle multiplicity distributions will provide a direct connection between experimental observables and Lattice Gauge Theory calculations [45]. Note that the product of the fourth and second moments (Fig. 3-10) not only provides a strong signal but also is particularly convenient from the experimental point of view, because all unknown volume terms cancel out.

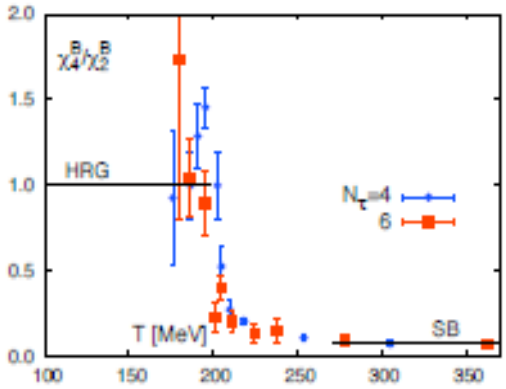

Fig. 3-10: The ratio of the fourth and second order cumulants of baryon number as a function of temperature. The value from the hadron gas model (HRG) is for the temperature range from100 to 200 MeV

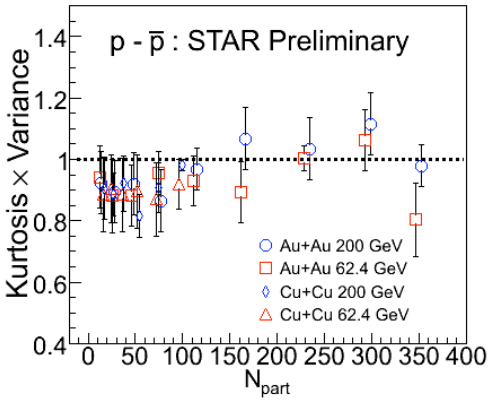

Fig. 3-11: Product of the kurtosis (fourth moment) and variance (second moment) of net-proton distribution at midrapidity ($|y| < 0.5$) for $0.4 < p_T < 0.8$ GeV/c in Au+Au and Cu+Cu collisions at $\sqrt{s_{NN}}$= 62.4 and 200 GeV. The errors are systematic.

Using STAR's large acceptance and excellent PID capabilities at mid-rapidity, protons and anti-protons can be cleanly identified. One can therefore carry out both net-charge and net-proton kurtosis analyses, as motivated by lattice QCD calculations. First measurements are shown in Fig. 3-11. The product of the second and fourth moments is found to be approximately unity, independent of beam energy and colliding ion studied, for the same N_{part}. These measurements are made in a baryon chemical potential (μ_B) range of 14 - 60 MeV [47], where Lattice QCD calculations predict a crossover transition. The QCD critical point is estimated to occur at much large chemical

potentials μ_B >160 MeV [48]. As such, current measurements can be used to constrain the contribution to this observable of physical processes unrelated to the Critical Point.

Statistics of the order of 5M events at each energy point across the energy range from 7.7 GeV and up will allow a net proton kurtosis analysis with an uncertainty of 0.1 [49].

3.4. B: Turn-off of QGP Signatures and Other New Phenomena

(B-1) Constituent-quark-number scaling

When elliptic flow v_2 is plotted versus transverse kinetic energy ($m_T - m_0$), v_2 for all identified particles below $m_T - m_0 = 0.9$ GeV/c^2 falls on a universal curve. Above that, meson and baryon v_2 deviates, with baryon v_2 rising above meson v_2 and saturating at a value approximately 50% larger than for mesons; however, upon dividing each axis by the number of constituent quarks ($n_q = 2$ for mesons and 3 for baryons), the meson and baryon curves merge very impressively into a single curve over a wide range of $m_T - m_0$, as seen in Fig. 3-12. This well-known scaling behavior is one of the most striking pieces of evidence for the existence of partonic degrees of freedom during the Au + Au collision process at 200 GeV. It is very hard to explain this pattern in a scenario where only hadronic matter exists throughout the interaction, whereas the hypothesis of coalescence of hadrons from deconfined quarks offers a ready explanation.

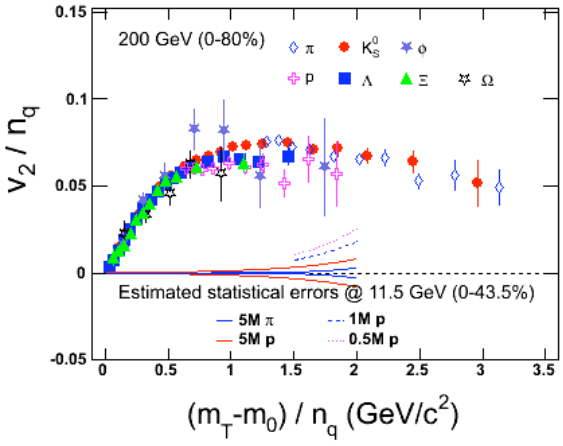

Fig. 3-12: Elliptic flow per constituent quark versus transverse mass per constituent quark for Au + Au collisions at 200 GeV at RHIC. See text for explanation of solid and dashed curves near $v_2 = 0$.

An observation of this n_q scaling behavior turning off below some threshold beam energy would be a very powerful confirmation of our current understanding of the deconfined phase. The $(m_T - m_0)/n_q$ reach of the NA49 data at the top SPS energy is only 0.9 GeV/c^2 [50]. Data in this range does not test quark number scaling and is therefore not sufficient to answer the question of whether a similar v_2/n_q-scaling extends to lower beam energies. Extending the n_q scaling studies to BES energies, with a reach to 2.0 GeV/c^2 should provide a definitive answer to this question.

The solid and dashed curves in Fig. 3-12 near $v_2 = 0$ show the simulated magnitude of v_2/n_q error bars in the scenario of running Au + Au at $\sqrt{s_{NN}} = 11.5$ GeV with the full ToF barrel in operation. With 5 million events, error bars are very small on protons, and even smaller on pions. Table 3-2 includes additional information about the energy dependence of STAR's simulated performance for this hallmark observable, including our capabilities for heavier mesons and baryons. Elliptic flow measurements for φ and Ω, particles that have relatively low hadronic interaction cross sections and are more promising probes of the early stages of the collision, open the door to testing partonic collectivity with improved confidence [51]. For testing π, K, p and Λ up to $(m_T - m_0)/n_q \sim 2$ GeV/c^2 with strong statistical significance,

we need on the order of 5 million events at each BES energy point, whereas for φ and Ω, the statistical requirement become prohibitive below injection energy. In summary, we are confident that STAR has some capability to search for the crucial turn-off of n_q scaling at all BES energies where on the order of a million events are collected, as illustrated by Fig. 3-12.

(B-2) High & Intermediate p_T Spectra: QGP Opacity and the Baryon Anomaly

Hadron suppression through jet quenching has been a key observable for estimating the density of the matter created in heavy-ion collisions. In 200 GeV Au+Au collisions, high p_T hadron yields are suppressed by a factor of five relative to N_{binary}-scaled p+p collisions. In 22.4 GeV Cu+Cu collisions, however, neutral pion yields at p_T = 4 GeV/c are enhanced by a factor of 2, as shown in Fig. 3-13. Such a behavior is characteristic of lighter systems (the number of participants is about a factor 3 lower in Cu+Cu than in Au+Au). This conclusion is not yet firm, however, because the p_T-reach of the 22.4 GeV Cu+Cu measurements extends only to 4 GeV/c. In this momentum range, the baryon to meson ratio is enhanced. In 62.4 GeV Au+Au collisions, the suppression is similar to that at 200 GeV, indicating that the strong jet quenching seen at top RHIC energies may set in somewhere below 62.4 GeV. A similar degree of suppression is observed also in Pb+Pb collisions at 17.3 GeV. The two CERN experiments NA49 [52] and WA98 [53] report $R_{AA} < 1$ up to p_T of 3.5 GeV/c, which indicates that suppression may set in at even lower energies, below 17.3 GeV. The particle type dependence of the nuclear modification factor R_{CP} shows a dependence on constituent quark number rather than mass, indicating that baryon yields increase faster with the matter density than meson yields. This dependence, coupled with the quark number scaling observed in v_2, suggests that fragmentation does not dominate hadron production here, but rather some multi-quark or gluon process and/or flow.

Measurements of the baryon to meson ratios and identified particle R_{CP} for p_T up to and above 4.5 GeV/c in the $\sqrt{s_{NN}}$ range between 17.3 and 62.4 GeV will allow STAR to disentangle effects that appear to dominate the intermediate p_T region. This is required to infer whether there is an onset of QGP opacity between 17.3 GeV and 62.4 GeV. At beam energies above 28 GeV, the R_{CP} and baryon-to-meson ratio studies can be bolstered with studies of the jet cone through triggered di-hadron correlations.

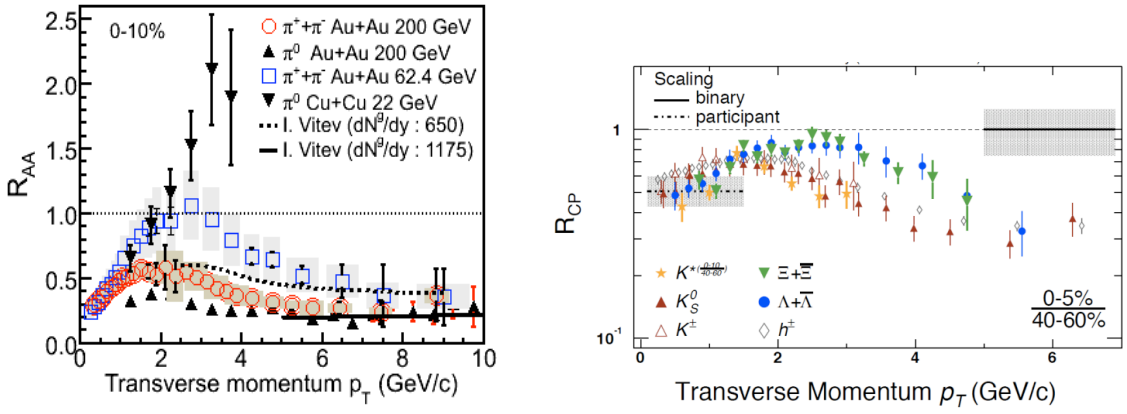

Fig. 3-13: The left panel shows STAR measurements of charged pion R_{AA} in Au+Au collisions at 62.4 and 200 GeV, and PHENIX measurements of neutral pion R_{AA} in Au+Au at 200 GeV, and in Cu+Cu at 22.4 GeV. The 22.4 GeV data are based on 6 million collisions. The right panel shows STAR measurements of identified particle R_{CP} in 200 GeV Au+Au collisions. Baryons are less suppressed than mesons. At intermediate p_T, all baryons lie in one group above the mesons.

The number of events required for high-p_T di-hadron studies was estimated based on PYTHIA. The estimates depend strongly on the p_T of the trigger and associated particle. For the high p_T spectra studies at 17.3 GeV, we base our estimates on existing measurements from NA49 and PHENIX. PHENIX measured neutral pion R_{AA} up to p_T = 4 GeV/c with 6 million 22.4 GeV Cu+Cu collisions. NA49 measured identified particle spectra up to p_T = 4.5 GeV/c with 800 thousand central 17.3 GeV Pb+Pb collisions. The acceptance of the STAR detector is roughly a factor of 1.8 larger than NA49 (-0.3<y<0.7 vs. 0.9<y<0.9) and a factor of 5 larger than PHENIX. We are confident therefore that 15 million minimum bias Au+Au collisions at 17.3 GeV will allow STAR to measure R_{CP} up to p_T = 4.5 GeV/c, where it is believed that fragmentation begins to dominate particle yields. Samples of 33 and 24 million events at 28 and 39 GeV will provide enough statistics to reach p_T values of 5 and 5.5 GeV/c, respectively, and will also provide the statistics needed to resolve the jet cone using triggered di-hadron correlations. These data sets will therefore allow STAR to perform definitive tests for an onset of QGP opacity and to test models for multi-quark and gluon hadron production, such as the recombination and coalescence models. The energy dependence of the baryon to meson ratio will be a particularly stringent test of models that rely on the interplay between a falling p_T spectrum and recombination or flow to describe the baryon enhancement.

(B-3) Pair Correlations in the Space of Pair Separation in Azimuth and Pseudorapidity

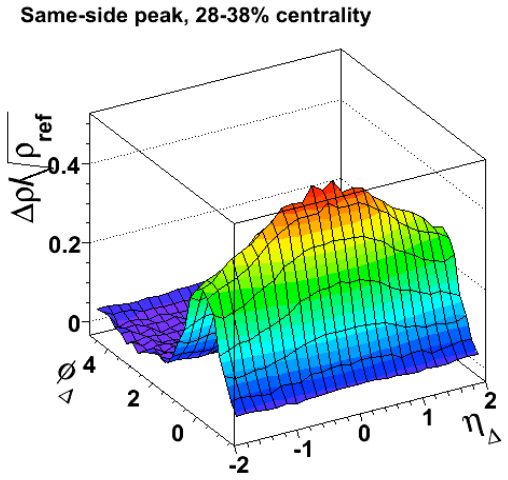

Fig. 3-14: Pair correlations for 200 GeV Au+Au as a function of pair separation in azimuth and pseudorapidity, after subtracting elliptic flow and an unrelated enhancement in the region where both differences are very small.

STAR's broad and uniform acceptance in both azimuth and pseudorapidity make it the ideal detector to reveal the full structure of many classes of correlation. The quantity $\Delta\rho/\sqrt{\rho_{ref}}$ plotted in Fig. 3-14 is constructed from the number of particle pairs separated by ϕ_Δ in azimuth and η_Δ in pseudorapidity. ρ_{ref} is a mixed-event reference, and $\Delta\rho$ is the number of real pairs minus ρ_{ref}[54]. This type of observable is sensitive to the familiar cos 2ϕ modulation arising from elliptic flow, but this flow has already been subtracted in Fig. 3-14. A spike at (0, 0) due to photon conversions and HBT has also been subtracted; what remains is a correlation strongly elongated in η_Δ at small ϕ_Δ known as the "ridge". This structure is fit quite well with a 2D Gaussian, and Fig. 3-15 provides further details about the parameters of this Gaussian as a function of the centrality measure ν. The most striking feature of the ridge is its steep increase in both amplitude and pseudorapidity width as collision centrality increases. Over the same centrality range, the width along the ϕ axis decreases slightly, and the behavior is qualitatively similar in Cu+Cu collisions at 62 and 200 GeV.

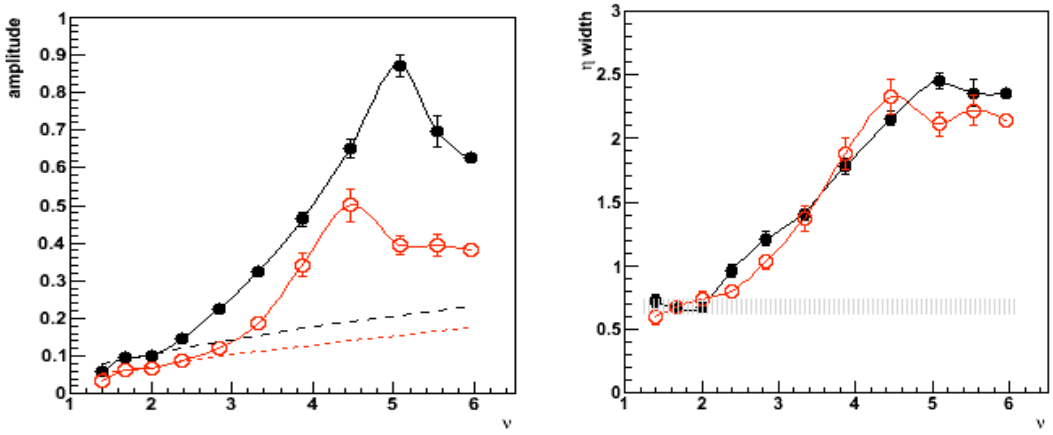

Fig. 3-15: Amplitude (left panel) and pseudorapidity width (right panel) of 2-D Gaussian fits to the ridge for Au+Au at 200 GeV (black / solid circles) and 62 GeV (red / open circles), as a function of the centrality parameter ν. Larger ν corresponds to smaller impact parameter. The broken lines on the left and the shaded band on the right correspond to Glauber Linear Superposition scaling.

The large extent of the ridge in pseudorapidity can be understood only if the underlying correlation is imparted early in the collision process. Calculations featuring Glasma flux tubes coupled with a flowing sQGP [55] make rather specific predictions related to the onset of the ridge, with a testable dependence on both beam energy and centrality. Ref. [55] implies that the beam energy region of greatest interest should lie between $\sqrt{s_{NN}} = 13$ GeV and 35 GeV. Studying the energy dependence of the ridge will allow us to test the conjectured relationship between the ridge, Glasma flux tubes, and the formation of strongly interacting quark gluon plasma. The ridge has featured prominently in overviews of the most important RHIC developments and we regard it as a promising analysis topic for an energy scan.

As before, Table 3-2 provides quantitative details about statistics requirements for the signals discussed in this section. We expect to have ample statistics to pursue all of the above ridge-related studies down to $\sqrt{s_{NN}} \sim 17.3$ GeV.

(B-4) Local Parity Violation in Strong Interactions

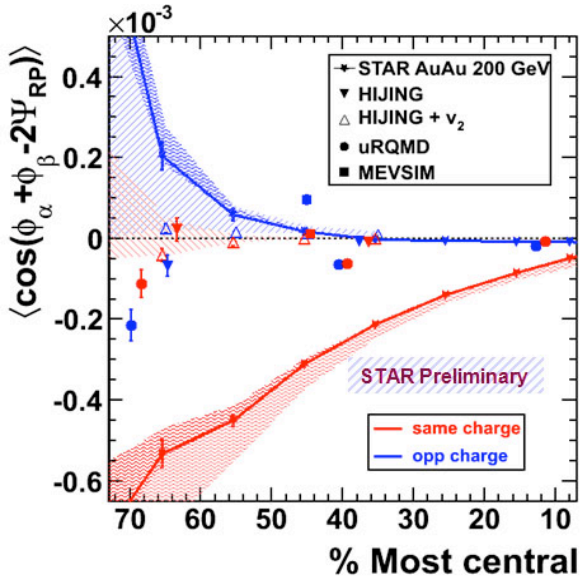

Fig. 3-16: Centrality dependence of the parity violation signal for Au+Au at 200 GeV. The shaded regions indicate systematic uncertainties, and such uncertainties will be smaller when the analysis is repeated at lower energies.

There are still many open questions related to the non-trivial structure of the QCD vacuum. The generation of mass from spontaneous chiral symmetry breaking, and topological solutions (instantons, sphalerons) are relevant to this discussion. Event-by-event local strong parity violation would be highly important new evidence that would lend support to current theoretical understanding, and would have an immediate impact, not just on relativistic heavy ion physics, but on all spheres of physics touched by QCD (high energy physics, cosmology, etc.)

The observation of a local parity-violating signal assumes the following chain of circumstances. In non-central heavy-ion collisions, a large orbital angular momentum vector ($\boldsymbol{L}$) exists at 90° to the reaction plane, leading to a very intense localized magnetic field (due to the net charge of the system). If the system is deconfined, there can be strong parity-violating domains, and different numbers of left- and right-hand quarks, leading to preferential emission of like-sign charged particles along $\boldsymbol{L}$. In the azimuthally anisotropic emission of particles,

$$\frac{dN_{\pm}}{d\phi} \propto 1 + 2a_{\pm}\sin(\phi - \Psi_{RP}) + \ldots$$

the coefficient a represents the size of the parity-violating signal, and the remaining terms (not shown explicitly) are the familiar ones with coefficients v_n for directed and elliptic flow, etc. However, the coefficient a averages to zero when integrated over many parity-violating domains in many events. If parity violation takes place, a non-zero average signal can be obtained by forming a correlation between pairs of emitted particles (azimuths ϕ_α and ϕ_β) relative to the reaction plane (azimuth Ψ_{RP}), as plotted on the vertical axis of Fig. 3-16. The observed results [56] are consistent with the expected signal for parity violation, especially the centrality dependence, as seen in Fig. 3-16. There are caveats attached to this observation – the expected parity violation is parity-odd, whereas the only accessible observable to measure it is parity-even, which means that effects not related to parity violation (e.g., jets and resonances) can contribute to the measured signal [56]. So far, there is no known background, or effect predicted by existing event-generating models, that could account for the observed signals. The shaded regions in Fig. 3-16 illustrate the limited extent to which background effects could contribute.

There are two separate ways in which the Beam Energy Scan is highly relevant in discussion of local strong parity violation. First, the violation is generally accepted as

needing deconfinement to happen. So apart from its very high intrinsic importance, with implications well beyond heavy ion physics, parity violation is a deconfinement signal that we expect to turn-off at some point if we go down low enough in energy. Second is the aspect of how the parity-violating signal and background effects might behave as we scan down in beam energy. Simulations of backgrounds suggest that if the signal survives after the analysis has been repeated over a range of beam energies, the argument that background effects cannot explain it will be even more compelling.

As documented in Table 3-2, this study of local strong parity violation needs about 5 million events at each BES energy, and thus our run plan will allow this study to be pursued at all energies down to 7.7 GeV. These measurements illustrate a unique capability offered by STAR's large acceptance: multi-dimensional imaging of correlations and fluctuations give better insight into the source and nature of observed signals.

3.5. Flexibility of STAR and Readiness for Unanticipated Observations

The energy range of the BES program at RHIC covers the span of most available Lattice QCD estimates of the location of the critical point. It will span from the cross-over regime, past the location of the critical point in several estimates, and into the region dominated by the first-order transition (T, μ_B) ~ (170-100 MeV, 20-500 MeV). The experiments must be capable of making comprehensive measurements of all the signals related to critical phenomena and the evolution with beam energy of unusual medium properties attributed to the new state of matter already studied at the upper RHIC energies (how they vary and, eventually, disappear). And, of course, all experimenters must be open to new surprises in unexplored regions, and should have the most flexible tools for investigating any unforeseen discoveries.

While the energy scan program at the CERN SPS (with beams from 20 to 158 GeV/c in fixed target mode, equivalent to $\sqrt{s_{NN}}$ = 6.3 – 17.3 GeV) reported interesting phenomena with possible relevance to a phase transition, the evidence remains inconclusive [57]. With the BES program at RHIC, we expect to greatly expand the scope and range of relevant measurements, and thus bring much improved clarity to the situation. Using a collider for energy scan studies brings two tremendous advantages over a fixed-target facility:

(1) The phase space covered by the detectors in collider experiments changes very little with beam energy. In fixed target experiments, the detector acceptance changes significantly with energy and in order to understand how the underlying physics evolves with beam energy, extrapolation to a common phase space is necessary. This process is based on assumptions and therefore introduces additional systematic uncertainties.

(2) Track density at mid-rapidity varies very slowly with energy for collider geometry, while it increases dramatically with energy in fixed-target experiments. This results in increased technical difficulties in tracking (e.g. changes in hit sharing and track merging, changes in *dE/dx* and momentum resolution). When going down to lower beam energy from 200 GeV, due to the low multiplicity and luminosity, the STAR TPC will perform slightly better in terms of efficiency and other performance parameters.

The STAR detector, due to its large and uniform acceptance and excellent particle identification capabilities (enhanced by the completed Time of Flight barrel in 2010), is uniquely positioned to carry out this program in unprecedented depth and detail.

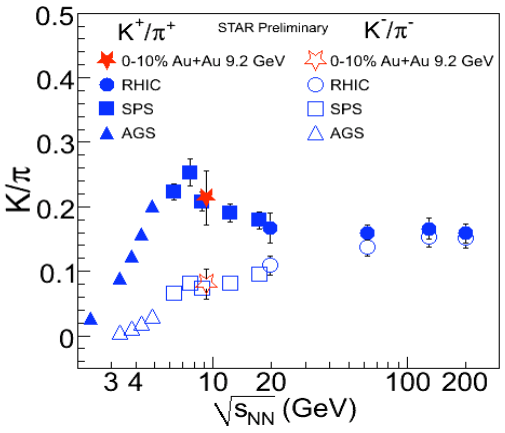

Fig. 3-17: The K/π ratio as a function of beam energy. The STAR 9.2 GeV test data are shown in comparison to world data. The error bars for the 9.2 GeV result is dominated by statistical errors.

The STAR experiment already has a proven performance record and significant experience with low energy running. Low energy runs were taken with 19.6 GeV Au+Au collisions in 2001 and 22.4 GeV Cu+Cu in 2004. During a brief machine development test in 2008, the STAR detector successfully took data (about three thousand good events) at $\sqrt{s_{NN}}$= 9.2 GeV. All systems performed well, and as an example of physics results from this short test run, Fig. 3-17 shows a comparison of 9.2 GeV data (marked with the red stars) with data from other experiments at different energies. The K/π ratio vs. $\sqrt{s_{NN}}$ is in very good agreement with the rest of the world data. All other STAR measurements at 9.2 GeV [58] are also consistent with those reported by earlier experiments. We are confident that STAR's capability over the proposed energy scan region is fully understood, and we are ready for the proposed run.

3.6. STAR Run Plan for First Energy Scan

The BES program is planned in at least two stages. For the first BES run (RHIC Run-10) we propose to run a wide range of energies, from $\sqrt{s_{NN}}$ 7.7 to 39 GeV (see Tables 3-1 and 3-2) with an additional 100 k events at 5 GeV for measurement of K/π fluctuations (nominally utilizing a machine development test at that energy). We have selected lower $\sqrt{s_{NN}}$ values that give the greatest discovery potential for the critical point, as well as higher energies to cover the current gap between RHIC and the SPS. It is important to run at a $\sqrt{s_{NN}}$ value as low as practically achievable since this provides the highest potential for identifying signatures of a first order phase transition, thus bracketing the location of the critical point. We have chosen energy steps spaced uniformly between top SPS energies and RHIC's 62.4 GeV.

It is highly preferable for the first run to take place in 2010 prior to the beam pipe change in STAR and PHENIX, and prior to removal of FTPCs in STAR. The new 4-cm diameter beam pipe may seriously complicate successful running at sub-injection energies due to increased transverse size of the beams below injection energy [59]. The STAR FTPCs play an important role in providing information about the 1st-order event plane as well as extending pseudorapidity coverage out to 4 units on each side.

Data from the 9.2 GeV Au+Au test run allowed us to estimate the actual rate of triggered events within a useable range of vertex positions. The test run was very short with emphasis on demonstrating capability rather than tuning for the highest possible event rate. BNL Collider Accelerator Division (C-AD) staff have indicated a high degree of confidence that these rates can be increased by a factor of about 6 via improvements in injection

efficiency and by increasing the number of bunches in the machine. Additional tuning is likely to provide further incremental rate improvements. Another option being explored is continuous injection to fill the bunches and extend the beam lifetime. This is expected to increase the integrated rate by a factor of about 2.

To be very conservative, none of these further possible enhancements are included in the event rate estimates presented in Table 3-1 and 3-2. Based on consultation with C-AD, it is estimated that the rates will scale according to γ^3 up to injection energy and by roughly γ^2 above that. These estimates were crosschecked against actual data rates taken by STAR during the early injection-energy run and also against measurements of the injection energy luminosity under current operating conditions. Results are found to be consistent. From these estimated event rates, and assuming that we take data for an average of 8 hours per day of beam, we determine the number of days necessary to acquire one million events at each of the proposed energies, as shown in Table 3-1. Note that all estimates in Tables 3-1 and 3-2 already allow for detector acceptance and vertex position cuts.

The observables listed in the white part of Table 3-2 are not considered at the present moment to be highest priority analyses that determine the structure of our overall run plan for RHIC Run-10, but nonetheless are priorities for individual groups within the STAR collaboration and will definitely be carried out. If the past history of heavy-ion physics is any guide, the most striking and unexpected discoveries of the BES program may well emerge from the analyses listed in this white area of Table 3-2, and we consider STAR's greatest strength to be its ability, through flexibility and broad acceptance, to make serendipitous discoveries.

The lower beam energies are specifically chosen to map out a region around the "horn" in the K/π ratio observed by SPS experiments. All the selected energies allow collisions at both STAR and PHENIX. After analysis of the first BES run, we propose that a second scan be performed, probably focused more specifically on a few collision energies. These energies and physics topics will be chosen to explore in more depth the most interesting regions found via the first scan.

We argue that the most important energy region for the physics of the BES program is the lower end of the proposed energy span where the potential to identify signatures of a first order phase transition is largest, and therefore we propose to start the energy scan at 7.7 GeV. After about two weeks of data taking, we will be able to test and refine the accuracy of the estimates provided in Tables 3-1 and 3-2 of this document, and adjust the allocation of time, if needed. At the time of writing, to the best of our knowledge, we will require 5 M events at 7.7 GeV. We expect that the second run, with more data at fewer energies, will take advantage of further luminosity upgrades proposed by BNL C-AD.

Beam Energy	Event Rate	8-hr Days/ 1M Events	Events proposed	8-hr days proposed
5	0.8	45	100 k	5
7.7	3	11	5 M	56
11.5	10	3.7	5M	19
17.3	33	1.1	15M	16
27	92	0.4	33M	12
39	190	0.2	24M	5

Table 3-1: The proposed run duration at each energy is determined by the number of Minimum Bias events needed to perform the detailed measurements discussed in the previous sections; see Table 3-2.

	Collision Energies (GeV)	**5**	**7.7**	**11.5**	**17.3**	**27**	**39**
Section	Observables	Millions of Events Needed					
A1	v_2 (up to ~1.5 GeV/c)	**0.3**	**0.2**	**0.1**	**0.1**	**0.1**	**0.1**
A1	v_1	0.5	**0.5**	**0.5**	**0.5**	**0.5**	**0.5**
A2	Azimuthally sensitive HBT	4	**4**	**3.5**	**3.5**	**3**	**3**
A3	PID fluctuations (K/π)	1	**1**	**1**	**1**	**1**	**1**
A3	net-proton kurtosis	5	**5**	**5**	**5**	**5**	**5**
A3	differential corr & fluct vs. centrality	4	**5**	**5**	**5**	**5**	**5**
A3	integrated p_T fluct (T fluct)						
B1	n_q scaling π/K/p/Λ $(m_T-m_0)/n$<2GeV		**6**	**5**	**5**	**4.5**	**4.5**
B1	ϕ/Ω up to p_T/n_q=2 GeV/c		56	25	**18**	**13**	**12**
B2	R_{CP} up to p_T ~4.5 GeV/c (at 17.3) 5.5 (at 27) & 6 GeV/c (at 39)				**15**	**33**	**24**
B3	untriggered ridge correlations		27	13	**8**	**6**	**6**
B4	parity violation		**5**	**5**	**5**	**5**	**5**
See[1]:	charge-photon fluctuations (DCC)	1	**1**	**1**	**1**	**1**	**1**
	kink/step/horn	**0.1**	**0.1**	**0.1**	**0.1**	**0.1**	**0.1**
	v_2 fluctuations	0.5	**0.5**	**0.5**	**0.5**	**0.5**	**0.5**
	HBT (R_l, R_o/R_s)	0.8	**0.8**	**0.5**	**0.5**	**0.5**	**0.5**
	Jet/ridge 2<trig<4, 1<assoc<trig				30	**8.8**	**4.5**
	Jet/ridge 3<trig<6, 1.5<assoc<trig					53	**24**
	Baryon-Strangeness cor (hypernuc)						50
	Forward π^- yield (rapidity scaling)						
	Forw. $\gamma(\pi^0)$ yield (rapidity scaling)						
	Long-range forward-backward corr.						
	Other PID fluctuations (esp. K/p)						
	Particle ratios (many examples)						
	p_T spectra						
	Prod. of light nuclei & antinuclei						
	Yields of species & stat model fits						

Table 3-2: Observables and statistics needed for the first BES run. The observables in the yellow-shaded area relate to the search for a phase transition or critical point (see section A), while observables in the blue-shaded area search for turn-off of new phenomena already established at higher RHIC energies (see section B). The numbers listed in boldface above are all within reach (nominally require no more than 1.5 times the proposed statistics) in the first BES run plan as set out in Table 3-1. The remaining numbers (not boldface) will need to wait for higher

statistics in a subsequent run. The white part above is briefly introduced in this document., and is explained in detail in Ref. [1].

References

[1] *Experimental Exploration of the QCD Phase Diagram: Search for the Critical Point* - in preparation.
[2] J. Adams *et al.*, Nucl. Phys. A 757, 102 (2005); also whitepapers from the other three RHIC experiments.
[3] For a recent review of the topic of multifragmentation and the liquid-vapor phase transition, providing many insights into the general topic of phase transitions in small systems, see B. Borderie and M.F. Rivet, e-print arXiv:0812.3524 (and references therein).
[4] F.R. Brown *et al.*, Phys. Rev. Lett. 65, 2491 (1990).
[5] M. Asakawa and K. Yazaki, Nucl. Phys. A504, 668 (1989); A. Barducci *et al.*, Phys. Lett. B231, 463 (1989), Phys. Rev. D41, 1610 (1990), Phys. Rev. D49, 426 (1994); J. Berges and K. Rajagopal, Nucl. Phys. B538, 215 (1999), M.A. Halasz *et al.*, Phys. Rev. D58, 096007 (1998); Y. Hatta and T. Ikeda, Phys. Rev. D 67, 014028 (2003).
[6] M.A. Stephanov, Prog. Theor. Phys. Suppl. 153, 139 (2004) [Int. J. Mod. Phys. A 20, 4387 (2005)].
[7] M. Asakawa *et al*., Phys. Rev. Lett. 101, 122302 (2008).
[8] H. Sorge, Phys. Rev. Lett. 78, 2309 (1997), nucl-th/9610026.
[9] P.F. Kolb, J. Sollfrank, and U.W. Heinz, Phys. Rev. C 62, 054909 (2000).
[10] S.A. Voloshin, A.M. Poskanzer, and R. Snellings, arXiv: nucl-ex/0809.2949.
[11] T. Hirano *et al.*, J. Phys. G 34, S879 (2007).
[12] U. Heinz, QM 2009.
[13] P. Huovinen, Nucl. Phys. A761, 296 (2005).
[14] P. Huovinen, P. Kolb, U. Heinz, P.V. Ruuskanen, S.A. Voloshin, Phys. Lett. B 503, 58 (2001).
[15] For an overview, see H. Stoecker, arXiv:0710.5089, published in PoS CPOD07:025, 2007.
[16] C. Alt *et al.* (NA49 collaboration), Phys. Rev. C 68, 034903 (2003), nucl-ex/0303001.
[17] R. Snellings *et al.,* Phys. Rev. Lett. 84, 2803-2805 (2000); J. Brachmann *et al.*, Phys. Rev. C 61, 024909 (2000), nucl-th/9908010; L. P. Csernai and D. Rohrich, Phys. Lett. B 458, 454 (1999), nucl-th/9908034; H. Stoecker, Nucl. Phys. A 750, 121 (2005).
[18] F. Retiere and M.A. Lisa, Phys. Rev. C 70, 044907 (2004) .
[19] M.A. Lisa, U. Heinz, U. Wiedemann, Phys. Lett. B489, 287 (2000).
[20] U. Heinz and P. Kolb, Phys. Lett. B542, 216 (2002).
[21] J. Adams *et al.* (STAR), Phys. Rev. Lett. 93, 12301 (2004).
[22] U. Heinz and P. Kolb, Phys. Lett. B 459, 667 (1999).
[23] M. Gyulassy, K.A. Frankel and H. Stoecker, Phys. Lett. B 110, 185 (1982); W. Reisdorf and H.G. Ritter, Ann. Rev. Nucl. Part. Sci. 47, 663 (1997).
[24] M.A. Lisa and S. Pratt, arXiv: 0811.1352.
[25] J. Randrup, arXiv:nucl-th.0406031.
[26] B.I. Abelev et al. (STAR Collaboration), arXiv:0901.1795 [nucl-ex]
[27] L.F. Pahares, E.S. Fraga, and T. Kodama, arXiv:0904.4830 [nucl-th]
[28] Y. Aoki, G. Androni, Z. Fodor, S.D. Katz and K.K. Szabo, Nature 443, 675 (2006).
[29] V. Koch, e-print arXiv: 0810.2520.
[30] M. Cheng *et al.*, Phys. Rev. D 79,074505 (2009).
[31] Y. Hatta, M. Stepanov, Phys. Rev. Lett. 91, 102003 (2003).

[32] M. Stepanov, K. Rojagopal, E.V. Shuryak, Phys. Rev. D60 114028 (1999), hep-ph/9903292.
[33] J. Adams *et al*., (STAR collaboration) Phys. Rev. C 72, 044902 (2005).
[34] M. Bleicher *et al*., J. Phys. G 25, 1859 (1999).
[35] M.I. Gorenstein *et al.*, e-print arXiv: 0811.3089.
[36] Z.-W. Lin *et al*., Phys. Rev. C 72, 064901 (2005).
[37] C. Alt *et al*., (NA49 collaboration) e-print arXiv: 0808.1237.
[38] M. Stepanov, K. Rojagopol, E.V. Shuryak, Phys. Rev. Lett. 81 4816 (1998), hep-ph/9806219.
[39] S. Jeon, V. Koch, "Event-by-event fluctuations" in *Quark Gluon Plasma 3*, R. Hwa, X. Wang eds., p. 430, World Scientific, Singapore, 2004.
[40] J. Adams *et al*., (STAR Collaboration), PRC 71, 044902 (2005).
[41] D. Adamova *et al*., (CERES Collaboration), Nucl. Phys. A 811, 179 (2008).
[42] H. Appelshauser *et al*., (NA49 Collaboration), Phys. Lett. B 459, 679 (1999); M. Rybczynski *et al*., (NA49 Collaboration), nucl-ex/0805.2245
[43] D. Adamova *et al*., (CERES Collaboration), Nucl. Phys. A 727, 97 (2003).
[44] J. Adams *et al*., (STAR Collaboration), Phys. Rev. C 72, 044902 (2005).
[45] M.A. Stepanov, e-print arXiv: 0809.3450.
[46] R.V. Gavai and S. Gupta, Phys. Rev. D 71, 114014 (2005).
[47] B.I. Abelev et al., STAR Collaboration, Phys. Rev. C 79 (2009) 34909.
[48] Z. Fodor and S.D. Katz, JHEP 0404 (2004) 50.
[49] T. Schuster et al., e-print arXiv: 0903.2911.
[50] C. Blume et al. (NA49 Collaboration), J. Phys. G. Nucl. Part. Phys. 35, 044004 (2008).
[51] B.I. Abelev *et al*., (STAR Collaboration), Phys. Rev. Lett. 99, 112301 (2007); J. Adams *et al*., (STAR Collaboration), Phys. Rev. Lett. 95, 122301 (2005).
[52] C. Alt *et al*., (NA49 Collaboration), Phys. Rev. C 77, 034906 (2008).
[53] M.M. Aggarwal *et al*., (WA 98 Collaboration), Phys. Rev. Lett. 100, 242301 (2008).
[54] M. Daugherity *et al.* (STAR collaboration), J. Phys. G **35**, 104090 (2008).
[55] A. Dumitru, F. Gelis, L. McLerran, and R. Venugopalan, Nucl. Phys. A 810, 91 (2008); P. Sorensen, arXiv: 0811.2959
[56] S.A. Voloshin *et al*., (STAR collaboration), e-print arXiv: 0806.0029 and B.I. Abelev *et al*., (STAR collaboration), in preparation.
[57] S.V. Afanasiev *et al*., (NA49 Collaboration), Phys. Rev. C 66, 054902 (2002); C. Alt *et al*., (NA49 Collaboration), Phys. Rev. C 68, 034903 (2003); C. Roland *et al*., (NA49 Collaboration), J. Phys. G 30, S1381 (2004).
[58] L. Kumar *et al.* (STAR collaboration), SQM 2008, QM 2009.
[59] C-AD communication.

4. Returning to Au+Au at 200 GeV in Run 10

4.1. Introduction and rationale

The last physics run with Au+Au collisions at 200 GeV was in Run 7, in which STAR accumulated 70M minimum bias events and sampled ~0.5 nb^{-1} with rare triggers. Much has improved in the detector in the intervening three years, which leads to this request to return to full energy Au+Au collisions. As of Run 9, the DAQ1000 data acquisition upgrade and 75% of the Time of Flight barrel are in place and fully functioning. By Run 10 the remaining 25% of the ToF will be installed. In addition, the Silicon Vertex Tracker and Silicon Strip Detector were removed prior to Run 8, which greatly reduced the material between the vertex and the Time Projection Chamber, and so greatly reduced background in all electron channels from conversions. This reduced background is especially important in heavy flavor measurements, both with non-photonic electrons and quarkonia.

The DAQ1000 upgrade, coupled with improvements in the luminosity deliverable by the machine, leads to a major jump in the statistics STAR can accumulate. Datasets in STAR can be divided into two types: "triggered" and "non-triggered". Triggered datasets rely on the ability of the Barrel Electromagnetic Calorimeter to trigger, at RHIC clock frequency, on rare processes such as high p_T electrons and photons. Non-triggered datasets do not use the calorimeter to trigger, and so are limited by the maximum rate at which the STAR detector can be read out. In Run 7, competition between these datasets led to ~30% livetime for triggered processes when STAR was running, at a readout rate of ~70 Hz at maximum for non-triggered datasets. Experience in Run 9 shows that the full STAR system can read at >500 Hz with maximal livetime, from 80-95% depending on the complement of detectors read in for each trigger condition. With this major improvement, we expect to be able to have large increases in sample sizes: factor of 4-5 increase in the minimum bias dataset relative to Run 7, factor of 10 increase in central datasets relative to Run 4 (the largest central dataset to date), and a factor of 4 increase in sampled luminosity in the triggered datasets.

In addition to sample size, the ToF brings major qualitative improvements in measurements such as identified particle correlations that simply could not be done in Run 7.

4.2. Triggered Datasets and Heavy Flavor

With the luminosities available at RHIC, collision rates are too large for all events to be written to tape with the STAR DAQ. Therefore, triggers are needed to sample the events for rare probes, the most discriminating of which use the Barrel Electromagnetic Calorimeter in a number of ways. A simplified history of sampled luminosity is shown in Table 4-1, which compares by run and species the integrated luminosity sampled by the Barrel EMC High Tower trigger with the highest threshold, requiring all detectors to be read out. A comparison between species can be made based on the binary scaling hypothesis, in which the pp-equivalent luminosity in collisions between species A and B

scales as A*B. This approximation is only roughly correct: for probes that are suppressed, such as hadrons at high p_T, the combination of suppression and centrality cuts can reduce the rates of triggered probes relative to this expectation by up to an order of magnitude. The integrated luminosity has been steadily progressing, so that we now have on the order of 10 pb^{-1} pp-equivalent integrated luminosity sampled in p+p, d+Au, and Au+Au collisions at 200 GeV.

Table 4-1: Integrated luminosity in highest threshold Barrel EMC high tower trigger with full detector readout. pp-equivalent luminosity for collisions between species A and species B is calculated as A*B*luminosity.

Run	System	Threshold [GeV]	Integrated Luminosity	pp-equivalent L [pb^{-1}]
3	d+Au	4.5	1.7 nb^{-1}	0.7
	p+p	4.5	0.17 pb^{-1}	0.17
4	Au+Au	3/sin(theta)	50 ub^{-1}	2
	p+p	4.6/sin(theta)	0.15 pb^{-1}	0.15
5	Cu+Cu	3.75	860 ub^{-1}	3.4
	p+p	4.2	2.8 pb^{-1}	2.8
6	p+p	5.4	11 pb^{-1}	11
7	Au+Au	5.5	0.5 nb^{-1}	20
8	d+Au	8.4	36 nb^{-1}	14
	p+p	4.3	3.1 pb^{-1}	3.1
9	p+p	4.2[(a)] 5.9[(b)]	20-50 pb^{-1}	20-50

[(a)] With Full ToF readout for Particle Identification
[(b)] Independent of ToF readout

Before Run 9, the STAR TPC has limited the luminosity that can be sampled, since it had linear deadtime that would rise with the rate of triggers that are written to tape. In practice, this led to a loss of 50-70% of the events that could be sampled by the trigger, since triggered programs competed with large samples of minbias and central events, and the size of the triggered datasets themselves also need to be considered. With DAQ1000 for Run 9 and beyond, this limitation has been largely removed, so that the triggered program can both easily coexist with the untriggered program and essentially double its efficiency in sampling the integrated luminosity delivered by the accelerator.

The next step is to increase these sampled luminosities by orders of magnitude. With stochastic cooling in RHIC II, in one RHIC year STAR can sample up to 20 nb^{-1} in Au+Au collisions. A strawman for the progression of luminosities is shown in Table 4-2. The following section will demonstrate a sample of the measurements that can be made within this scenario.

Table 4-2: Strawman for increase in integrated sampled luminosity at $\sqrt{s_{NN}}$ = 200 GeV. Integrated luminosities are cumulative, meaning that luminosities from previous runs of the same species add into the total quoted for a given year. Table lists only $\sqrt{s_{NN}}$ = 200 GeV, the energy most relevant for studies in Au+Au.

Run	System	Cumulative Integrated Sampled Luminosity	pp-equivalent Sampled Luminosity	Physics from run
9	p+p	50 pb^{-1}	50 pb^{-1}	Reference data for: First attempt at separation of Upsilon 1S from 2S+3S Further study of e-D from B J/Psi to high p_T
10	Au+Au	2 nb^{-1}	80 pb^{-1}	Electron spectra for R_{AA} with low material to resolve PHENIX/STAR discrepancy
11	p+p	80 pb^{-1}	80 pb^{-1}	Extension of reference data from Run 9
Future	p+p	200 pb^{-1}	200 pb^{-1}	Reference for Au+Au
Future	Au+Au	20 nb^{-1}	800 pb^{-1}	High precision utilization of RHIC II luminosity

γ-hadron correlations: Correlations between a direct photon and a hadron have been termed a "golden probe" of parton energy loss in the medium. A direct photon does not interact with the medium, and so does not lose energy. RHIC sits at a sweet spot in terms of backgrounds, as the nearly exclusive source of coincident photons and hadrons in the relevant kinematic regime is QCD Compton scattering between a quark and a gluon. Photons from pion decay are subdominant, and can be largely removed by cluster shape analysis, and Next-to-Leading-Order processes such as parton fragmentation into photons are expected to be small, on the order of 10%, as a first measurement from PHENIX indicates. From this clean process, both the identity and kinematics of the parent parton of the associated hadron are cleanly tagged. This allows for a precise measurement of the modification of the fragmentation function of a quark due to its interactions in medium.

The challenge with photon-hadron correlations is the low production rate. Figure 4-1 shows results to date, shown at QM2008, for measurements of direct photon-hadron correlations. While the results are within errors of theoretical predictions, the size of the uncertainties do not provide sufficient distinguishing power between different theoretical scenarios.

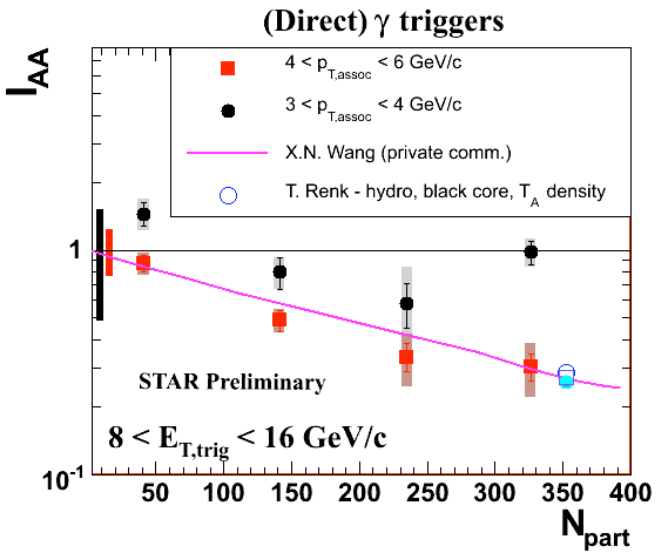

Figure 4-1: Suppression of away-side hadrons associated with direct photons from Run 7 Au+Au (0.5 nb^{-1}) and Run 6 p+p (9 pb^{-1}). Bars at the origin at unity denote uncertainty in the p+p reference, error bars indicate Au+Au statistical uncertainties, and grey bands denote systematic uncertainties.

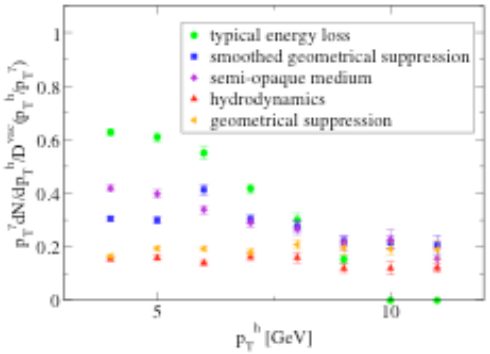

Figure 4-2: Prediction for sensitivity of suppression of γ-hadron away-side correlations to different scenarios, where E_T^γ > 15 GeV. From T. Renk, Phys. Rev. C74 (2006) 034906.

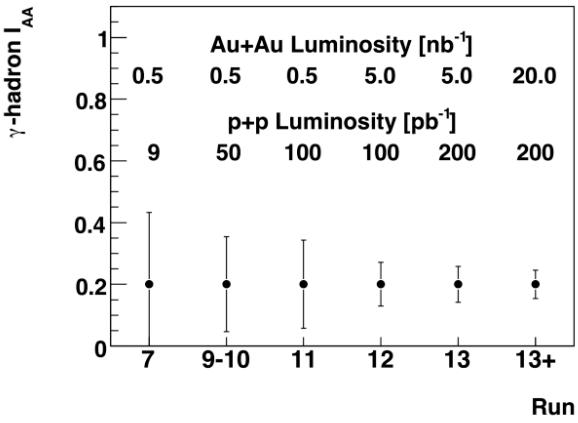

Figure 4-3: Projection for statistical uncertainties in γ-hadron suppression in a scenario of luminosity progression in different years. Projection is for E_T^γ> 15 GeV, associated particle p_T from 4-6 GeV/c.

In order to make progress, more luminosity is needed. Figure 4-2 shows one set of predictions under different theoretical scenarios of the suppression pattern, for a somewhat higher trigger E_T, > 15 GeV, than STAR has measured to date. This higher trigger E_T is needed to ensure that the associated hadron is both at relatively low fractional momentum with respect to the trigger photon and at high enough p_T to be cleanly associated with jet phenomena. Figure 4-3 shows a projection of the evolution of the uncertainties in a representative bin, 4-6 GeV/c associated particle p_T for one scenario of evolving luminosity sampled by STAR in the coming runs. This bin shows the largest deviation between theoretical scenarios, though the scenarios with the largest deviations are currently

disfavored. As shown in the figure, incremental progress can be made over the next five years, as cooling in RHIC ramps up to the full luminosity of RHIC II. Beyond this, studies of suppression focusing on the orientation of the trigger with respect to the reaction plane, and for identified hadrons combining the full Barrel Time of Flight detector with dE/dx in the TPC, will be possible in certain kinematic regions. With RHIC II luminosities, precise determination of the modification of quark fragmentation functions in medium will be possible with these correlation measurements.

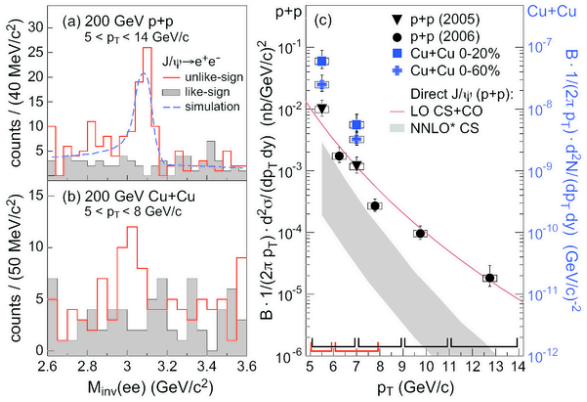

Figure 4-4: J/Psi differential cross section at mid-rapidity from p+p collisions at √s=200 GeV.

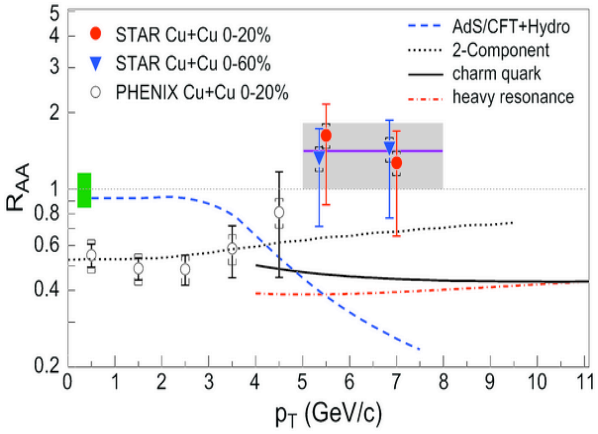

Figure 4-5: J/Psi R_{AA} in Cu+Cu collisions, as comported to theoretical expectations.

Quarkonia: STAR has submitted for publication J/Psi spectra out to transverse momenta of 14 GeV/c from triggered data from p+p and Cu+Cu collisions in Runs 5 and 6, as shown in Figure 4-4. By comparing STAR data across species and with PHENIX data, it appears that J/Psi suppression decreases at high p_T and R_{AA} approaches unity, in contradiction to some theoretical expectations, see Figure 4-5. However, this statement is statistically limited, at approximately 2-sigma, so further measurements are sorely needed. Figure 4-6 shows a projection of statistical uncertainties after the integrated sampled luminosities proposed for Runs 9-10, assuming that the increased bandwidth of DAQ1000 allows the thresholds to remain constant as luminosity increases, and that R_{AA} is unity. Should J/Psi be suppressed at high p_T, uncertainties will increase accordingly. While such integrated luminosities would greatly extend the reach of J/Psi measurements at RHIC, precision measurements await the higher luminosities of RHIC II, as shown in Figure 4-7 for luminosities expected by Run 13. At lower p_T, the addition of the full Time of Flight barrel will greatly decrease backgrounds, and should enable significant measurements, though effective triggering is still under study to understand the statistical significance that can be achieved.

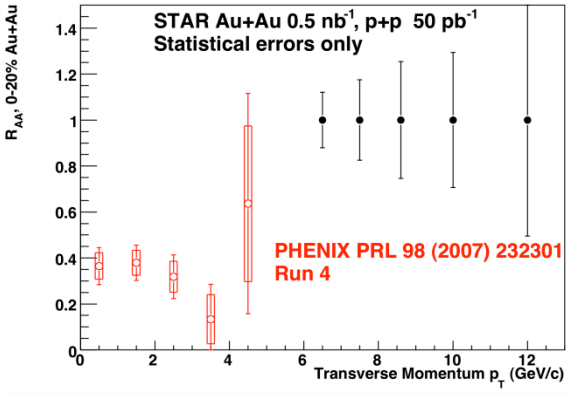

Figure 4-6: Projection for statistical uncertainty in J/Psi R_{AA} at high p_T, assuming R_{AA}=1, from integrated sampled luminosity of 0.5 nb^{-1} in Au+Au collisions and 50 pb^{-1} in p+p collisions, as proposed in Runs 9-10.

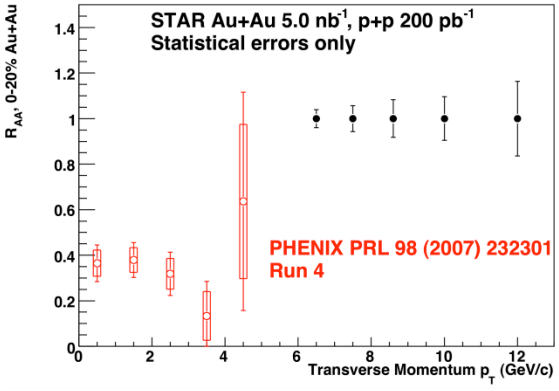

Figure 4-7: Projection for statistical uncertainty in J/Psi R_{AA} at high p_T, assuming R_{AA}=1, from integrated sampled luminosity of 5 nb^{-1} in Au+Au and 200 pb^{-1} in p+p collisions, as proposed to occur by the end of Run 13.

Upsilons remove many of the ambiguities that surround J/Psi suppression, since the b quark production cross-section is not large enough for recombination to be appreciable, and interactions between the Upsilon and co-moving hadrons are expected to be weak, leading to a cleaner signature of suppression at early times. Different states of Upsilon (1S, 2S, and 3S) are expected to be affected by the medium at different levels: the 1S state is expected to be unsuppressed due to its tight binding, while the 2S and 3S will be successively more strongly suppressed. By studying the full pattern of suppression, one can place constraints on the temperature and/or energy density of the medium. STAR has begun the Upsilon program with Runs 6-8. Shown in Figure 4-8 and Figure 4-9 are mass peaks from p+p collisions in Run 6 and Au+Au collisions in Run 7, both peaks of which have significance of approximately 4-sigma. A comparable dataset was collected in d+Au collisions in Run 8.

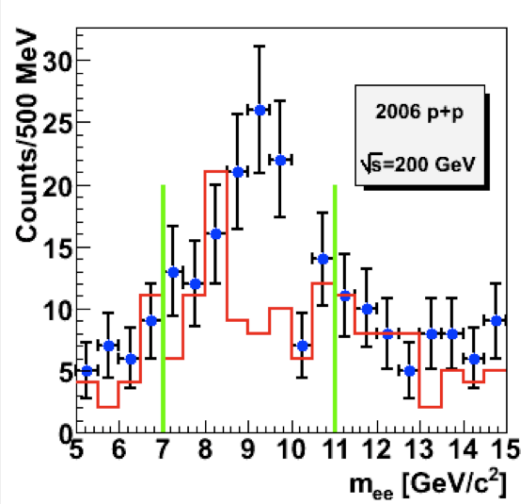

Figure 4-8: Upsilon (1S+2S+3S) mass peak from p+p run 6, 9 pb^{-1}. Points are from unlike-sign pairs, histogram from like-sign pairs.

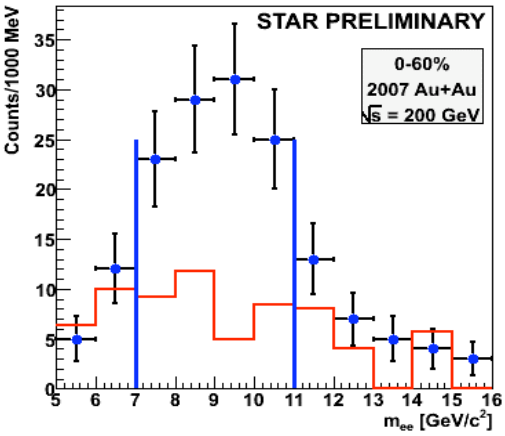

Figure 4-9: Upsilon (1S+2S+3S) mass peak from Au+Au Run 7, 0.3 nb^{-1}. . Points are from unlike-sign pairs, histogram from like-sign pairs.

After Run 7, STAR removed the inner tracking detectors the SVT and SSD, which greatly reduce the amount of material seen by electrons, and so reduces the broadening in the mass resolution in the di-electron channel from Bremsstrahlung. Figure 4-10 shows the expected resolution from simulation in the current configuration, while Figure 4-11 and Figure 4-12 show measured invariant mass distributions from Run 8. With this resolution, and 50 pb^{-1} sampled integrated luminosity from p+p collisions in Run 9, a first measurement separating the 1S from the 2S and 3S states appears to be feasible. This will need to be followed up with later runs integrating larger sampled luminosity in both p+p and Au+Au.

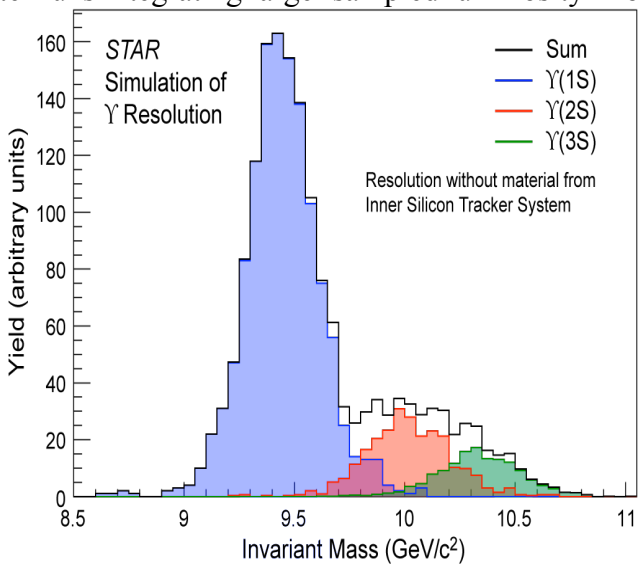

Figure 4-10: Expected mass resolution in Runs 8 and beyond, with no inner tracking detectors

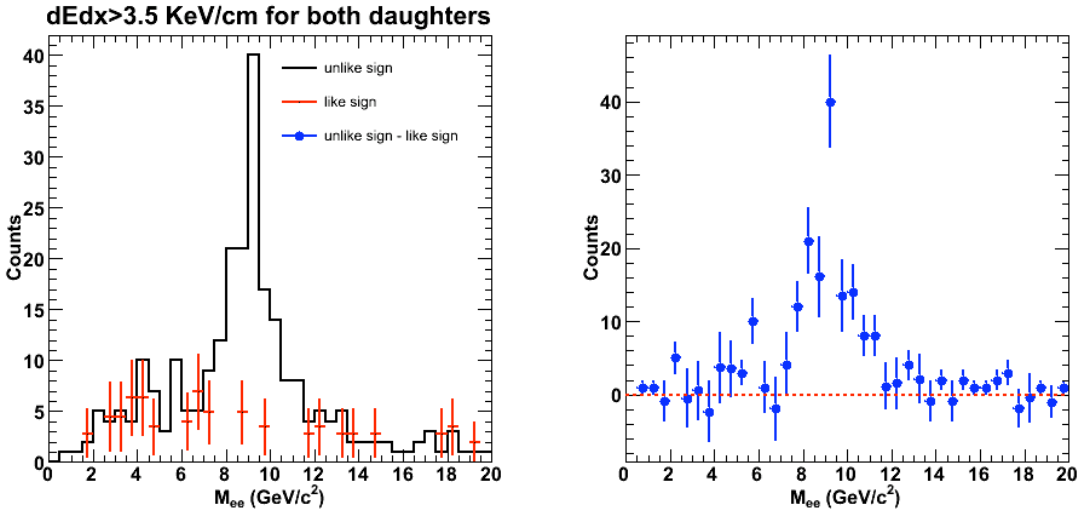

Figure 4-11: Upsilon invariant mass distribution as measured in Run 8 d+Au collisions. Left panel is like and unlike sign, showing the level of background. Right panel shows the distribution of unlike-sign pairs after subtracting the like-sign background.

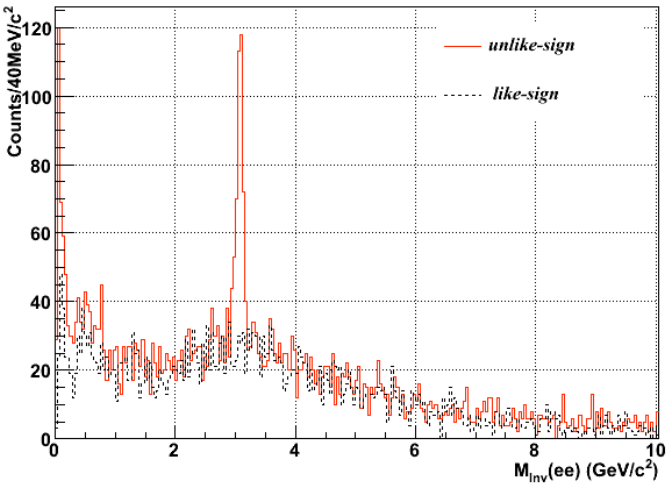

Figure 4-12: J/Psi invariant mass distribution as measured in Run 8 d+Au collisions

The ultimate goal from RHIC II luminosity is shown in Figure 4-13, which shows expected uncertainties in Upsilon(1S) that can be achieved with 20 nb^{-1} sampled integrated luminosity in Au+Au collisions and 100 pb^{-1} sampled integrated luminosity in p+p collisions. With this dataset, precision measurements of the dissociation of quarkonium states will be made possible.

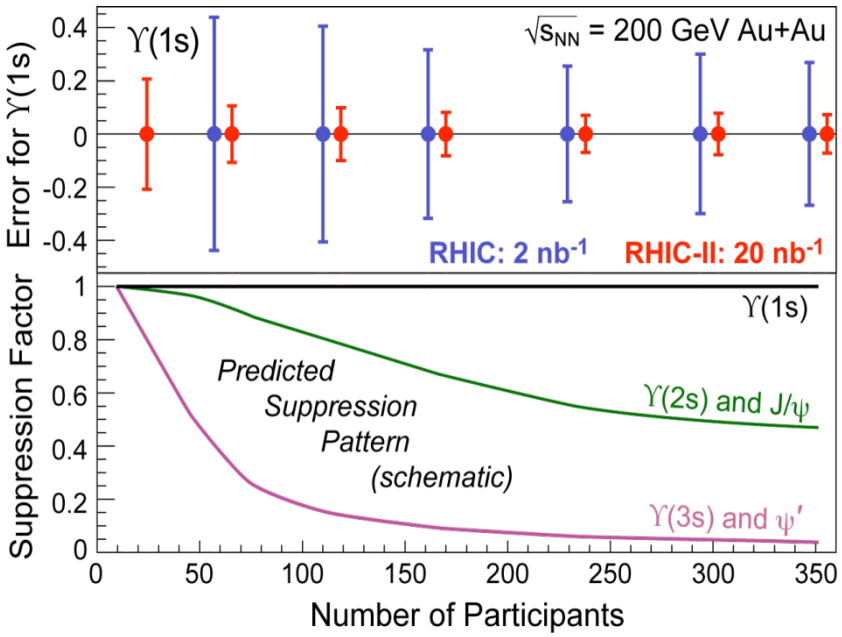

Figure 4-13: Projection of uncertainties in Upsilon(1S) R_{AA} for two sets of integrated luminosity.

Open Heavy Flavor: Energy loss of heavy quarks tests perturbative calculations of partonic energy loss in the medium in a way orthogonal to photon-hadron correlations. Non-photonic electrons, produced predominantly from decays of beauty and charm, are strongly suppressed, providing a strong challenge to these calculations. There are, however, a number of limitations to the measurements that cloud their interpretation.

First, as shown in Figure 4-14, the uncertainties on the spectrum of non-photonic electrons are quite large, and there is an apparent discrepancy between STAR and PHENIX (though R_{AA} is consistent between the experiments). Data from Runs 8 and 9 will help to resolve these issues, since the sampled integrated luminosity increased by a factor of 30 relative to the published results, and without the SVT and SSD the backgrounds from conversion electrons in STAR are comparable to those in PHENIX. However this measurement turns out, we need to return to Au+Au to do comparable measurements to study the suppression pattern, for which Run 10 provides a perfect window of opportunity.

The major limitation comes from the uncertainty in the relative contribution of charm and beauty to the non-photonic electrons. Energy loss calculations predict significant differences between the suppression of charm and beauty, but perturbative calculations cannot accurately predict the relative contribution of charm and beauty to these non-photonic electrons. Without measuring this fraction accurately, we are left with an unconstrained problem. First attempts at measuring this fraction in p+p collisions, using correlations between the electron and hadrons or fully reconstructed D's, are shown in

Figure 4-15. The measurements are consistent with the most advanced calculation, a Fixed-Order Next-to-Leading-Log calculation, but the data do not strongly constrain the uncertainties in the calculation.

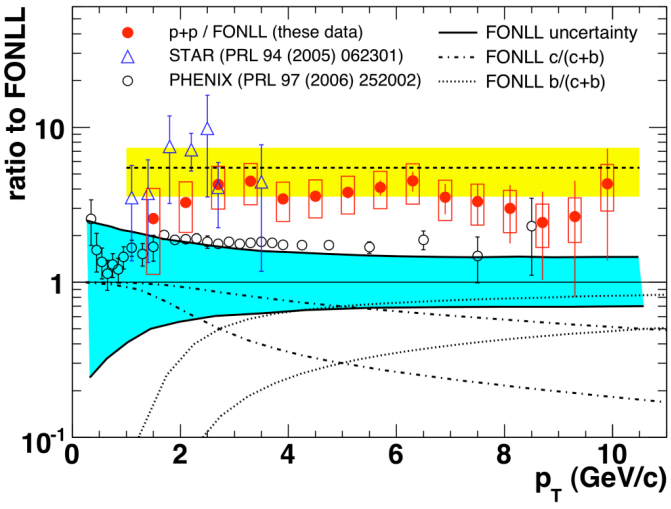

Figure 4-14: Ratio of non-photonic electron spectrum in p+p collisions at 200 GeV to a theoretical FONLL calculation. From a sampled integrated luminosity of 0.1 pb^{-1}.

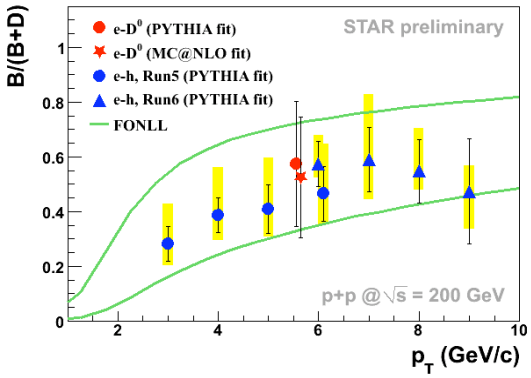

Figure 4-15: Relative contribution of beauty to non-photonic electrons, from correlation measurements, as compared to the uncertainty band from a FONLL calculation. Sampled integrated luminosity in Run 6 was 9 pb^{-1}.

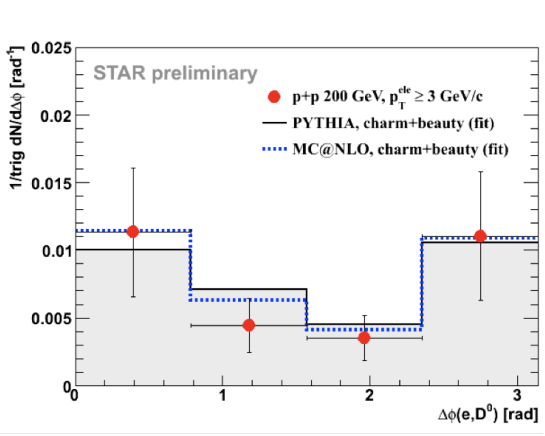

Figure 4-16: Per-trigger yields of reconstructed D mesons as a function of azimuth relative to a trigger non-photonic electron with p_T between 4 and 8 GeV/c. From 9 pb^{-1} of p+p collisions in Run 6.

There are a number of future directions to constrain this situation. First, with larger untriggered datasets, and with the Heavy Flavor Tracker, direct D measurements out to high p_T will be possible. With the TPC and TOF, with 200M events of any system D spectra can be measured with 3-sigma accuracy out to p_T of 4-5 GeV. In p+p, with DAQ1000, this is

planned for Run 9 and accompanying measurements are planned in Au+Au collisions in Run 10. Beyond the timescale of this document, with the Heavy Flavor Tracker, D spectra and R_{AA} can be measured with high accuracy out to 10 GeV.

4.2.1. Run 10 in the longer-term context of luminosity improvements

Table 4-2, in the previous section, provides a strawman plan for the year-by-year increase in luminosity towards the ultimate goal of RHIC II for triggered probes. In Run 10, the main goal is to make use of moderate amounts of integrated luminosity in Au+Au, in the time window between the removal of the SVT/SSD and the installation of the HFT, to make measurements in the electron sector that benefit from a low amount of material. Beyond the timescale of this document, we expect to begin the precision program of RHIC II in earnest, with an order-of-magnitude increase in sampled integrated luminosity in Au+Au collisions and the installation of the Heavy Flavor Tracker.

4.3. Untriggered Datasets in Au+Au at 200 GeV

A key strength of STAR is the ability to identify a wide variety of the hadron species produced in the collision. Stable charged particles are identified through dE/dx measurements and weakly decaying strange and multi-strange hadrons from their decay vertices. Various resonance peaks can be revealed by combining particles in pairs either without identification, or by using one or both of the identification techniques mentioned above. These capabilities have allowed us to address a variety of physics topics by measuring the yields and transverse momentum spectra of a wide range of particles. With ToF, these capabilities will be expanded dramatically in Run 10. The other major advantage of the STAR detector is the large azimuthal acceptance, which has allowed many correlation and other event-by-event analyses to be made. RHIC has provided A+A collisions at several energies and with two species (Au and Cu). This has enabled detailed systematic studies as a function of system size, geometry and energy to be performed.

4.3.1. High-p_T kaon measurements as Probe of Nuclear matter with jet conversion

"The coupling of jets to nuclear matter naturally leads to an alteration of jet chemistry even at high transverse momentum. In particular, QCD jets coupling to chemically equilibrated quark gluon plasma in nuclear collisions, will lead to hadron ratios at high transverse momentum that can differ significantly from their counterparts in p + p collisions. Flavor measurements could complement energy loss as a way to study interactions of hard QCD jets with nuclear matter."[1]

The study of identified hadron spectra at high p_t in p+p collisions also provides a good test of perturbative quantum chromodynamics (pQCD) [2, 3, 4]. In different NLO pQCD calculations, the inclusive production of single hadrons is described by the convolution of parton distribution functions (PDFs), parton-parton interaction cross-sections and fragmentation functions (FF). The PDFs were derived from deep inelastic scattering while the FFs [5] were derived from elementary electron positron collisions. The flavor-separated quark and gluon FFs are not well constrained, especially for baryons. In order to further understand particle production mechanisms, it is necessary to provide a stringent constraint on the quark and gluon FFs by comparing theoretical calculations with experimental data in

the same kinematics. This also provides a baseline to understand the mechanism of jet interaction with the medium created at the relativistic heavy ion collisions.

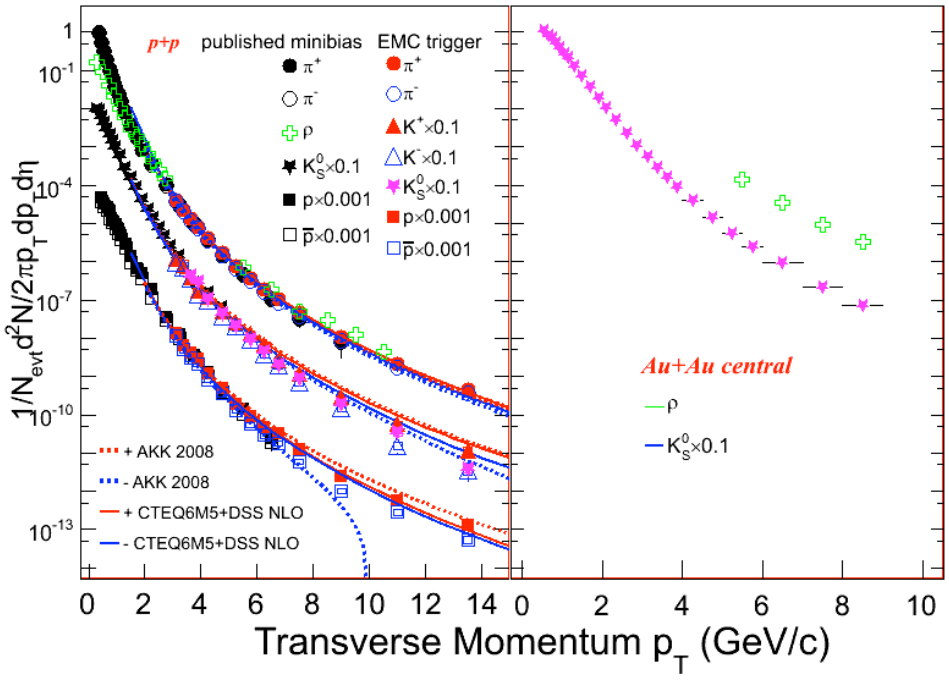

Figure 4-17 K^{+-}, K_s, p, pbar, π^{+-}, and ρ spectra up to p_t=15 GeV/c in p+p and central Au+Au collisions.

A parton produced through a hard process loses energy when traversing medium. This leads to a suppression of hadron spectra, compared to those in p+p collisions, scaled by the number of binary nucleon nucleon collisions [6, 7, 8]. The centrality dependence of proton and pion spectra indicates that the suppression magnitude for protons is similar to that for pions [9]. This is somewhat surprising since protons (more so for antiproton) are dominated by gluon fragmentation while pions have significant contribution from quark jets [10]. The Casimir factor for gluons is 9/4 times that for quarks, which leads to more energy loss for gluons than for quarks when traversing the medium [11, 12]. Naively, this will result in proton spectra more suppressed compared to pion spectra, which is contradictory with our experimental results.

Jet conversion mechanisms have been proposed by Liu and Ko to understand this result[13]. In this mechanism, the parton can change flavor or color charge after interaction with the medium. A large jet conversion cross-section leads to better agreement between the calculations and data, with the suppression pattern of protons similar to that of pions. Using the same factors, Fries and Liu [1] predicted that the kaon suppression pattern would be significantly different when compared to pion suppression pattern, since the initially produced hard strange quarks are fewer compared to the strange quarks in quark gluon plasma. Put another way, the interaction between the initially produced light quark (gluon) and the medium will lead to more strangeness production at high p_T at RHIC energies as compared to the case without jet conversion. Experimental measurements of charged kaon and neutral kaon at high p_T in pp and Au+Au collisions are called for to test these

predictions, and to understand more about the jet interaction with the medium as well as the chemistry of the medium.

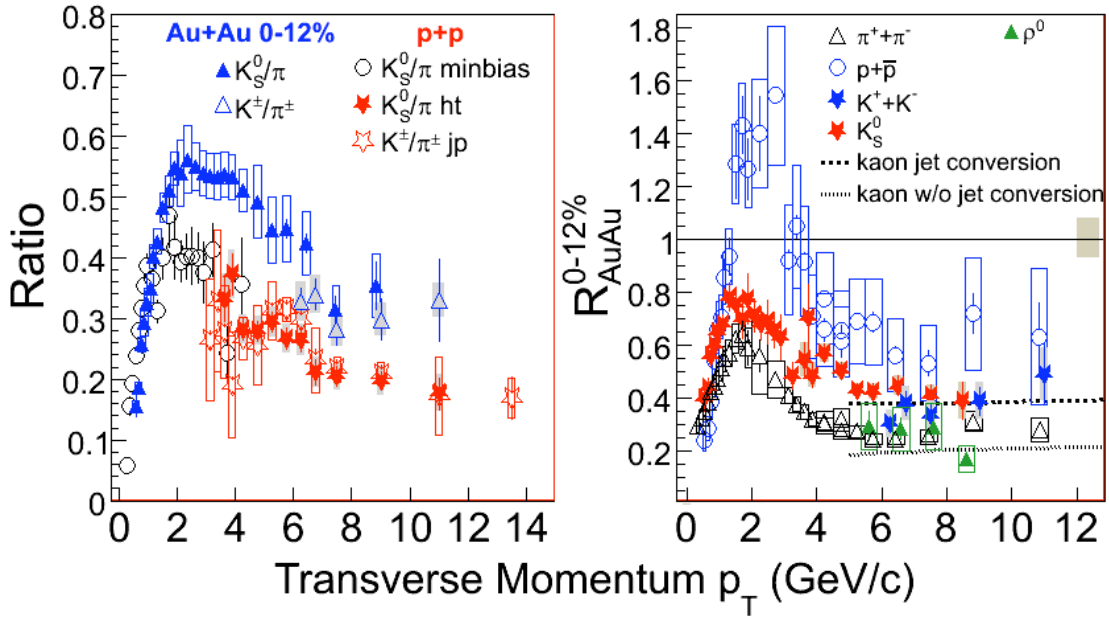

Figure 4-18 a) K_s/π, K^{+-}/π ratio in p+p and central Au+Au collisions, b)R_{AA} of K_s, K^{+-}, p+antiproton, π^{+-} and ρ for central Au+Au collisions, as compared to model calculations with and without jet conversion for kaons

At QM09, STAR presented the charged kaon and K_s spectra at high p_T in both p+p and central Au+Au collisions [14], as shown in Figure 4-17. Figure 4-18 shows the K/π ratio and identified particle R_{AA} for central Au+Au collisions [14]. The trend at high p_T is quite clear: R_{AA} of ρ [15] and π are the same, while R_{AA} of Kaon is larger than π (ρ) and smaller than proton (antiproton). This is consistent with the prediction [1].

We also attempted to extend this study to peripheral collisions, since one would naively expect that the effect should disappear at peripheral Au+Au collisions, as the phenomenon is purely a signature of flavor equilibrium in a hot and dense matter. However, due to limited statistics in peripheral collisions, the spectra for K_s reach only to p_t =~ 6 GeV/c. Figure 4-19 shows the R_{AA} for p_t -integrated Ks yields with p_t>5.5 GeV/c as function of centrality [16]. Indeed, we see larger R_{AA} for K_s than π through all centralities. Such an enhancement is possibly due to the Cronin effect or coalescence, since this p_t range is where these effects are at its maximum. We propose to take more minimum bias Au+Au data to extend the K_s and K^{+-} measurements to higher pt where such effects decrease in importance. For 300M minimum bias Au+Au collisions, we expect 50—100 charged kaons at p_t>10 GeV/c for 60—80% Au+Au centrality, and an increase in the statistics for K_s by an order of magnitude. This will provide a definitive test of the jet conversion phenomenon.

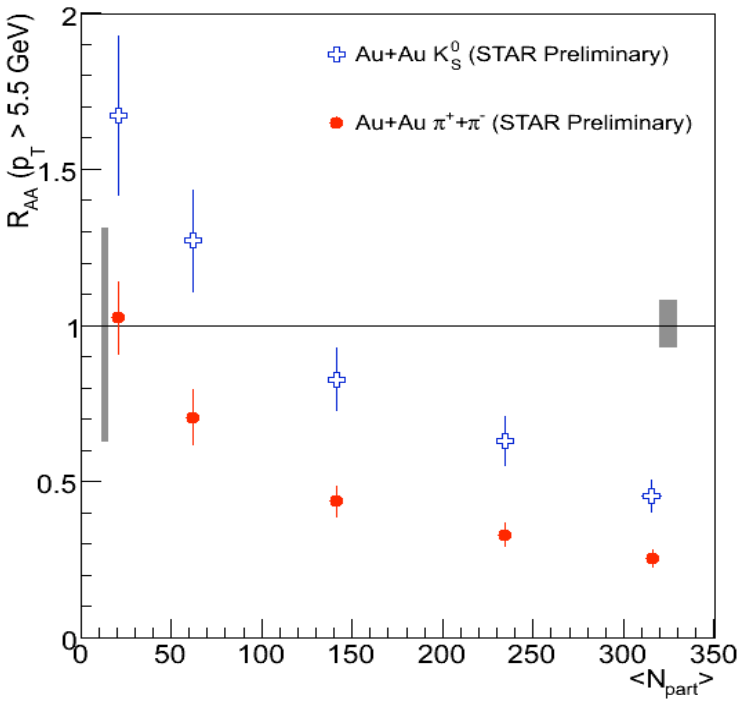

Figure 4-19: R_{AA} vs. centrality (N_{part}) of K_s and π^{+-} for p_t>5.5 GeV/c

4.3.2. Full Jet Reconstruction

Much has been learned from jetlike signatures in di- and tri-hadron correlations in heavy ion collisions, and in Run 10 the larger data samples and ToF detector will greatly improve the interpretability of these results. In the past year, major improvements in theoretical and experimental techniques have enabled a major step past such measurements. Full reconstruction of jets in heavy ion collisions, previously thought to be beyond reach at RHIC, has been successfully demonstrated. Figure 4-23 shows one such event from Run 7.

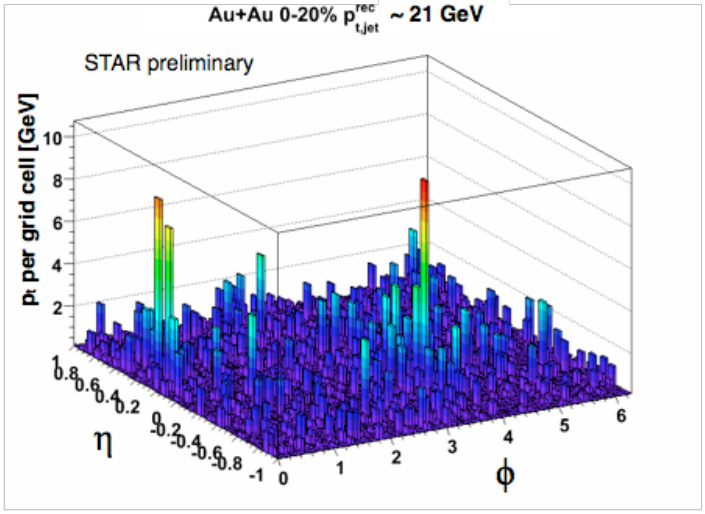

Fig. 4-23: A di-jet event in central Au+Au

Full jet reconstruction in heavy-ion collisions can conceptually provide a direct measurement of the energy of the scattered parton before energy loss, alleviating well known biases in di-hadron correlations and allowing reconstruction of the partonic kinematics in an unbiased way, independent of the fragmentation details (quenched or unquenched). This would result in a direct measurement of the energy loss probability distribution in a model-independent way.

The current jet cross-section and jet R_{AA} measurements suggest that, as compared to single hadron measurements, with full jet reconstruction one is able to recover a larger fraction of the jet population (see Fig. 4-24). Conclusions about a possible decrease of the jet R_{AA} for higher jet energies are currently limited by statistics. Measurements of the jet fragmentation function and their modification, especially at high z, are currently limited to jet energies around 25-30 GeV and $z<0.7$ in the High Tower triggered Year 7 data-set utilizing the recoil jet. Statistics are further limited in the Minimum Bias Year 7 dataset. With the Year 10 Au+Au data, STAR would be able to significantly extend the kinematical reach, and further explore the systematics, of jet quenching measurements at RHIC energies.

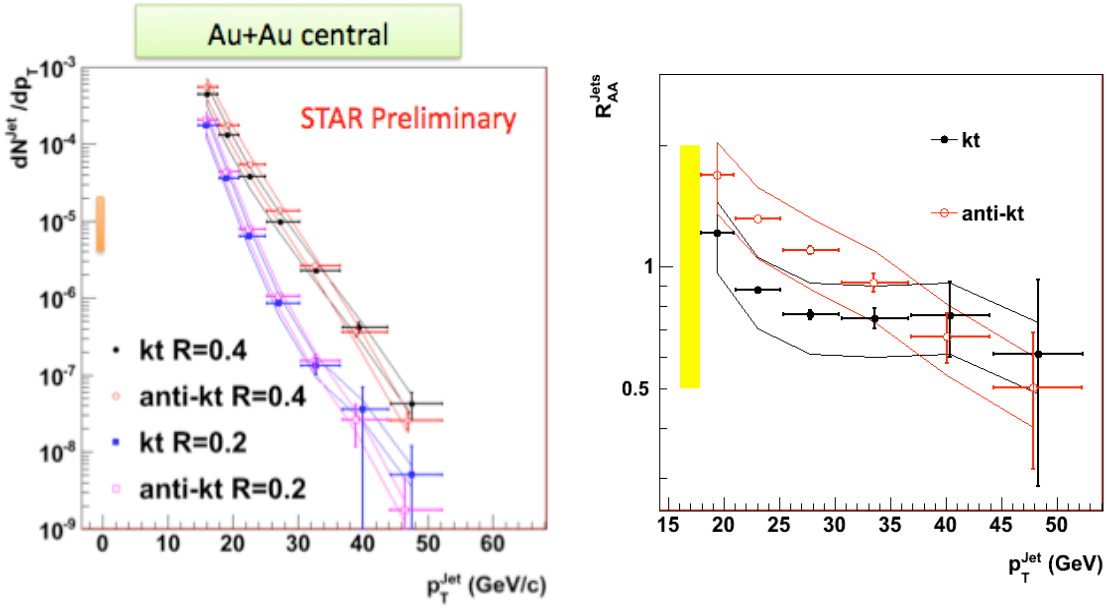

Fig.4-24: (left) Inclusive jet spectrum in 0-10% central Au+Au collisions Year 7 (right) R_{AA} for fully reconstructed jets in 0-10% central Au+Au collisions.

With the Year 7 minbias Au+Au data the inclusive jet spectrum in 0-10% central Au+Au collisions (~7M) was measured up to jet energies ~40 GeV (see Fig. 4-24). 250M central Au+Au collisions (~30x more statistics) would allow cross-section measurements above 50 GeV in jet energy and would allow jet R_{AA} measurements as well as jet-energy flow measurements (by comparing the jet x-section for different resolution parameters R) with high statistics up to 45 -50 GeV (see Fig. 4-24). An increase of 4-5x in the minbias Au+Au data would open up the possibility to study the jet R_{AA} as function of centrality, testing the path length dependence of partonic energy loss. The centrality dependence would also provide important insights and systematics concerning background fluctuations in the underlying heavy-ion event and how elliptic flow affects the current background subtraction scheme. Furthermore the increased statistics would allow fragmentation function measurements in 0-10% central Au+Au collisions for jet energies above 25-30 GeV. A comparison of these measurements with the High Tower triggered recoil fragmentation functions (see Fig. 4-25) will further test the dependence of different average path lengths of the reconstructed jets. By comparing Au+Au minbias to Au+Au High Tower recoil jet-by-jet measurements, most of the systematics caused by uncertainties in the background subtraction and fluctuation will cancel out as compared to measurements using p+p as a reference (see Fig. 4-24).

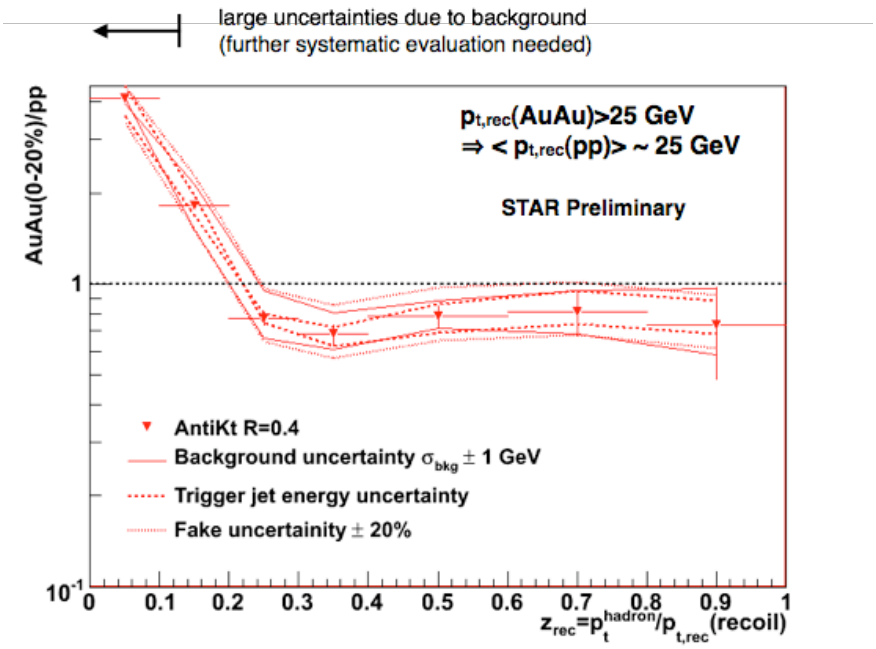

Fig.4-25: Recoil fragmentation function ratio Au+Au/p+p for 0-20% central Au+Au collisions (Year 7 High Tower triggered).

A High Tower triggered data-set of 2 nb^{-1} in addition to the Au+Au minbias would allow recoil jet fragmentation function measurements up to 40-45 GeV, in a kinematic regime where the systematics are better understood. Furthermore a measurement of the di-jet cross-section as well as fragmentation functions as function of centrality could be carried out. Triggering, while it allows for sampling of the full luminosity delivered, introduces a number of biases (fragmentation and parton species-dependent) that can severely complicate interpretation of the results. Studies are ongoing to determine if alternative, less biased, trigger schemes, such as Jet Patch triggers which trigger on total energy over a broader range of η and φ than a High Tower trigger, can be made viable in the challenging environment of Au+Au collisions.

With the full TOF acceptance high statistics PID (π, K, p) fragmentation function measurements will be accessible to study the flavor dependence of jet quenching.

4.3.3. Future EM probes in STAR

Electromagnetic probes[17] uniquely provide direct access to the in-medium modifications of hadronic states (vector mesons ρ(770), ω(782), φ(1020)) via dilepton invariant-mass spectra, which can illuminate the nature of hadron mass generation and thus the origin of ~ 98% of the visible mass in the universe (as well as related changes in the structure of the QCD vacuum including the restoration of chiral symmetry). In addition, at masses above ~1 GeV there exists the possibility of detecting novel nonperturbative (resonant) correlations in

a sQGP. Electromagnetic probes are also unique in inferring the temperature of the system during its hottest phases via direct thermal radiation of photons and dileptons radiation.

At STAR electron identification is made possible by a combination of a measurement of the energy loss by charged particles due to ionization (dE/dx) of the Time Projection Chamber (TPC) gas and a velocity measurement with the TOF system [18]. The relativistic rise of the electron dE/dx separates electrons from hadrons, except where electrons cross with pions at momenta of ~0.2GeV/c, with kaons at ~0.6GeV/c, with protons at ~1.1GeV/c, and with deuterons at ~1.5GeV/c. A time-of-flight measurement, with the requirement that $|1 - \beta| < 0.03$, eliminates slow hadrons and cleans up the crossing regions. This results in clean electron identification. In addition to direct measurements of open-charm hadrons (via $K\pi$ decays), the STAR HFT [19] will serve as a powerful device to discriminate primordial electrons from background electrons, both from photonic sources such as conversions and from correlated decay of charm and beauty. Rejection of π^0 and η Dalitz decays by a factor of 3 (single track) can be achieved by measuring both electrons of the pair, which is possible due to the large acceptance of the STAR TPC. The large reduction in electron background will enable us to observe the electromagnetic signal from low-mass vector mesons and the radiation of intermediate-mass dileptons with a few hundred thousand central Au+Au events in STAR. With the upgrades we expect to detect 6K φ and 22K ω decays in 200 Million recorded central Au+Au collisions [17,19]. These measurements will be of comparable accuracy to those presented by NA60 at QM05 [20] in central In+In collisions, which consisted of signals ~ 6K for the ω and ~ 10K for the φ, but recorded at RHIC energies.

In the absence of the HFT, we expect that the electron background level will be similar to that of the PHENIX detector. From ϕ yields measured by STAR in the hadronic decay channel ($\phi \rightarrow K^+K^-$), we estimate that in the electron channel ($\phi \rightarrow e^+e^-$) a signal with 25σ significance and signal-to-background ratio between 1:25 to 1:10 will be obtained in 300M minimum bias events. This is an example of the high quality measurements that can be made with electron pairs in such a configuration.

4.3.4. Hypernuclei and anti-hypernuclei

A hypernucleus is a nucleus which contains at least one hyperon in addition to nucleons. The first hypernucleus was discovered by Marian Danysz and Jerzy Pniewski in 1952 in a cosmic ray emulsion experiment [21]. The smallest and simplest hypernucleus is the hypertriton ($^3_{\Lambda}H$, or $_{\Lambda}t$), consisting of a Lambda, a proton and a neutron. Hyperons inside a hypernucleus contain strangeness, and therefore provide one more degree of freedom for nuclear spectroscopy than the normal nucleus. Hypernuclei also provide an ideal laboratory for studying the force between a hyperon and a nucleon (the Y-N interaction), which is otherwise not possible with normal nuclei or with traditional hadron-hadron or electron-positron beams. This information is needed to understand the configuration of a neutron star, which, depending on the strength of the Y-N interaction, can be an object with strange quark matter, a hyperon star, or a kaon condensate at the core [22].

Conventional methods of producing hypernuclei use cosmic ray interactions, kaon capture, or strangeness exchange reactions [23]. There are currently several hypernucleus

experiments in major nuclear facilities: MAMIC at Mainz and JLab (photo-production), FINUDA at DAϕNE (stopped kaon beam from e+e- collider), J-PARC (stopped kaon from hadron beam), PANDA at FAIR (stopped anti-proton annihilation), and HypHI at FAIR and SPHERE at JINR (using heavy ion beams). All these experiments require a target or baryon-rich dense nuclear matter to provide the nucleons necessary for hypernucleus production: only RHIC and the LHC are capable of producing an anti-hypernucleus, which contains anti-protons, anti-neutrons, and anti-hyperons.

Understanding the asymmetry of anti-matter and matter in the observable universe is one of the frontiers of modern physics. There is an abundance of nuclei in the universe, but anti-nuclei (A>=2) have not been found in nature. Relativistic heavy ion collisions, simulating the conditions in the early universe, not only can provide an environment with abundant anti-nucleons and anti-hyperons, but also produce anti-nuclei and anti-hypernuclei through coalescence. RHIC offers the first opportunity for discovery of anti-hypernuclei as well as anti-nuclei having A>3. The antinuclei $\bar{d}$, $\bar{t}$ and $^3\bar{H}\bar{e}$ have been observed, but no one has claimed detection of an $\bar{\alpha}$: we expect to produce and observe the first $\bar{\alpha}$ in the next long 200 GeV AuAu run based on our understanding of the coalescence parameters. The coalescence process for formation of hypernuclei (anti-hypernuclei) requires that nucleons (anti-nucleons) and hyperons (anti-hyperons) be produced in proximity in phase space, Hypernucleus (anti-hypernucleus) production is sensitive to correlations of the coordinate and momentum space distributions of their constituent particles. A similar yield of nucleus-antinucleus pairs is one of the signatures of QGP formation. The hypertriton ($_\Lambda$t) yields can be compared to the yields of ^{3}He and of t which have the same atomic mass number; the anti-hypertriton ($_{\bar{\Lambda}}\bar{t}$) can be compared to $^3\bar{H}\bar{e}$ and $\bar{t}$.

STAR recently reported the first observation ever of an anti-hypernucleus, identified via the secondary vertex of the hypertriton decay to (helium3 + pion). A total of 70 ± 17 anti-hypertritons and 157 ± 30 hypertritons were identified in Au+Au collisions at √s=200 GeV as shown in Fig. 4-26. The lifetime of the hypertriton was measured as $c\tau=182 \pm {}^{89}_{45} \pm 27$ ps (Fig. 4-27). We also measured the anti-hypertriton/hypertriton = 0.49 ± 0.18 ± 0.07, anti-helium3/helium3 = 0.45 ± 0.02 ± 0.04, anti-hypertriton/anti-helium3 = 0.89 ± 0.28 ± 0.13, and hypertriton/helium3 = 0.82 ± 0.16 ± 0.12. In Fig. 4-28 these ratios are compared to the results at AGS and SPS, where available.

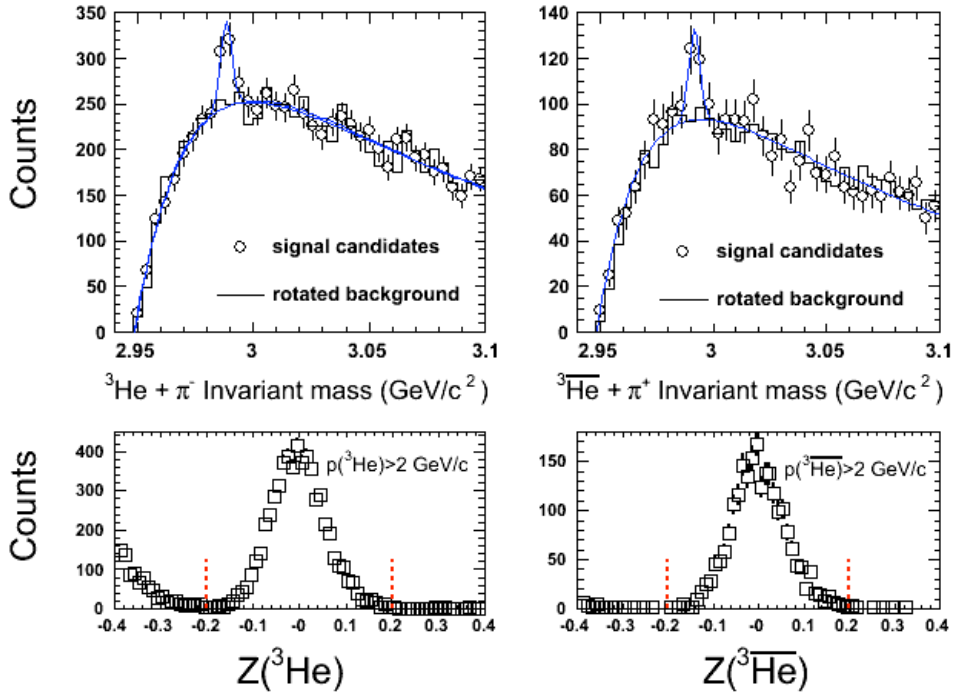

Fig.4-26: Upper panels show the invariant mass distribution of helium3 + pion in Au+Au collisions at 200 GeV. Open circles represent the signal candidate distributions, solid black lines are background distributions. Lower panels show the helium3 candidates Z ($\log((dE/dx)_{measured}/(dE/dx)_{expected})$) distribution from the same data set.

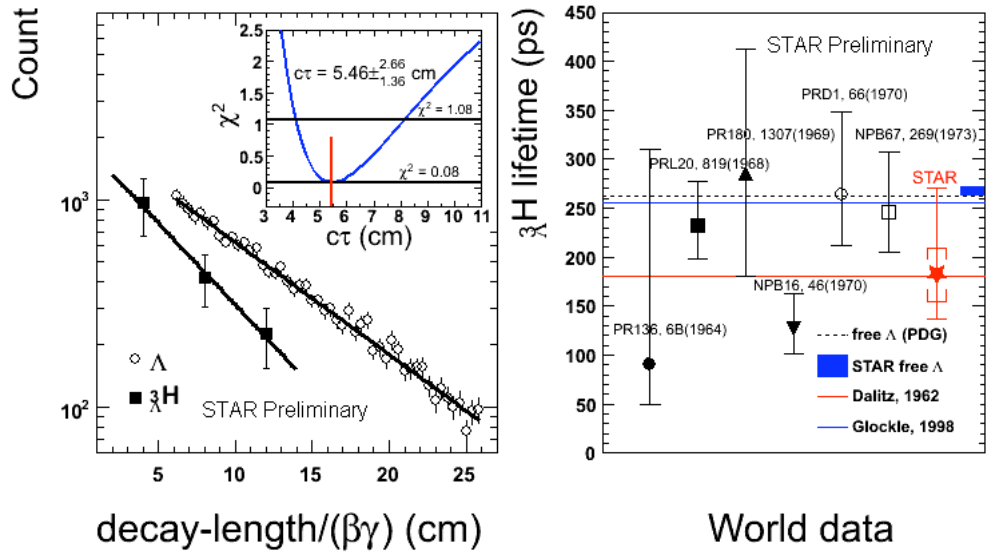

Fig. 4-27, Left panel show the hypertriton and lambda yield distribution in various cτ bins. Solid lines represent the cτ fitting. The insert panel shows the χ^2 distribution of the hypertriton cτ fitting. Right panel show the worlds data of hypertriton lifetime measurements.

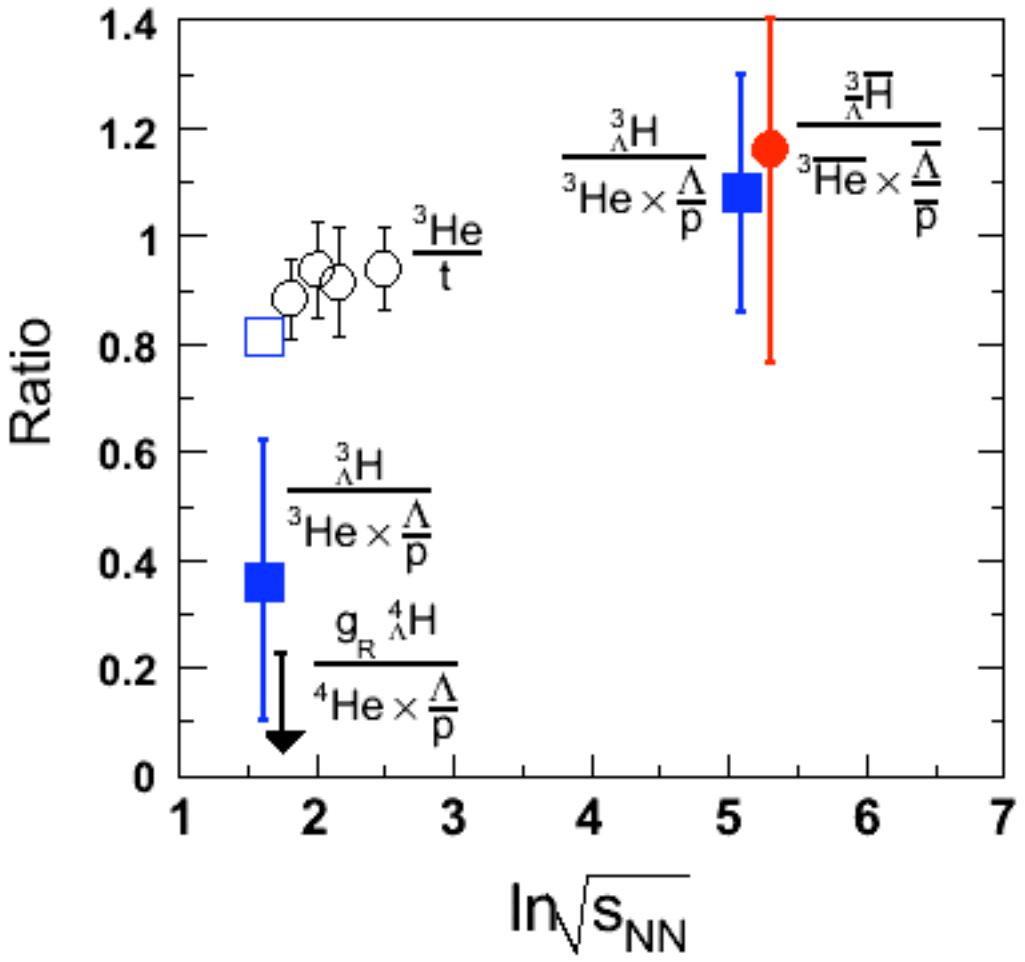

Fig.4-28: Ratios of various nuclear states from AGS, SPS and RHIC experiments

We plan to increase the statistics for the anti-hypernucleus discovery, and to provide a more precise lifetime measurement for the ${}_{\Lambda}t$ and ${}_{\bar{\Lambda}}\bar{t}$. Measurement of hypernucleus production will provide information about the hyperon and nucleon correlation and Y-N force. A dataset of 300 million minimum-bias events in Au+Au collisions at 200 GeV will provide a total collection of hypertriton+anti-hypertriton with more than 10σ significance. The energy scan will provide data points between the AGS and RHIC top energies to establish the trend of hypertriton/^{3}He ratio. This can then be compared to calculations at quantitative level based on p,n and Λ spectra. In Table 4-3 we estimate the number of minimum-bias Au+Au events required to reconstruct the hypertriton at the 5σ level. This assumes that the reconstruction efficiency is the same at all energies. In reality, the background and hyperon yields decrease with decreasing beam energy while reconstruction efficiency increases due to lower TPC occupancy.

Table 4-3 Number of minbias Au+Au events required for an observation of hypertriton in STAR at 5σ level. The penalty factors are provided by [24].

Beam energy	200 GeV	~17 GeV	~5 GeV
Minbias events# (5σ)	**300M**	**~10—100M**	**~1—10M**
Penalty factor	1448	368	48
^{3}He invariant yields	1.6×10^{-6}	2×10^{-4}	0.01
$^3_\Lambda$H/^{3}He assumed	1.0	0.3	0.05

4.3.5. Ultra-Peripheral Collisions

STAR plans to continue its ultra-peripheral collisions (UPC) program in Au+Au events. The Au+Au UPC analysis of STAR focuses on heavy vector mesons, in particular J/ψ, ϕ production, and four-prong particle decays. The four-prong data will be used to improve the previous reported measurement of the parameters of the ρ′(~1450) and/or ρ′(1700) resonance, and a search for heavier resonances decaying to 4 pions. With 50 M minbias UPC triggered Au+Au events, the collection of which is made possible via DAQ1000, we expect to reconstruct ~1500 ρ' candidates. A search for the four-pronged KKππ and, statistics permitting, KKKK final states will also be performed. With such high statistics a 6-prong final state study will also be feasible as will the first attempt to observe the two-photon production of the $f_2(1270)$. Meanwhile the reconstruction of the J/ψ will enable the study of the gluon distribution functions around x=0.01 and $Q^2=(1.5\ \text{GeV})^2$. Finally, multiple vector meson production in a single ion-ion collision is within reach with such a data set. Approximately 1 out of 1,000 ρ^0 should be accompanied by a second ρ^0. Quantum correlations in the production and in the decay can then be studied: for example with $\rho^0\rho^0$ in the same quantum state, stimulated decay becomes a possibility.

4.4. Au+Au Beam Use Request at 200 GeV for Run 10

In an 8-week run in Run 10 at 200 GeV, STAR can collect a dataset that represents a major step both in size and scope beyond past datasets. The addition of the full barrel ToF, combined with a low material budget in front of the TPC, enables a qualitative step in the interpretability of the results. The main statistical drivers are summarized below.

Triggered: 2 nb^{-1} sampled (x4 relative to Run 7)

Non-photonic electrons with low material to investigate Open Heavy Flavor R_{AA}
Quarkonia: Upsilon and high-p_T J/Ψ with low material
γ-hadron: hadron z_T~0.3 at hadron p_T~5 GeV/c to distinguish E_{loss} scenarios
Triggered fully reconstructed jets for jet-jet and identified jet-hadron correlations

Central: 250M (x10 relative to Run 4 and x30 relative to Run 7)

Extension of fully reconstructed jets, unbiased by trigger, to 40-50 GeV
Di- and tri-hadron identified particle correlations to study jet-medium interactions

Minimum bias: 300M (x4 relative to Run 7)

Jet conversion via K for p_T>10 GeV/c in peripheral collisions
Low-mass dileptons with low material to begin using the ToF for E.M. probes
10σ measurement of hyperon and anti-hypertriton production

In addition to the above measurements, the requested sample allows for detailed measurements of all the Fourier harmonics (v_n) for identified particles. For instance, as noted in section 3.3, the observation of a "wiggle" in the v_1 measurement around mid-rapidity could indicate a change in the compressibility of the matter created. The higher order harmonics can be used as a more sensitive test of the initial conditions. Both v_1 and v_4 measurements have been performed by STAR with limited statistics, but measurements using full PID and finer granularity in rapidity are needed to further constrain models of both the initial conditions and the dynamical evolution of the system**.** Other physics topics that would become feasible with the requested sample include jet-induced Lambda polarization and resonance production in jets. Additionally, rare particle searches and resonance studies will become possible even in central Au+Au collisions, benefiting greatly from TOF availability.

References

[1] W. Liu and R.L. Fries, Phys.Rev. C 77:054902, 2008
[2] J. C. Collins and D. E. Soper, Ann. Rev. Nucl. Part. Sci. 37 (1987)
383; J. C. Collins, D. E. Soper and G. Sterman in Perturbative Quantum
Chromodynamics (World Scientific, 1989) edited by A. H. Muller and Adv.
Ser. Direct. High Energy Phys. 5 (1988) 1; G. Sterman et al., Rev. Mod. Phys.
67 (1995) 157.
[3] J. Adams et al., Phys. Lett. B 616, 8 (2005); J. Adams et al., Phys. Lett. B 637, 161 (2006).
[4] J. Adams et al., Phys. Rev. C 75, 64901 (2007).
[5] R. D. Field and R. P. Feynman, Nucl. Phys. B 136 (1978) 1; J. F. Owens, Rev.

Mod. Phys. 59 (1987) 465.
[6] M. Gyulassy et al., nucl-th/0302077; A. Kovner et al., hep-ph/0304151, Review for: Quark Gluon Plasma 3, Editors: R.C. Hwa and X.N.Wang, World Scientific, Singapore.
[7] J. Adams et al., Phys. Rev. Lett. 91, 172302 (2003).
[8] S.S. Adler et al., Phys. Rev. Lett. 91, 072301 (2003); S.S. Adler et al., Phys. Rev. Lett. 91, 241803 (2003); B.B. Back et al., Phys. Lett. B 578, 297 (2004); I. Arsene et al., Phys. Rev. Lett. 91, 072305 (2003).
[9] B.I. Abelev et al., Phys. Rev. Lett. 97, 152301 (2006); B.I. Abelev et al., Phys. Lett. B 655, 104 (2007).
[10] S. Albino et al., Nucl. Phys. B 725, 181 (2005).
[11] X.N. Wang, Phys. Rev. C 58, 2321 (1998).
[12] Y. Dokshitzer et al., Phys. Lett. B 519, 199 (2001).
[13] W. Liu, C.M. Ko, B.W. Zhang, Phys. Rev. C 75, 051901 (2007).
[14] Y. Xu, QM2009 presentation.
[15] P. Fachini, QM2008 presentation.
[16] A. Timmins, QM2009 presentation.
[17] G. David, R. Rapp and Z. Xu, arXiv: nucl-ex/0611009 v2
[18] M. Shao et al. NIMA **558**, 419 (2006).
[19]STAR HFT: http://rnc.lbl.gov/~wieman/hft_final_submission_version.pdf
K. Schweda et al., NPA **774**, 907 (2006).
[20]E. Scomparin et al. (NA60 Collaboration), NPA **774**, 67 (2006).
[21] M. Danysz and J. Pniewski, Phil. Mag. 44 (1953) 348.
[22] J.M. Lattimer and M. Prakash, Science 304 (2004) 536.
[23] D.H. Davis, Nucl. Phys. A547 (1992) 369c-378c.
[24] H. Liu and Z. Xu, nucl-ex/0610035.

5. Run 11: U+U Collisions at 200 GeV

5.1. Physics of U+U collisions at RHIC Top Energy

The commissioning of the EBIS upgrade will enable Uranium beams to be accelerated at RHIC. The peculiar geometry of Uranium opens up a new horizon of measurements at RHIC, in which we can probe matter which has both higher densities than achievable in Au+Au collisions and non-trivial geometrical shape.

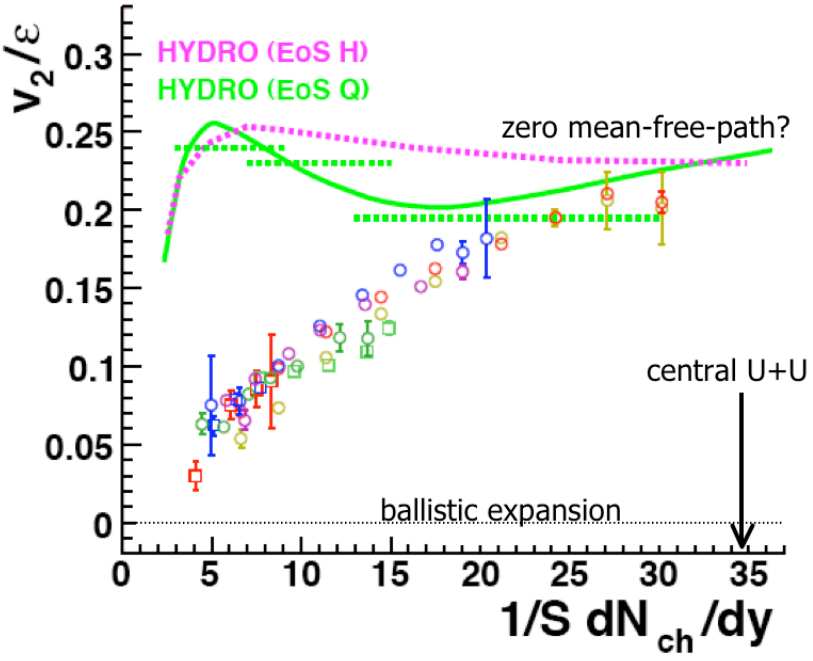

Figure 5-1: Heavy ion data on eccentricity scaled v_2 vs. transverse particle density. A central U+U collision is expected to reach densities 30% larger than central Au+Au while the eccentricity is large. Estimates for 1/S dN_{ch}/dy from [1].

Grazing (non-central) collisions of spherical nuclei produce elliptic shaped overlap areas. The expansion of and radiation from the produced spatially asymmetric fireball, assumed to be thermally equilibrated, can yield large asymmetries in momentum space. The momentum space anisotropy is therefore a sensitive probe of the dynamics of the expanding system. These anisotropies are quantified by the various coefficients in the Fourier expansion of the azimuthal distribution of the transverse momenta (or number of particles). The second coefficient, v_2, is a measure of anisotropy arising due to the elliptic shaped overlap zone. In the low density limit of the matter in the overlap region, v_2 is proportional to the initial state spatial anisotropy (eccentricity ε) and the amount of scattering, where the latter enables thermalisation and is large for a large particle density in the transverse plane. The hydrodynamic limit assumes complete thermalization, with a mean free path much smaller than the system size, where the values of v_2 may depend only on the initial state spatial

anisotropy. While results on v_2 scaled with the initial state spatial anisotropy ε for smaller colliding systems at lower center of mass energies have shown a linear dependence on the transverse particle density, as expected from the low density approximation, v_2/ε for nearly central Au+Au collisions at 200 GeV approaches values close to those predicted for a system with zero mean-free-path where a hydrodynamic description of the expansion may be valid. Ideally, one would like to investigate the effect of increase in transverse particle densities on values of v_2/ε, to probe well into the region of hydrodynamic scaling to confirm the relevance of a hydro limit. While saturation of scaled anisotropy with increasing transverse particle densities would validate the existing hydro models, a linear increase in its value would imply a different value of the hydro limit arising from a stiffer equation of state.

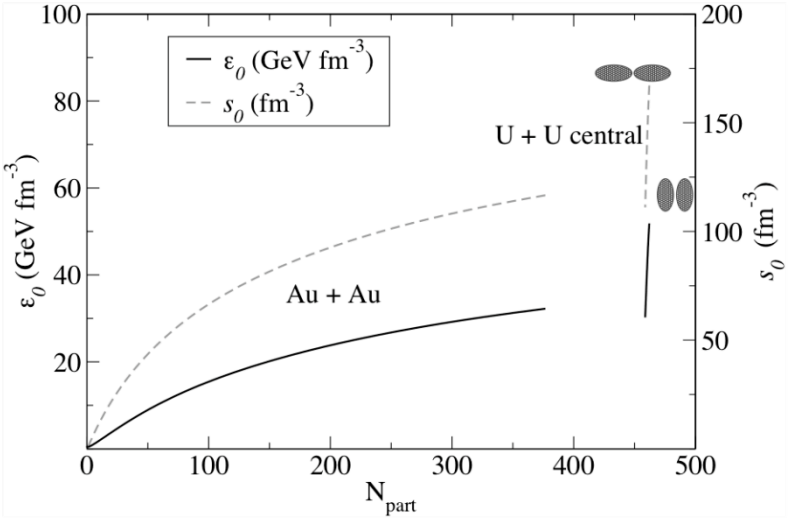

Figure 5-2: Schematic of achievable energy density (ε_0) and entropy density (s_0) in U+U collisions, for two extreme geometrical cases. Figure from [4].

The Pb ion beams at the Large Hadron Collider at CERN will provide an opportunity to probe the hydro limit by increasing the transverse particle densities by approximately a factor of 2 above those at RHIC. U+U collisions can bring experiments at RHIC a significant fraction towards this increase, with estimates ranging from a 30% to 50% increase in entropy and energy density in central U+U collisions as compared to central Au+Au collisions [1-5].

One major advantage of accelerating the Uranium nuclei, as compared to any spherical nuclei, is the possibility of a large initial state spatial anisotropy in central collisions, depending upon the relative orientation of the two nuclei at the time of collision. The large particle densities in central collisions, along with the large values of the eccentricity, will provide a unique opportunity to probe the hydro limit at available RHIC energies. It is imperative that one estimates the effect of the non-spherical shape of Uranium nuclei on the various parameters that help probe the hydro limit.

Model calculations using an initial state geometry based on Glauber model and using a two component model for obtaining the charged particle multiplicities are used to estimate the

multiplicities expected in Uranium+Uranium collisions in different orientations. The free parameters of the two component models have been fixed using Au+Au data at RHIC energies. The multiplicities for different centralities and different orientations have also been estimated using the KLN model, incorporating saturation physics through the Color Glass Condensate. Both models can reproduce existing multiplicity data in Au+Au collisions, and both models predict that the highest multiplicities in U+U will occur in tip-on-tip collisions. The challenge of the program is to be able to trigger on events that selects preferential eccentricities. It has been shown that by triggering both on the number of spectator nucleons, and the total multiplicities, it should be possible to select events with a given average source eccentricity, as shown in Figures 5-3 and 5-4.

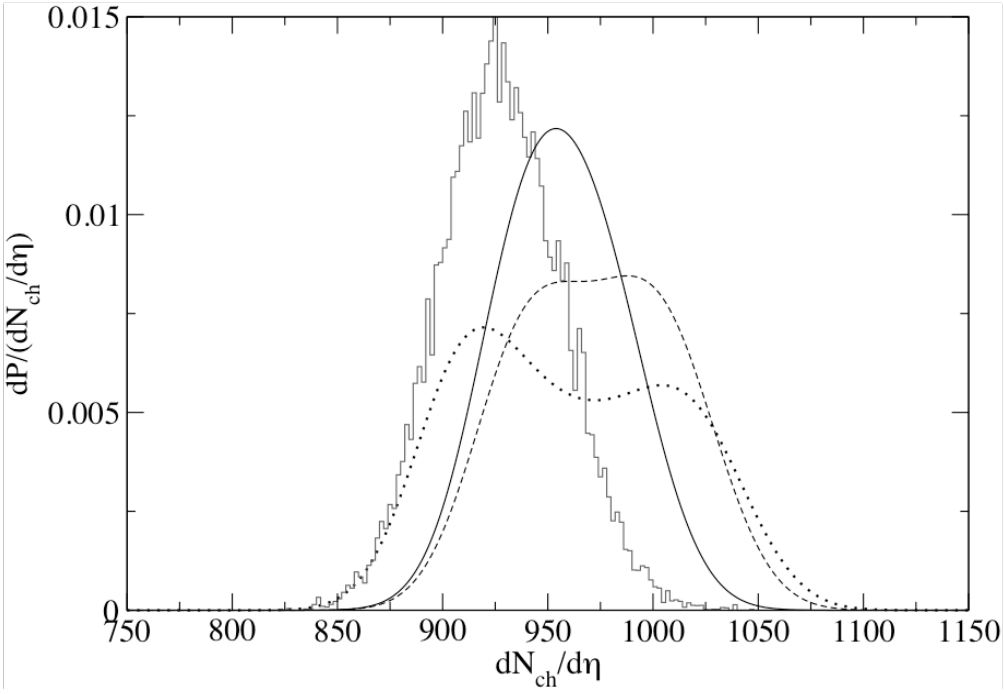

Figure 5-3: $dN_{ch}/d\eta$ for full-overlap U+U collisions. Dotted curve from Glauber + 2-component model, dashed and solid curves from CGC-related KLN model with two p_T cuts, histogram from cutting on the 0.5% fraction with lowest number of spectators. Figure from [5].

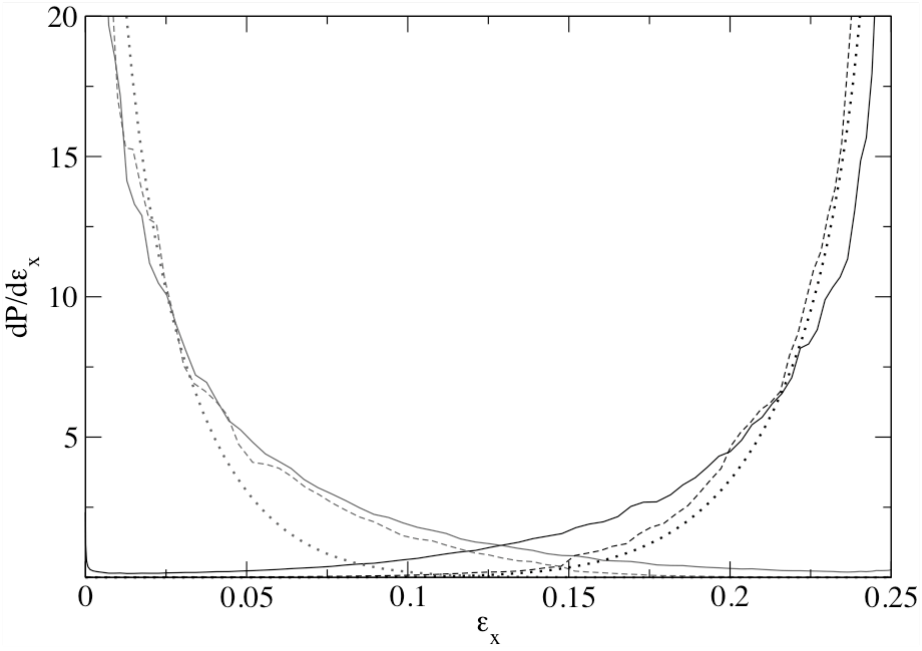

Figure 5-4: Eccentricity distribution for full-overlap U+U collisions, obtained by cutting the multiplicity distribution in Figure 5-3 on the 10% lowest (black) or highest (grey) multiplicities. Dotted curve from Glauber + 2-component model, dashed and solid curves from CGC-related KLN model with two p_T cuts. Figure from [5].

While the model calculations show promise in sampling the cutspace, significant uncertainties remain, which need data to fully resolve. Two different mechanisms are able to explain the multiplicity distributions in Au+Au collisions: the Glauber model, along with a two-component model of particle production, and KLN models incorporating saturation physics through the Color Glass Condensate. These two models give significantly different predictions for multiplicity distributions, as shown in Figure 5-3. The Glauber calculation has the largest range of multiplicities, and so distinguishing power for geometries, while the KLN calculation has a more limited range. Distinguishing between these models is a matter for experimental measurement. This is both an advantage, in that new constraints can be placed on the mechanism underlying bulk particle production at RHIC, and a disadvantage, in that this mechanism needs to be understood before more complicated measurements relying on geometry, such as elliptic flow, can be interpreted.

The values of initial state eccentricity also depend on the model used for its estimate. The distributions of eccentricities for the class of events obtained using the above mentioned models are shown in Figure 5-4.

Despite quantitative differences between results of model calculations, in Figure 5-4 the qualitative features of U+U collisions remain: there are broad classes of central U+U events, either tip-on-tip with large multiplicity and small eccentricity or side-on-side with small multiplicity and large eccentricity, which can be selected with distinct experimental signatures. Other selection criteria, such as directly selecting on the strength of v_2 event-by-event [3] or selecting asymmetries in rapidity, are under active investigation.

Beyond investigating geometry and hydrodynamic behavior, the grossly deformed overlap zone will enable an investigation of the path length dependence of energy lost by a parton. Current theories assume a non-linear dependence, but this has not yet been tested in experiment, partially because of the small difference in path lengths for the parton traversing in plane and out of plane. Side by side U+U collisions are expected to provide almost twice as much difference between the in plane and out of plane path lengths for the same eccentricity as semi-peripheral Au+Au collisions. With modest data samples, these path length effects can be investigated via single-hadron and di-hadron suppression, as done in RHIC Runs 1,2, and 4. More detailed investigations utilizing rarer probes await high luminosity running.

The unique geometry of U+U collisions opens up an exciting possibility in Ultra-Peripheral Collisions studies. These studies are based in coherent phenomena across the entire nucleus, which can be affected significantly by quantum correlations. The geometry of U+U collisions can enhance the probability for multiple vector meson production and multi-photon interactions to occur. Based on the production rates for single and double ρ production [6] and assuming the cross-section scales as $Z^8*[A^{5/3}]^2$, about 1 out of 1,000 ρ^0 should be accompanied by a second ρ^0. Such multi-ρ samples enable the study of quantum correlations in production and decay, in which stimulated decay is a possibility.

5.2. U+U Beam Use Request for Run 11

The physics of U+U collisions can be split into two distinct classes, which have distinct requirements for beam conditions. The first class consists of bulk observables, such as multiplicity, elliptic flow, HBT, and the like. These have relatively small requirements in terms of the number of events, and are mainly focused on hydrodynamic behavior of the medium, though some measurements related to hadron quenching in medium can be made with such samples (as in the first years of RHIC Au+Au). This class also contains the light vector meson portion of the Ultra-Peripheral Collision program.

The second class of measurements consists of rare, triggered probes, such as γ-hadron, jets, and heavy flavor suppression, which are extremely luminosity hungry. Due to the large configuration space for the relative orientation of the two U nuclei at the collision point, restrictive cuts on data samples need to be made in order to select the most interesting densities and geometries. The authors of [4] and [5] advocate placing 0.5% cuts on spectators, combined with 5-10% cuts on multiplicity, decreasing sample sizes from minimum bias by a factor of a few thousand. This implies that rare probes need high luminosities, which are likely not achievable in Run 11.

With DAQ1000 and a modest collision rate of 5-10 kHz, we estimate that STAR can accumulate 400M events, approximately half central and half minimum bias, in 4 weeks' time. The central trigger will likely be based on the number of spectator neutrons seen in the ZDC, which has single-neutron resolution and has been used successfully in all previous Au runs as a centrality trigger. The precise selection of centrality fraction in this trigger will depend on available collision rates.

Such a sample should allow for sufficiently fine-grained selection of geometries to investigate the behavior of v_2, HBT with respect to the reaction plane, and related measurements. It will also allow for some measurements related to jet quenching, such as

suppression of single-hadron spectra and di-hadron correlations, at accuracies approximately at the level investigated in Au+Au collisions in Runs 2 and 4. Should the machine deliver higher luminosities, we would begin the program of triggered probes analogous to that in Au+Au Run 10.

References

[1] C. Nepali et al., Phys. Rev. C 73, 034911 (2006).
[2] A.J. Kuhlman and U.W. Heinz, Phys. Rev. C 72, 037901 (2005).
[3] C. Nepali et al., Phys. Rev. C 76, 051902(R) (2007).
[4] U.W. Heinz and A.J. Kuhlman, Phys. Rev. Lett. 94 132301 (2005).
[5] A.J. Kuhlman, U.W. Heinz, and Y. Kovchegov, Phys. Lett. B 638, 171 (2006).
[3] S. Klein, J. Nystrand, Phys. Rev. C 60, 014903 (1999).

6. Run 11: Return to p+p Collisions

6.1. Recent spin physics results

6.1.1. STAR transverse spin program

The study of transverse spin effects, both theoretically and experimentally, has received a great deal of attention in recent years. The ultimate goal of this effort is to extract transversity distribution functions and determine possible orbital angular momentum effects.

The first measurement of a transverse single-spin asymmetry, A_N, for forward neutral pion production at $3.3 < \eta < 4.1$ by the STAR collaboration [1] was found to increase with x_F similar in magnitude to the measurement of A_N performed by the E704 experiment at $\sqrt{s}$ =20 GeV [2]. The STAR collaboration has performed cross-section measurements for forward neutral pion production at $\langle\eta\rangle$=3.3, 3.8 and 4.0, which are found to be in good agreement with next-to-leading order (NLO) perturbative QCD calculations [3]. This provides an important basis for the interpretation of the sizable measured asymmetries at forward rapidity.

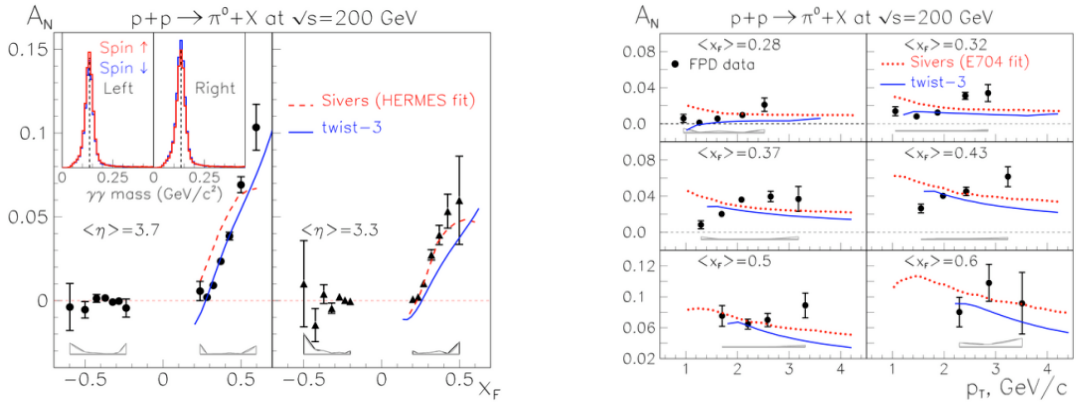

Figure 6-1: (Left) A_N as a function of x_F for p+p → π^0+X from Run 6. The error bars represent statistical errors only. Systematic uncertainties are indicated by the bands at the bottom of the plots. The solid blue line represents the result of a twist-3 calculation; the dashed red line is the result of a calculation based on the Sivers effect. (Right) A_N as a function of p_T for p+p → π^0+X from Run 6 in bins of x_F in comparison to a calculation based on the Sivers effect (dashed red line) and twist-3.

The STAR collaboration performed an upgrade of the Forward Pion Detector (FPD) for Run 6 as a prototype for the Forward Meson Spectrometer (FMS). These results are shown in Figure 6-1 and are found to be in good agreement with previous results [4]. The measured asymmetry A_N is found to be consistent with zero at negative x_F and grows from 0 at x ~ 0.2-0.3 up to 0.1 at x_F ~ 0.6. The figure also shows the results of two calculations at different $\langle\eta\rangle$ values [5,6]. The extended kinematic region in x_F and p_T and the increase in the available data sample from Run 6 allow a mapping of A_N in x_F and p_T. Figure 6-1 (right) shows A_N as a function of p_T in fine bins of x_F. The current measured results for A_N do not support a decreasing behavior of A_N with p_T in all x_F bins as expected by various theoretical models. The Run 8 data sample provided not only an important reference pp data sample for the dAu data set in Run 8, but also provided a first measurement of the transverse single-spin asymmetry A_N using the FMS, which provides about a factor of 20 increase in acceptance compared to the previous modular FPD detectors. It is anticipated that the FMS will provide new information about transverse single spin-asymmetries. To make a point of contact with previous work, a first analysis of the x_F dependence of the A_N for the $p\uparrow+p \rightarrow \pi^0 +X$ from the FMS was completed. Figure 6-2 shows the FMS result for A_N as a function of x_F covering a pseudo-rapidity range of $2.5<\eta<4$.

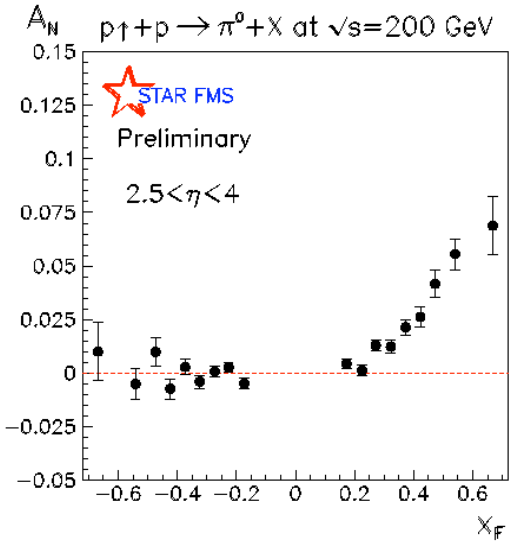

Figure 6-2: A_N result as a function of x_F for forward neutral pion production in Run 8 using the FMS detector.

The STAR collaboration extended the well-established result for forward neutral pion production for transverse single-spin asymmetries to forward η production based on the Run 6 data sample. Figure 6-3 shows the first η result for A_N as a function of x_F. The surprising observation is that in this kinematic region, the η asymmetry is larger than the already large π^0 asymmetry. This is similar to the finding by E704. The errors in this figure are statistical, with preliminary estimates of systematic error much smaller

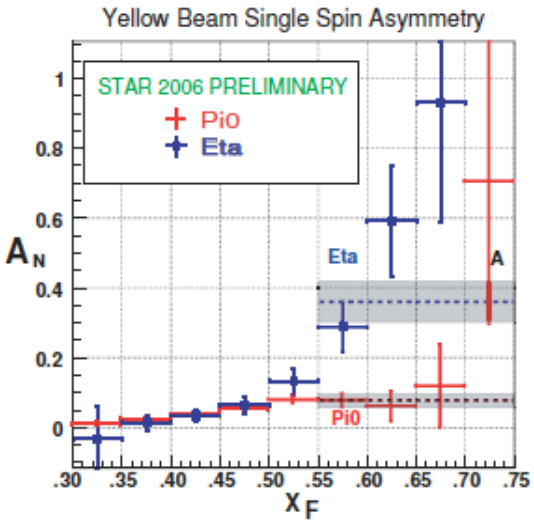

Figure 6-3: A_N result as a function of x_F for forward η production in Run 6.

6.1.2. STAR longitudinal spin program

The longitudinal STAR spin physics program profits enormously from the unique capabilities of the STAR experiment for large acceptance jet production, identified hadron production and photon production [7]. The measurement of the gluon polarization through inclusive measurements such as jet production and π^0 production has so far been the prime focus of the physics analysis program of the Runs 3, 4, 5, and 6 data samples. The sensitivity of these inclusive measurements to the underlying gluon polarization in high-energy polarized proton-proton collisions has been discussed in detail [8]. Inclusive hadron production and jet production are strongly affected by the relative contributions from quark-quark, quark-gluon and gluon-gluon subprocesses. The low p_T region is dominated by gluon-gluon scattering, while at high p_T the quark-gluon contribution starts to become important. As a result, the sign of A_{LL} in this high p_T region indicates the sign of the gluon polarization. The fact that the inclusive photon channel is dominated by quark-gluon scattering results in a strong sensitivity to the underlying gluon polarization, despite the small production cross-section. Throughout the following discussion, four gluon polarization scenarios have been used as input to NLO perturbative QCD calculations of A_{LL}. The GRSV standard case refers to the best global analysis fit to polarized DIS data [13]. The case for a vanishing gluon polarization (GRSV-ZERO) and the case of a maximally positive (GRSV-MAX) or negative (GRSV-MIN) gluon polarization have been also considered. In addition, the global analysis result by the group of Gehrmann and Sterling (GS) has been used, specifically the set C of polarized parton distribution functions[14]. The polarized gluon distribution function has a node in the measured kinematic region being negative at large x and positive at low x values which results overall in a larger first moment value compared to the GRSV-STD scenario.

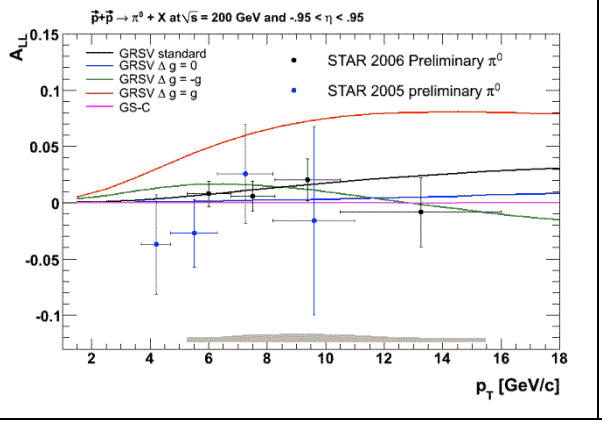

Figure 6-4: Longitudinal double-spin asymmetry A_{LL} for neutral pion production at $\sqrt{s} = 200$ GeV as a function of p_T for Runs 5 and 6 in comparison to several gluon polarization scenarios.

The Run 6 measurement of the longitudinal double-spin asymmetry for inclusive jet production provides a substantial improvement over previous measurements and clearly rules out extreme gluon polarization scenarios, suggesting that the gluon polarization in the measured kinematic region is rather small. Furthermore, an update of the preliminary result on neutral pion production based on Run 6 data has been released. A new measurement of charged-pion / jet correlations in Run 6 allows to reduce trigger bias uncertainties, which are the dominant systematic uncertainty of the Run 5 charged pion result.

Figure 6-4 shows A_{LL} for neutral pion production at mid-rapidity as a function of p_T based on the 2006 data sample. This new measurement is shown in comparison to NLO calculations assuming different Δg scenarios. This measurement reaches to higher p_T values compared to previous measurements by PHENIX and STAR. At the present level of precision, the data excludes extreme ΔG scenarios. The STAR collaboration has recently presented also results for neutral pion production at forward rapidity based on the STAR Electromagnetic Endcap Calorimeter (EEMC) and the STAR Forward Pion Detector (FPD). These measurements provide an important milestone for future photon-jet coincidence measurements at STAR.

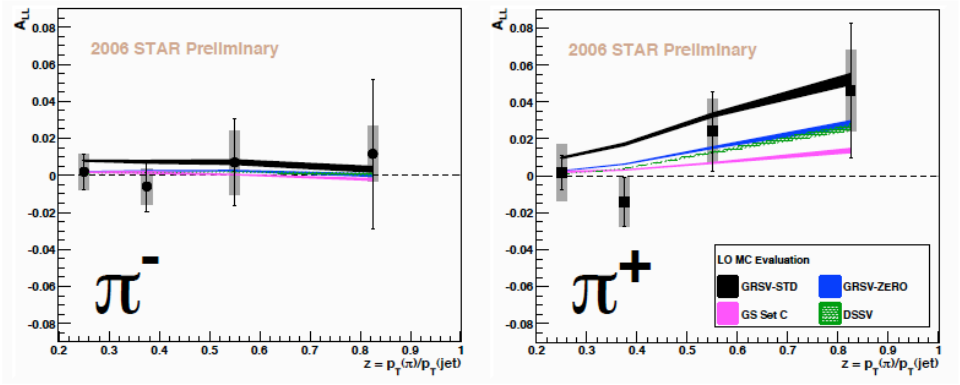

Figure 6-5: Longitudinal double-spin asymmetry A_{LL} for charged pion production at √s=200 GeV as a function of p_T (-1 < η < 1) for Run 6 in comparison to several gluon polarization scenarios.

Figure 6-5 shows STAR's new preliminary result of A_{LL} for π^- and π^+ pions that are produced at mid-rapidity and reconstructed opposite a jet that triggered the experiment. The data are shown versus $z \sim p_T(\pi^0)/p_T(\text{jet})$ and were obtained in 2006. Full NLO calculations for this observable are now available. These calculations will provide the basis for charged pion results to be included in a global analysis. The data shown for charged pion production are compared to a LO MC evaluation of A_{LL} excluding extreme scenarios of ΔG. The measurement of $A_{LL}(\pi^+)$ is of particular interest, since its gluon spin sensitivity is large because of the large ug scattering contribution to the production cross section and sizable $\Delta u/u$. Future, more precise measurements of $A_{LL}(\pi^+)$ have a great potential for providing a better understanding of ΔG.

The STAR result for Run 5 of the measurement of the longitudinal double-spin asymmetry A_{LL} for inclusive jet production [9] is shown in Figure 6-6 as a function of p_T for $5 < p_T < 30$ GeV/c in comparison to several gluon polarization scenarios as described earlier. The 2005 A_{LL} inclusive jet measurement is found to be in good agreement with the previous 2003/2004 measurements. The current measurement extends the p_T region to larger values, where the quark-gluon contribution starts to become important. This analysis rules out most GRSV fits with ΔG much larger than the GRSV std. solution. The most recent A_{LL} result for inclusive jet production is shown in Figure 6-7 which provides the most precise measurement to date to constrain the gluon polarization of the proton at RHIC. This analysis is based on a luminosity of 4.7 pb^{-1} and an average polarization of approximately 60% which resulted together with the full STAR BEMC acceptance in a factor of 3-4 improvement in statistical precision for $p_T > 13$ GeV/c compared to the Run 5 jet result.

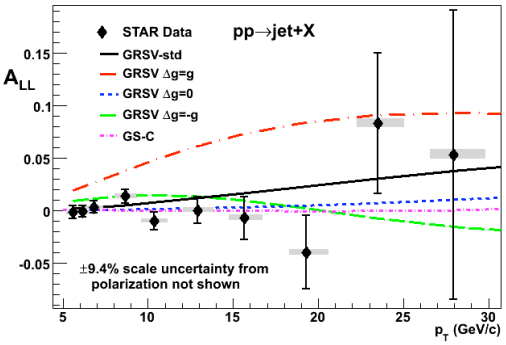

Figure 6-6: Longitudinal double-spin asymmetry A_{LL} for inclusive jet production $\sqrt{s} = 200$ GeV as a function of p_T ($0.2 < \eta < 0.8$) for Run 5 in comparison to several gluon polarization scenarios. The error bars are statistical. The gray bands show the systematic uncertainties in the measured A_{LL} and jet p_T. Figure from [9].

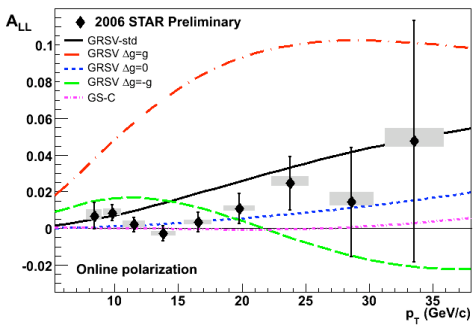

Figure 6-7: Longitudinal double-spin asymmetry A_{LL} for inclusive jet production at $\sqrt{s} = 200$ GeV as a function of p_T ($-0.7 < \eta < 0.9$) for Run 6 in comparison to several gluon polarization scenarios.

Taking all current PHENIX and STAR A_{LL} measurements together in comparison to different NLO perturbative QCD predictions for A_{LL} yields a consistent picture which clearly rules out extreme gluon polarization scenarios and suggests that the gluon polarization on average in the measured kinematic region is rather small.

6.2. Run 11 spin physics request

Run 11 presents the next opportunity to make important strides in the STAR spin physics program. With about 14 weeks in pp, there should be an opportunity to address transverse and longitudinal goals at 500 and 200 GeV It will certainly be important to see the end of run performance, look at the data from run 9 and see projected run 11 accelerator performance before setting final priorities. The current high priority goals are the following:

1) It is clear that additional experience with 500 GeV beams is required before embarking on the 300 pb^{-1} goal for the W program DOE milestone to determine the flavor asymmetry in the ubar/dbar sea quark polarizations. A seven-week run should allow for addressing some high priority transverse and longitudinal goals at this energy. A luminosity of 6.5 pb^{-1} (P=50%) integrated in transverse mode should allow for exploring the x_F dependence of the single spin asymmetry for π^0 production and forward jets. Another 15 pb^{-1} (P=50%) should allow a statistically significant parity violating A_L signal for the W^+ at mid-rapidity.

2) With the recent addition of the Forward Meson Spectrometer (FMS) it becomes a high priority to address goals in transverse polarization mode. An integrated luminosity of 15 pb^{-1} (P=65%) at 200 GeV would allow a gamma-jet A_N measurement representing 1/2 the

data required to meet the DOE milestone to check the change in sign between this channel and SIDIS expected from pQCD. In addition a proposed Forward Hadron Calorimeter would allow, in parallel, conclusive measurements on A_N for forward jets to separate Sivers from Collins mechanisms.

3) Completing a map of the x dependence of the gluon helicity contribution to the proton, a DOE milestone, remains of highest priority to our program. Completion of Run 9 and evaluation of results will be needed to asses our status with respect to our near term goal of 50 pb^{-1} (P=60%) and eventual need for 80 pb^{-1} and the increment required in Run 11 to reach the near term goal.

These physics goals, their requirements and impact are discussed in detail below.

6.3. Transverse spin program at 200 and 500 GeV

The initial STAR observations of large transverse single spin asymmetries in the production of π^0 at large x_F have attracted significant theoretical and experimental interest. Next to Leading Order Perturbative QCD forms a fairly good description of the observed π^0 spin averaged differential cross section. The asymmetries, however, vanish in leading twist QCD with collinear factorization. They thus provide the opportunity to sensitively study non-leading twist aspects of hadron interactions in processes where the underlying leading twist calculations have been shown to be meaningful.

Two basic parton model pictures have developed to explain how these asymmetries can come about. In the Sivers model, the initial transverse momentum distribution of large x quarks, in conjunction with absorptive effects, could lead to the required spin dependent transverse momentum that can explain these asymmetries. In the Collins model, corresponding higher twist effects are associated with the final state fragmentation process that produces the final state meson from a parton. The parton retains its (transverse) initial state polarization through the hard scattering process.

Subsequent STAR measurements at $\sqrt{s}$=200 GeV have studied the p_T and x_F dependence of A_N, as described before, to advance the understanding of the underlying dynamics. Large A_N have been observed also in the invariant mass region of the η meson and in the production of forward π^+, π^-, and *K* production in $\sqrt{s}$=200 GeV proton collisions at RHIC.

The HERMES and COMPASS experiments have observed transverse single spin asymmetries in semi-inclusive deep-inelastic scattering (SIDIS) from transversely polarized targets. A separation of the Sivers and Collins mechanisms from these data has been made on the basis of the orthogonal characteristic angular modulations in the SIDIS final state. The Collins asymmetries from HERMES and COMPASS proton data are comparable, with the COMPASS data extending to smaller values of *x* and having harder scales Q^2 in the *x*-region of overlap. The proton Collins asymmetries turn out non-zero for $x > 0.05$. They are negative in sign for positively charged hadrons and positive for negatively charged hadrons. The Collins asymmetries of unidentified and identified charged hadrons from COMPASS deuteron data are compatible with zero to within the statistical uncertainties, in line with the expected cancellation between the u- and d-quark contributions. The Sivers asymmetries from COMPASS data on both deuteron and proton targets are small and compatible with zero to within the statistical uncertainties. The deuteron values are consistent with the

present theoretical understanding that the Sivers functions for u- and d-quarks are opposite in sign and cancel for the isospin zero target. The COMPASS proton values form a surprise, in view of the distinctly non-zero values observed by HERMES for the proton Sivers asymmetries.

The separation of Collins and Sivers mechanisms at RHIC is a high priority goal that has thus far not been reached. The Collins asymmetries, when combined with Collins fragmentation functions, give insight in the quark transversity distributions. Collins fragmentation functions have been observed in e^+e^- collisions by the Belle Collaboration. If non-zero Sivers functions are found in both SIDIS and in polarized proton collisions at RHIC, this would provide observational evidence of parton orbital motion within the polarized proton. Further theoretical research is required to establish the connection with orbital momenta quantitatively, and additional transverse polarized proton operations at RHIC are needed to obtain such data. Theoretical research of the Sivers mechanism has led to the very interesting expectation that the Sivers function for the transverse single-spin asymmetry in Drell-Yan is exactly opposite in sign to the Sivers function from SIDIS. Experimental observation of this sign change would identify fundamental aspects of color charge interactions. Drell-Yan measurements are not presently possible with the STAR experiment at RHIC. Further theoretical research has led to the development of a similar expectation for the transverse spin asymmetries in the production of forward photons in conjunction with away-side jets in proton collisions at $\sqrt{s}$=200 GeV[17], which can be measured with STAR at RHIC using the FMS subsystem to measure the photon and the central TPC and BEMC subsystems to reconstruct the jet. This measurement forms the main motivation to request an integrated luminosity of 15 pb^{-1} with transverse proton polarizations of P=65% at $\sqrt{s}$=200 GeV in run 11. It represents a significant fraction (about 50%) of the data sample required to meet the 2015 DOE Performance Milestone (HP13) to *"test unique QCD predictions for relations between single-transverse spin phenomena in p-p scattering and those observed in deep-inelastic scattering."*

For direct photon detection with the FMS, a large-area hermetic electromagnetic calorimeter, the most effective method is to eliminate other sources of photons by direct detection. These other photon sources arise primarily from the decay of π^0 and η neutral mesons. Multiple aspects make this feasible with the FMS. First, because the calorimeter is at large rapidity, the typical photon energies are large (E_γ> 35 GeV) and in addition the hadronic response of the FMS is small. Direct simulation of the detector response via GSTAR simulations employing the GEISHA hadronic simulation, applied to full PYTHIA events of collisions have demonstrated that the hadronic response of the lead glass detectors is minimal for energy depositions in excess of 25 GeV. Second, the large Lorentz factors result in significant spatial correlations for the decay products from π^0 and η mesons. For example, when there is a candidate direct photon having E_γ = 25 GeV, 95% of the phase space for all π^0 decays that could potentially be the source of this energetic photon are contained in a circle of radius 23 cm (approximately four large cells of the FMS) around the 25-GeV photon at the face of the FMS. Finally, π^0 and η mesons are most typically produced via fragmentation in p+p collisions at RHIC energies. This means that other hadrons share the energy of the fragmenting quark or gluon, softening the decay photon spectrum. The daughter photons from π^0 and η decay then further divide this energy. In contrast, direct photons are produced in the hard scattering process. Their energy is not

shared via fragmentation nor is it shared by particle decay. The energy where direct photon probabilities exceed decay photon probabilities is ~50 GeV for $<\eta>$ ~ 3.2, with no other conditions on the event. The π^0 and η backgrounds can be reduced, and this energy can be lowered to ~25 GeV, by subdivision of the FMS into two volumes. The fiducial volume, used for identifying direct photon candidates, is a small annular region within the outer calorimeter. The remainder of the FMS is used as a veto to establish that other photons from the decay of neutral mesons are not present. The effectiveness of the discrimination between direct and decay photons is demonstrated via full collision event simulations in Figure 6-8.

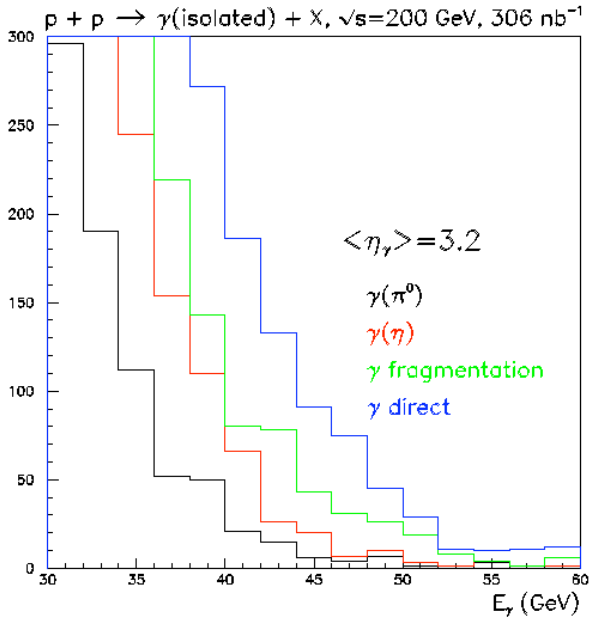

Figure 6-8: Simulation of inclusive forward photon spectrum. Direct photon candidates are detected in a small fiducial volume within the FMS. Isolation of radius, $\Delta R=(\Delta\eta^2+\Delta\varphi^2)^{1/2}$, is then required around the photon candidate, where Δη and Δφ refer to angular differences between near-side correlations with the direct photon candidate and potentially other particles.

Restricting the measurement of the forward photon to E_γ>35 GeV at $<\eta>$=3.2 produces a signal to background ratio of 2 to 1. Lower thresholds result in larger contamination, and so are undesirable. Substantial gains in yield can be realized by small changes in the fiducial volume towards smaller distance from the beam because of the very strong power law dependence on p_T. A detailed optimization of signal magnitude and signal to background ratio still must be completed.

Fragmentation photons are also a background for inclusive direct photon measurements that would require a careful study of jet asymmetries for forward jets that contain a fragmentation photon. The prediction for the sign change for transverse SSA is for a forward photon + recoil jet. The isolated fragmentation photon will have its momentum balanced by two jets, rather than one, as expected by the dominant *qg* Compton diagram. Consequently, the fragmentation photon contribution will be spread throughout a $\Delta\varphi=\varphi_\gamma-\varphi_{jet}-\pi$ distribution, whereas the signal of interest is on the sides of the peak in the Δφ

distribution, in the vicinity Δφ=0. More detailed simulations to quantify this argument are in progress.

Simulations of the Δϕ distribution for p+p → γ(forward)+jet at √*s*=200 GeV are shown in Figure 6-9. The simulations use a simple clustering algorithm to define the mid-rapidity jet, requiring a seed with transverse energy of at least 0.5 GeV. A cone radius of $R = (\delta\eta^2 + \delta\phi^2)^{1/2} = 0.7$ is used in the clustering. Here, δφ(δη) refer to the deviation of a hadron from the thrust axis of the reconstructed jet. Jet reconstruction, even at $p_{T,jet} > 2$ GeV/c, is found robust by comparison to recoil parton kinematics and by comparison to a leading particle analysis.

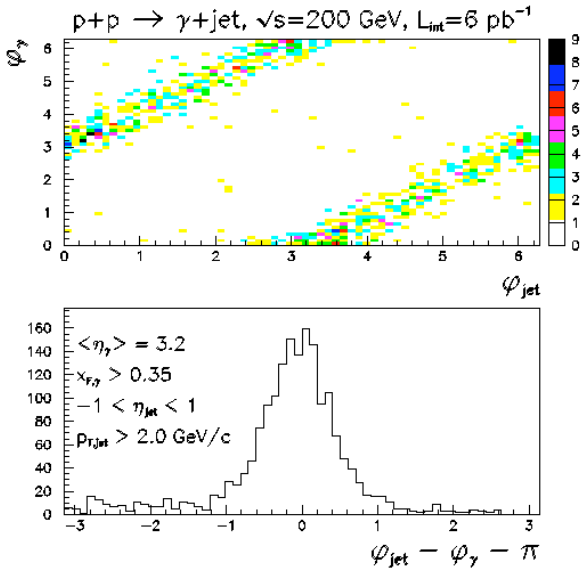

Figure 6-9: Simulation of forward photon + recoil jet for p+p collisions at √s=200 GeV.

The result of these simulations is that 10^4 useable forward photon + jet coincidences are expected in a 30 pb^1 data sample with 60% beam polarization. This thus forms our present estimate of the transverse data sample required to meet DOE performance milestone HP13. The γ(forward)+jet yield is sensitive to the jet-finding parameters and the fiducial volume requirement for the forward photon. A full optimization of the event selection to test the theoretical prediction is required, and possibly could result in robust sensitivity to the predicted sign change (>4σ) at smaller figure of merit. The request for a transverse sample of 15 pb^{-1} with P=65% in an initial run of would form a significant fraction of about 50% to perform the final measurement.

The proposed addition of two 8×8 stacks of E864 hadronic calorimeter modules immediately behind the forward meson spectrometer (FMS) would allow, if realized, to minimize the bias in triggering on and reconstructing jets that are produced at large rapidity in polarized proton collisions. In a pQCD description, jets are products of the hard scatterings of quarks and gluons. Symmetric integration about the thrust axis of hadronic fragments of the produced jet will eliminate spin-dependent fragmentation (Collins mechanism) as a contribution to the forward pion (kaon) transverse single-spin

asymmetries. Consequently, a non-zero SSA for inclusive jet production isolates contributions from the Sivers mechanism that explains transverse SSA forward pion (kaon) production by a spin-correlated transverse momentum of the partons within the proton (orbital motion). The realization of this Forward Hadron Calorimeter (FHC) in STAR is thus anticipated to enable conclusive measurements, concurrently with the γ (forward)+jet measurement, of the single transverse spin asymmetry A_N for jets to isolate the Sivers function. A proposal is in review within the collaboration. Figure 6-10 illustrates simulations of the forward jet reconstruction capability with the existing FMS and proposed FHC.

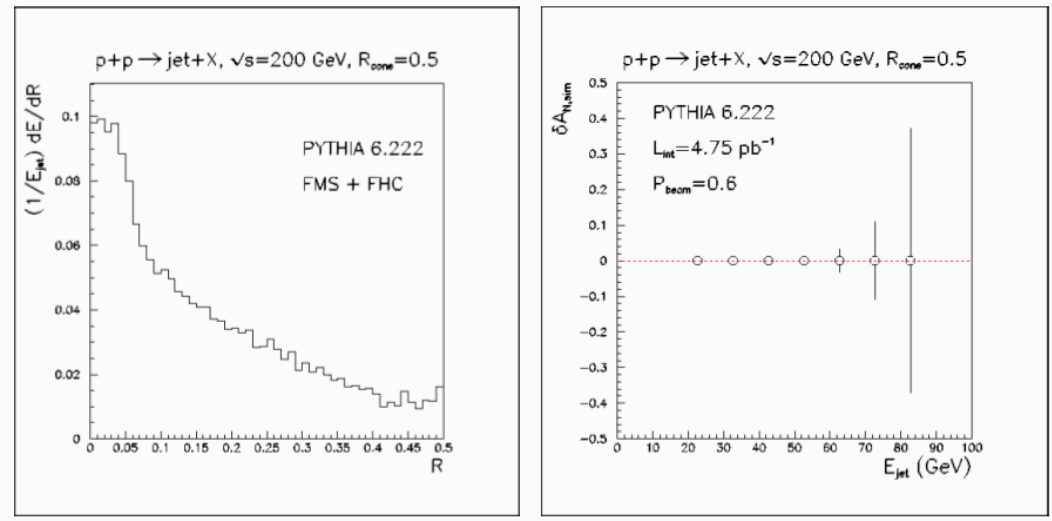

Figure 6-10: Simulations of forward jet reconstruction with the existing FMS and a forward hadron calorimeter (FHC) addition. Jets are reconstructed, using a standard jet finder used for previous studies, for electromagnetic energy and observable hadrons within the acceptance of an FMS half and a FHC module. The reconstructed jets are then subjected to acceptance cuts in η−φ space, to assure good acceptance for their hadronic fragments. The resulting narrow acceptance, centered at <η>~2.7, induces a strong x_F-p_T correlation for the jets.

Future measurements at √s=500 GeV may provide the opportunity to determine whether A_N scales with variables other than x_F and p_T, such as $x_T=2p_T/\sqrt{s}$. An integrated luminosity of 6.8 pb^{-1} with beam polarization of 55% is estimated to yield comparable quality data for $A_N(x_F)$ at √s = 500 GeV and <η>=4 as the published results at √s = 200 GeV and <η>=3.3 based on scaling properties of the unpolarized π^0 production cross section. The importance of completing this measurement is to establish if these effects persist to the highest collision energies. It is at this collision energy that a future transverse-spin Drell-Yan experiment could be completed. The requirements for specifying this future program include knowing that the spin effects persist, and benchmarking simulations against data, so they can fully establish remaining instrumentation required for a future transverse spin Drell-Yan experiment.

Above, we have described the main physics motivations and primary basis to request polarized proton operation in transverse mode for an integrated luminosity of 15 pb^{-1} with P=65% at √s=200 GeV and 6.5 pb^{-1} at P=50% at √s=500 GeV. We anticipate that these data samples will lead to many other interesting observations, including for example the

mapping of A_N in the invariant mass region of the η meson in x_F and p_T, as has been the case for proton operation in transverse mode in the past.

6.4. Longitudinal spin program at 500 GeV

Following year 11 it is expected that the focus of the STAR spin program will switch to W production with $\sqrt{s}$ =500 GeV polarized pp collisions. This channel has long been identified as a means to measure the polarization of sea quarks [10,11]. It can provide direct access to the difference between the polarizations of u-bar and d-bar quarks, a quantity sensitive to underlying mechanisms which produce the polarized sea [12]. In STAR, W detection will be primarily through $W^- \rightarrow e^- \nu$ and to e^+ for the W^+. Charge sign discrimination is essential to separate the u-bar and d-bar contributions. Construction of a Forward GEM Tracker to provide charge sign discrimination in the forward direction, $1 < \eta < 2$, is currently underway and will be fully installed for run 12. In Figure 6-11 we show predictions for various underlying quark and anti-quark distributions based on GRSV-STD, GRSV-VAL [13] and GS-A [14] calculated with RHICBOS [15], a program that incorporates an NLO calculation of spin observables in W production. GRSV-VAL considers a flavor asymmetric scenario of Δu and Δd. It is qualitatively similar to the sea quark distributions in DSSV. In contrast, GRSV-STD is based on a flavor symmetric description. Since the cross section for W production is small, a large integrated luminosity is required. The calculations show that $300 pb^{-1}$ provides significant discrimination between these models setting the scale for goals in the $\sqrt{s}$ =500 GeV spin program.

An extensive effort to simulate electron - hadron discrimination in the forward direction covered by the EEMC were completed in the last year. This analysis makes use of Pythia and GEANT simulations in the full STAR software framework. The effort is quite CPU intensive and special algorithms have been developed to preselect events capable of depositing significant energy in the EM calorimeters. Still it has required the use of a Tier2 grid facility to generate sufficient hadronic background samples for the studies. The projected sensitivities from these studies are shown in Fig. 6-11.

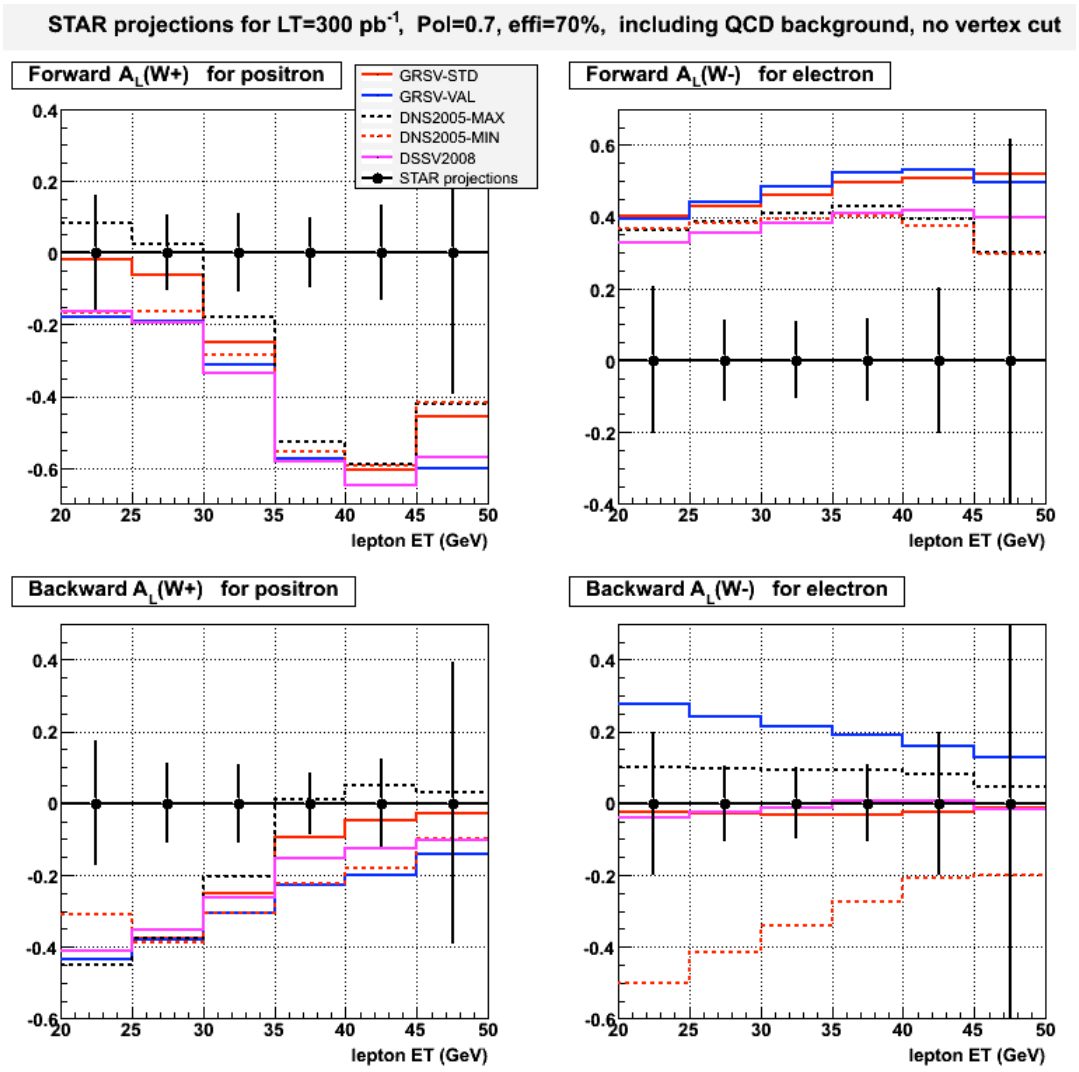

Figure 6-11. Estimation of expected precision for the single spin parity violating asymmetry for W production in proton - proton collisions at $\sqrt{s}$ =500 GeV. Full simulations of backgrounds are used along with necessary estimated background subtractions to arrive at the estimated errors.

It is clear that before embarking on the long high intensity, high polarization runs required for these measurements additional experience with the 500 GeV beam is required. An approximately 7 week run at this energy in run 11 would provide that experience while addressing the transverse goals for 500 GeV as discussed above. In addition if sufficient progress is made on luminosity there should also be time to switch to longitudinal mode and obtain a statistically significant non-zero measurement of the parity violating longitudinal single spin asymmetry for W^+ production as shown in Fig. 6-12. A minimum of 10 pb^{-1} and 50% beam polarization would be required.

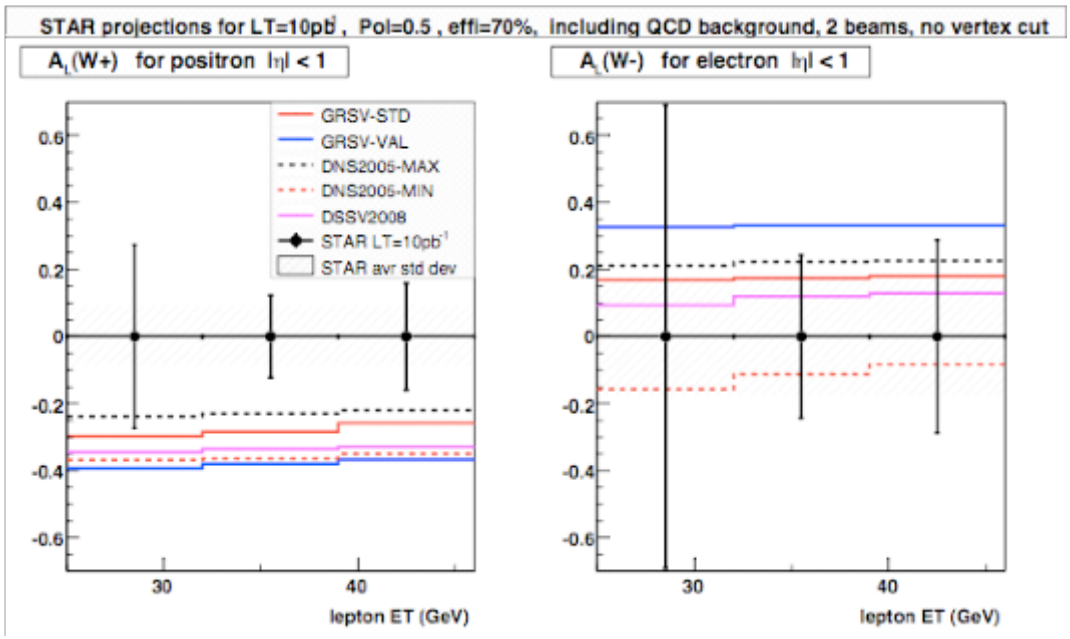

Figure 6-12. Projected sensitivity to the parity violating longitudinal single spin asymmetry for W+ production at 500 GeV with 10 pb-1 and P=50%.

It is also of interest to continue with the gluon polarization measurements at 500 GeV. In particular the higher energy allows for access to lower x. These measurements are double spin asymmetries, A_{LL}, and hence are affected more quickly by low polarization. In addition the asymmetries of interest are anticipated to be quite small as shown for full statistics at 300 pb^{-1} in Fig. 6-13 for inclusive jets and for dijets in Fig. 6-14. Improved polarization in run 11, above that of the 500 GeV run 9, running period should allow a serious start on the 500 GeV jet based program to study ΔG.

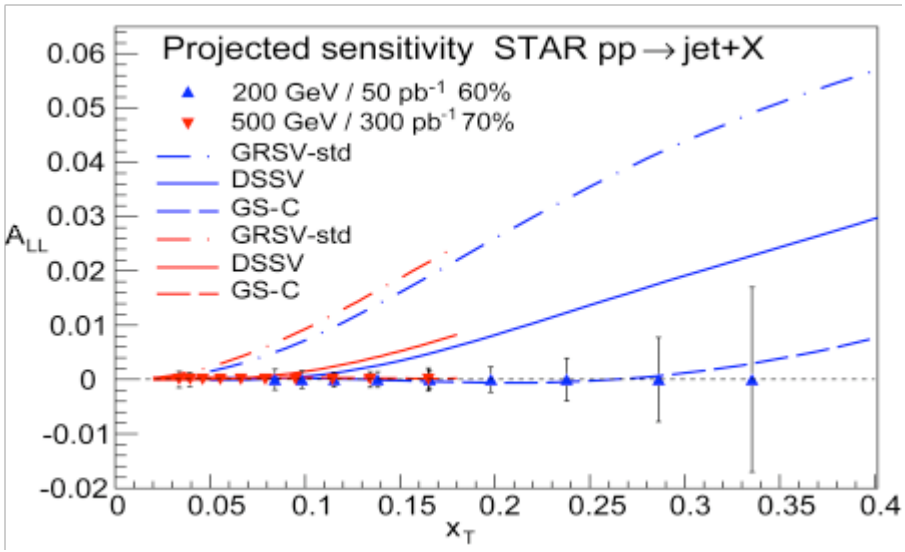

Fig. 6-13. Projections for the double spin asymmetry A_LL at 500 GeV for inclusive jets compared to expected precision at 200 GeV. The data is plotted vs. x_T to give the relative comparison at the same x_g for the different beam energies.

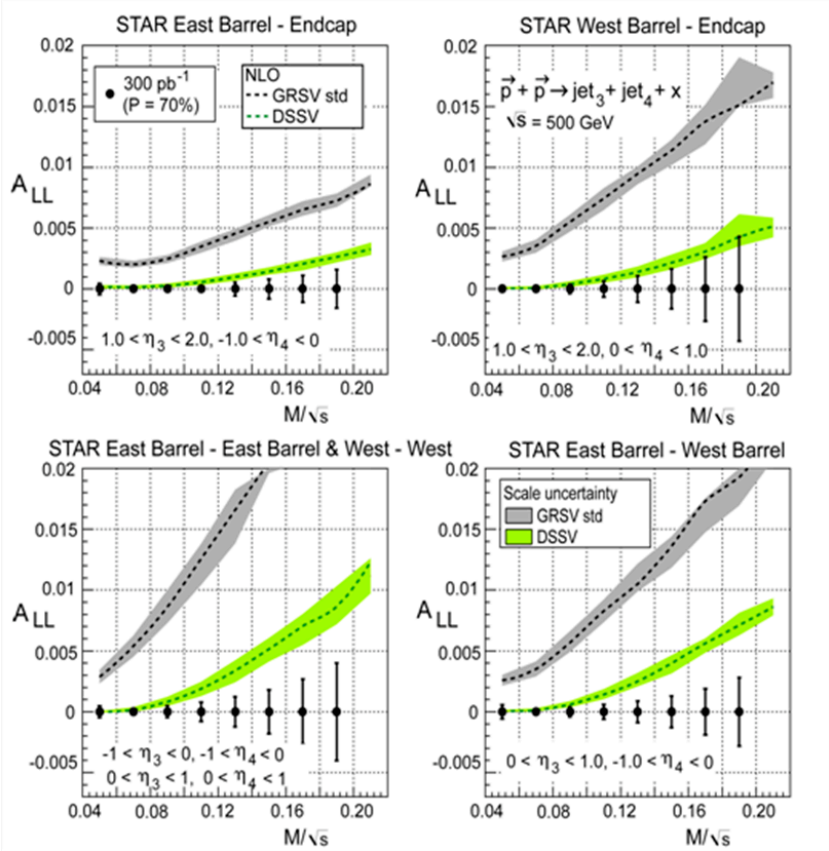

Figure 6-14: Dijet projections for 500 GeV collisions assuming 300 pb^{-1} and 70% beam polarization.

6.5. Longitudinal spin program at 200 GeV

The primary goal for the longitudinal spin program at 200 GeV is to advance our understanding of the gluon polarization based on three key measurements:

i) Di-Jet production over a wide kinematic region profiting from the large calorimetry coverage in STAR

ii) Precision inclusive measurements at large transverse momentum, in particular for the case of inclusive jet production, which had been so far the flagship of the STAR longitudinal spin program

iii) Embark on prompt photon measurements and photon-jet measurements

Di-Jet production is a key element of the STAR longitudinal spin program. As discussed previously, di-jet production provides sensitivity to the underlying partonic kinematics beyond inclusive measurements, which simply integrate over the measured kinematic region. The recent global analysis by DSSV [16] suggest a gluon polarization at the initial scale with a node around x=0.1 with a positive value for x>0.1 and a negative value for x<0.1. Although these features will evolve to the measurement scale it is extremely

important to enhance those Bjorken-x regions through specific kinematic cuts. Di-jet production in STAR does indeed allow such a unique selection. Figure 6-15 shows the longitudinal double-spin asymmetry A_{LL} for di-jet production as a function of the invariant mass M for different topological combinations of the STAR BEMC and STAR EEMC region. The projected uncertainties are shown for a luminosity of 50 pb^{-1} and a beam polarization of 60% (a fraction of which is currently being taken in run 9) including detector effects. Those projected uncertainties are compared to LO and NLO evaluations of A_{LL}. The A_{LL} curves at LO are shown for GRSV-STD and GRSV-ZERO, the former a best fit to DIS data circa 2001 and the latter with the gluon helicity set to zero at the input scale. In addition to those parton distribution functions, a LO calculation based on GS-C and GRSV-m0.3 has been performed, where the latter refers to the case of a GRSV-type gluon polarization with a first moment of -0.3 at a scale of 1 GeV^2. A_{LL} predictions at NLO are shown for GRSV-STD and DSSV, including an estimate of the uncertainty due to scale variations. The east barrel – west barrel combination probes symmetric partonic collisions at large x values, whereas the combination east barrel – endcap probes asymmetric partonic collisions allowing to access smaller x values. The projected uncertainties are such that discrimination between GRSV-ZERO and GS-C should be possible. Those gluon distribution functions have a rather different underlying behavior and in particular first moment. Di-Jet production with a minimum integrated luminosity of 50 pb^{-1} and a beam polarization of 60% would allow a substantial improvement of our understanding of the gluon polarization.

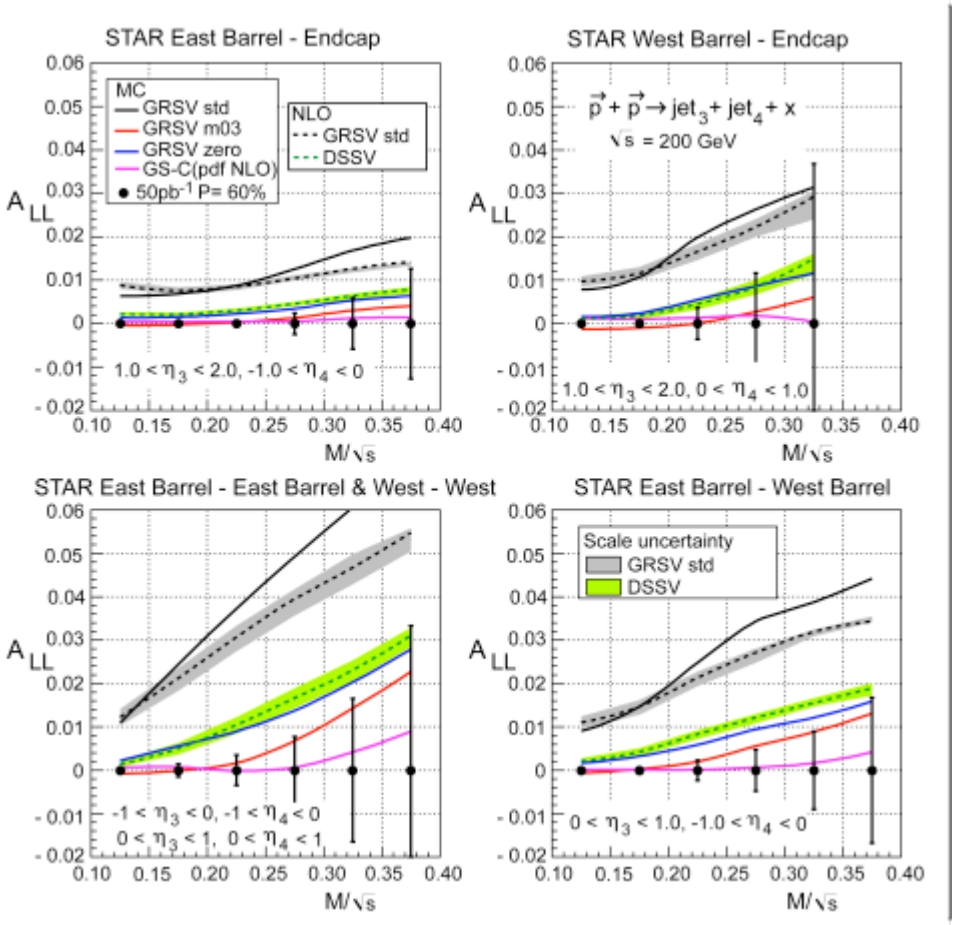

Figure 6-15: Longitudinal double-spin asymmetry A_{LL} for di-jet production as a function of the invariant mass M for different topological combinations of the STAR BEMC and STAR EEMC region. The projected uncertainties are shown for a luminosity of 50pb^{-1} and a beam polarization of 60%. Those projected uncertainties are compared to LO and NLO evaluations of A_{LL}.

The potential for inclusive jet production for Run 9 is discussed in the following in the context of the recent global analysis by DSSV [16]. Figure 6-16 shows the gluon polarization as a function of x including the inclusive jet result from STAR and the neutral pion result from PHENIX for Run 6 (top) and based on a data sample of 50pb^{-1} and a beam polarization of 60% (bottom). The uncertainty is substantially reduced which is shown as a variation of the total χ^2 by 1 unit in green and by a 2% variation of the total χ^2 in yellow. The corresponding current and projected χ^2 distributions are shown in Fig. 6-17. This underlines the clear potential of the inclusive jet program of STAR in Run 9 to further reduce the actual uncertainty on the extracted gluon polarization.

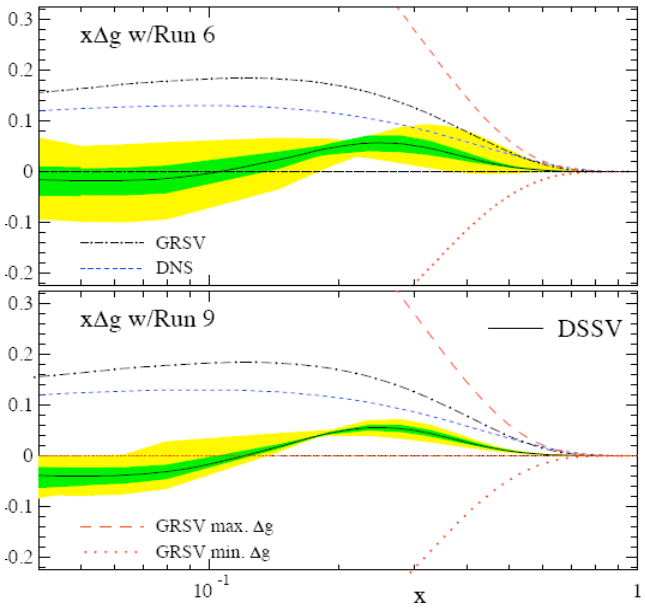

Figure 6-16: Gluon polarization as a function of x for the inclusive jet result from STAR and the neutral pion result from PHENIX for Run 6 (top) and the projected performance for Run 9 (bottom) based on a data sample of 50pb^{-1} and a beam polarization of 60%.

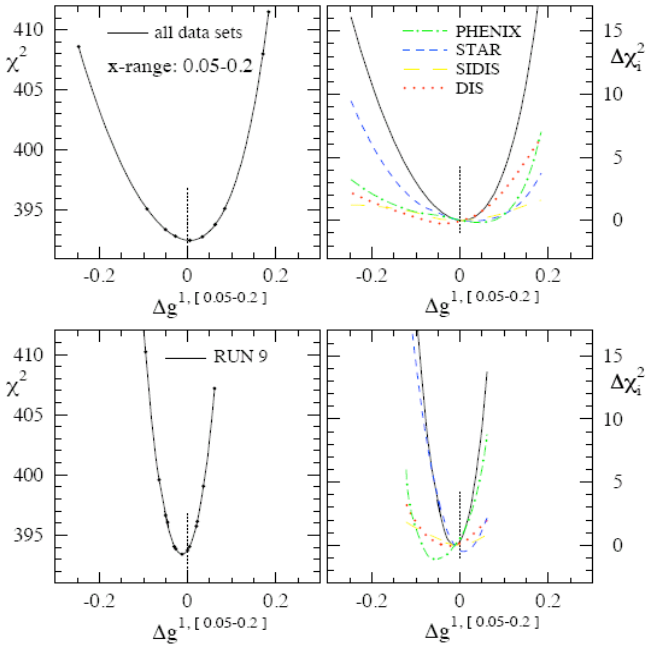

Figure 6-17: χ^2 as function of the truncated first moment (0.05, 0.2) including the inclusive jet result from STAR and the neutral pion result from PHENIX for Run 6 (top) and the projected performance for Run 9 (bottom) based on a data sample of 50pb^{-1} and a beam polarization of 60%.

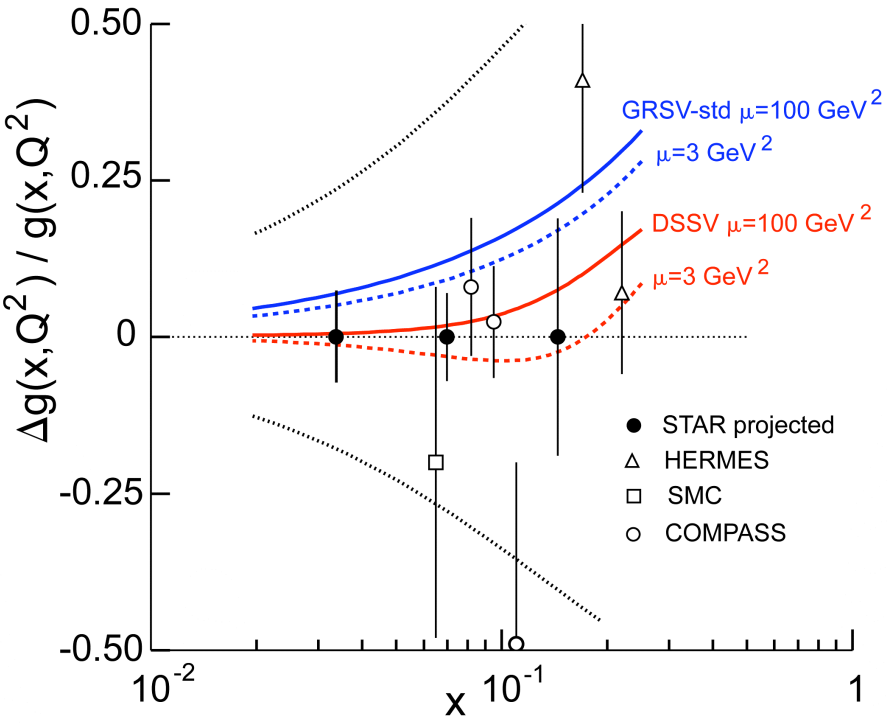

Figure 6-18: Projected uncertainties for Δg/g as a function of x for photon-jet measurements at $\sqrt{s}$ = 200 GeV for an integrated luminosity of 50pb^{-1} and 60% beam polarization. Experimental efficiencies are not yet taken into account. Also shown are current world data from high-p_T hadron (pair) and open charm production in fixed-target polarized lepton-nucleon experiments by the COMPASS, HERMES, and SMC collaborations.

In addition to the proposed measurements of inclusive jets and di-jets, we propose to make significant photon-jet coincidence measurements at $\sqrt{s}$ = 200 GeV and eventually $\sqrt{s}$ = 500 GeV. These measurements are sensitive mostly to quark-gluon scattering and thus allow the rather direct determination of the polarized gluon distribution Δg(x) as a function of gluon fractional momentum x.

At the time we have not yet completed a full evaluation of the sensitivities that STAR photon-jet measurements will yield. Analyses on previous years data is proving challenging but proceeding. We have estimated sensitivities in the acceptance of the barrel and endcap calorimeters at the PYTHIA event generator level for the nominal integrated luminosity of 50 pb^{-1} and 60% beam polarization expected to be achieved in the near term. It is anticipated that 80pb^{-1} will be necessary to fully exploit this channel. These projected sensitivities are shown in Figure 6-18, together with current world data from high-p_T hadron (pair) and open charm production in fixed-target polarized lepton-nucleon experiments by the COMPASS, HERMES, and SMC collaborations. In addition representative polarized gluon distributions are shown at the scales typical of the STAR proposed measurements, $\mu^2 \approx 100$ GeV^2, and of the lepton-nucleon measurements of high p_T hadron(s), $\mu^2 \approx 3$ GeV^2.

The scale, $\mu^2 \approx 13$ GeV^2, of the COMPASS open charm measurement is in between the shown scales. We expect Run 9 will provide us with the most substantial sample of gamma-jet events to date and allow further refinement of the analysis techniques and estimates of required luminosity.

At the writing of this document we are mid-way through the 200 GeV running period so the final integrated luminosity and polarization for this data set is very uncertain. However, it seems unlikely that the full run 9 goal of 50 pb^{-1} at 60% polarization will be met. The final performance of beam delivery and yield from the data set will be required to estimate the quantity of data required in future runs to achieve 80 pb^{-1} and our physics goals.

References

[1] J. Adams et al. (STAR Collaboration), PRL 92, 171801 (2004).

[2] D. Adams et al, (E704 Collaboration), PLB 261, 201 (1991); ibid 264, 462 (1991).

[3] J. Adams et al. (STAR Collaboration), PRL 97, 152302 (2006).

[4] B.I Abelev et al. (STAR Collaboration), PRL 101, 222001 (2008).

[5] C. Kouvaris et al., hep-ph/0609238.

[6] U. d'Alesio and F. Murgia, private communications.

[7] K.H. Ackermann et al. (STAR Collaboration), NIM A499, 624 (2003).

[8] B.Jaeger, M. Stratmann and W. Vogelsang, PRD 70, 034010 (2004).

[9] B.I. Abelev et al. (STAR Collaboration), Phys. Rev. Lett. 100, 232003 (2008).

[10] G. Bunce, N. Saito, J. Soffer, and W. Vogelsang, Ann. Rev. Nucl. Part. Sci. 50, 525 (2000), hep-ph/0007218.

[11] RHIC SPIN collaboration, G. Bunce et al., BNL internal document, Status and Prospects of the RHIC Spin Physics Program.

[12] D. de Florian, G. A. Navarro, and R. Sassot, Phys. Rev. D71, 094018 (2005).

[13] M. Gluck, E. Reya, M. Stratmann, and W. Vogelsang, Phys. Rev. D63, 094005 (2001), hep-ph/0011215.

[14] T. Gehrmann and W. J. Stirling, Phys. Rev. D53, 6100 (1996), hep-ph/9512406.

[15] P. M. Nadolsky and C. P. Yuan, Nucl. Phys. B666, 31 (2003), hep-ph/0304002.

[16] D. De Florian, R. Sassot, M. Stratmann, W. Vogelsang, Phys. Rev. Lett. 101:072001 (2008), arXiv:0904.3821 [hep-ph]

[17] A. Bacchetta et al., Phys. Rev. Lett. 99, 212002 (2007).

7. Physics with Tagged Forward Protons: Run 11 and Beyond

7.1. Introduction

We are assuming here that a five-day run will take place in Run 9 with transverse polarization. To finish our goals in Phase I, as outlined in the Run 9 BUR, we are requesting 5 days of beam time with longitudinal polarization to investigate the non-perturbative regime of QCD using the polarized proton beams at RHIC, the STAR detector and the Roman Pots of the pp2pp experiment [1-5]. The pp2pp Roman Pot detectors, already installed and debugged during Run 9, will be used to tag very forward protons, thus selecting processes in which the proton stays intact, and the exchange has quantum numbers of the vacuum. Fig. 7-1 shows a schematic of this so-called Pomeron (IP) exchange; in this figure both Feynman diagrams and corresponding azimuthal angle vs. pseudorapidity diagrams are shown. For such processes the probability of measuring reactions where colorless gluonic matter dominates the exchange is significantly enhanced. A discovery program of glueball production in the Central Production process, taking advantage of STAR detector capabilities and the Roman Pots, is also proposed. The use of polarized proton beams, unique at RHIC, will allow exploration of the unknown spin dependence of diffraction, including both elastic and inelastic processes [6-8]. Needs for Phase II, which includes running at $\sqrt{s}$ = 500 GeV, beyond Run 11 are also outlined.

7.2. Beam Use Request for Run 11

To finish our physics program at small t, outlined in the BUR for Run 9, one more five-day running period with longitudinal polarization is requested in Run 11. Such a run will enable the collection of sizeable data samples. In order to reach the t and ξ values needed for both diffractive and elastic data, beam scraping and special optics are needed; this necessitates dedicating beam time specifically to this program.

Three major topics of interest will be studied: two in diffractive physics (elastic scattering, diffractive scattering) and one with discovery potential (Central Production of Glueballs in Double Pomeron Exchange Process), see Fig. 7-1.

Using the capacity of existing power supplies, optics of $\beta^* = 21$ m at $\sqrt{s} = 200$ GeV can be produced allowing t coverage with 100% acceptance for elastic scattering for $0.003 < |t| < 0.024$ $(GeV/c)^2$.

The five-day run includes two days of beam commissioning, two days of data taking and one-day contingency.

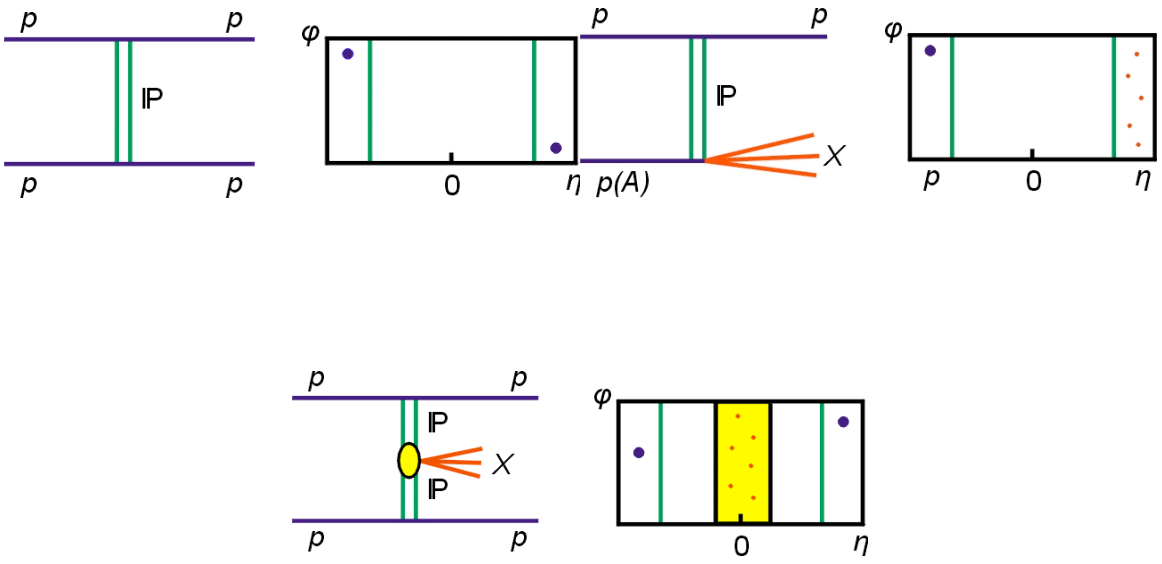

Figure 7-1. Elastic Scattering diagram (top left), Single Diffraction Dissociation (top right) and Central Production diagram (bottom center) diagrams. Both Feynman diagram and corresponding azimuthal angle vs. pseudorapidity diagram are shown.

Table 7-1

Luminosities at STAR and PHENIX for special run: emittance 12π mm mrad, 109 bunches 0.45×10^{11}/bunch

Luminosity	$cm^{-2}\ sec^{-1}$
STAR (β*=21m)	3.5×10^{29}
PHENIX (β*=0.7m)	1.1×10^{31}
Polarization	60-70%

With the above conditions at least 20×10^6 elastic events for each polarization could be collected. An estimated error on the slope parameter is $\Delta b = 0.31$ $(GeV/c)^{-2}$ and on the ratio of real to imaginary part $\Delta\rho = 0.01$, which is comparable to the existing measurements from the pp and $p\bar{p}$ data. The $\Delta\sigma_{tot}$ = 2-3 mb, where the biggest contribution is from the error on luminosity measurement. In four t subintervals we shall have 5×10^6 events in each resulting in corresponding errors $\delta A_{LL} = 0.003$.

With the expected luminosity we can also collect about 1.5×10^5, triggered DPE events, for which the proton momentum is reconstructed for each beam polarization.

During this period, STAR would also be able to acquire a large data sample (60 -100 million) of minimum bias events in an environment of low background and pileup.

7.3. Request beyond Run 11, Phase II

Our future plans include also running at $\sqrt{s}$ = 500 GeV. In addition, to maximize the acceptance and the range in t, ξ and M_X in this phase the Roman Pot system needs to be installed between DX-D0 magnets and will be used in conjunction with the STAR TPC to reconstruct and fully constrain events with resonances in central production processes. In Phase II taking data with STAR without a need for special optics will be possible.

The cost estimate for this step would have to be done since it requires modifications to the vacuum chamber in the DX-D0 region and new detectors. By the time this part is implemented, the controls, the readout and the trigger will already be done and ready, since it comes after executing of the program in Phase I. The Old Dominion University collaborators are planning to submit a proposal to NSF to fund this part of the program.

In Phase II the same physics topics will be studied over larger t, ξ and M_X, extending to pQCD regime at $\sqrt{s}$ = 500 GeV.

References

[1] S. Bültmann et al., Phys. Lett.**B579** (2004) 245.
[2] S. Bültmann et al., Nucl. Instr. Meth. **A535** (2004) 415.
[3] S. Bültmann et al.,Phys. Lett. **B632** (2006) 167-172.
[4] S. Bültmann et al., Phys. Lett. **B647** (2007) 98-103.
[5] W. Guryn et al., RHIC Proposal R7 (1994) (unpublished).
[6] V. Barone, E. Predazzi, *High-Energy Particle Diffraction*, Texts and Monographs in Physics, Springer-Verlag (2002) ISBN: 3540421076.
[7] S. Donnachie, G. Dosch, P. Landshoff, *Pomeron Physics and QCD*, Cambridge University Press (1998) ISBN: B0006Z3XLM.
[8] A. Bravar, W. Guryn, S.R. Klein, D. Milstead, B. Surrow, J.Phys. G28 (2002) 2885.